CORRELATION BETWEEN THE DEGREE OF CORROSION AND ULTRASONIC PARAMETERS IN STEEL

S.A.K.V.M.Piyathilake

168079R

Degree of Master of Philosophy

Department of Materials Science & Engineering

University of Moratuwa

Sri Lanka

July 2020

CORRELATION BETWEEN THE DEGREE OF CORROSION AND ULTRASONIC PARAMETERS IN STEEL

S.A.K.V.M.Piyathilake

168079R

Thesis submitted in partial fulfillment of the requirements for the degree Master of Philosophy

Department of Materials Science & Engineering

University of Moratuwa

Sri Lanka

July 2020

DECLARATION

I declare that this is my own work and this thesis does not incorporate without acknowledgement any material previously submitted for a Degree or Diploma in any other University or Institute of higher learning and to the best of my knowledge and belief it does not contain any material previously published or written by another person except where the acknowledgement is made in the text.

Also, I hereby grant to the University of Moratuwa the non-exclusive right to reproduce and distribute my thesis in whole or in part in print, electronic or other medium. I retain the right to use this content in whole or in part in the future work (such as articles or books).

Signature: S.A.K.V.M.Piyathilake Digitally signed by S.A.K.V.M.Piyathilake Date: 2020.07.28 00:03:11 -07'00' Date:

The above candidate has carried out research for the MPhil thesis under my supervision.

Signature of the supervisor: Date: Digitally signed by V Sivahar Date: 2020.07.29 10:41:12 +05'30'

Name of the Supervisor: Mr. V. Sivahar

Abstract

In metallurgical engineering, corrosion is considered as one of the main reasons for the failure of metallic components. The main reason for this is that, the corrosion is a phenomenon which is mainly influenced by the nature itself. It is very important to eliminate or reduce corrosion since it can lead to major disasters which can negatively affect the human lives and properties. Inaccurate estimations, inaccessibility of the areas of corrosion, limitations for the destructive tests can be identified as some of the main reasons for the wrong and misleading preliminary corrosion investigations, which lead to catastrophic failures. Conventionally, the degree of corrosion is determined using destructive testing methods. Also, most of the research work in this area has focused on the uniform corrosion/general attack faced by steels across a range of atmospheres. With those methods, the real degree of corrosion cannot be revealed since it is difficult to address regarding the corrosion penetrations or pits. Therefore, those are inaccurate up to some extent. In contrast to that, Ultrasonic testing methods would be more effective and convenient to overcome above limitations and would be able to open a new area of estimating the degree of corrosion accurately. Also this study sought to contribute to this field by examining whether the penetration of corrosion beyond the general attack has a significant effect on the load-bearing capacity of mild steel.

Also,in some cases such as in bridges and pipelines ultrasonic non-destructive method would be really advantageous since it is not only non-destructive but also it will allow reaching inaccessible locations easily. Further,an Ultrasonic wave can easily propagate through steel and its attenuation would provide a measurable reading to express the degree of corrosion including every minor detail.

The research work is basically focused on measuring the degree of corrosion accurately using ultrasound attenuation. The selected steel materials were subjected to corrosion in a standard accelerated environment for a defined period of time. Then after a set of experiments, the degree of corrosion has been represented by the weight loss per unit

area, corrosion rate and the corrosion penetration depth in to the material. Furthermore, the research work was able to cover the area of the mechanical property deterioration. The tensile samples were also corroded in the same standard accelerated environment as mentioned above, and subjected to periodic tensile testing and corrosion weight loss analyses. Further, the corroded samples were examined under optical and scanning electron microscopy to observe the penetration behavior of corrosion in to the material. The results showed that the actual breaking loads deviated negatively from the expected load-bearing capacity, which was determined through conventional methods. This deviation showed a close correlation to the increase of penetration of corrosion with time.

Meanwhile, the ultrasound attenuation related to each of those corroded samples was measured simultaneously. Finally, all the data were analyzed through mathematical software such as MATLAB and SPSS to generate final correlations. Thereby, a nondestructive method through ultrasound attenuation was developed to determine the accurate degree of corrosion and to predict the remaining load bearing capacity of corroded structures.

TABLE OF CONTENTS

LIST OF FIGURES

LIST OF TABLES

LIST OF ABRREVIATIONS

ASTM - American Society for Testing and Materials

CS – Carbon Steel

CR – Corrosion Rate

DAC – Difference in Attenuation Coefficient

EDX - Energy Dispersive X-Ray Analysis

EN - European Norm

EMAR – Electro Magnetic Acoustic Resonance

EMAT - Electro-Magnetic Acoustic Transducer

FEM -Finite Element Method

GDP - Gross Domestic Product

IGC – Inter-Granular Corrosion

ISO - International Organization for Standardization

PDC – Penetration Depth of Corrosion

RAC – Reference Attenuation coefficient

SEM – Scanning Electron Microscope

SCC - Stress Corrosion Cracking

TEM - Transmission Electron Microscope

TAC - Total Attenuation Coefficient

WLPA –Weight Loss Per unit Area

XRD - X-Ray Diffractometer

ACKNOWLEDGEMENT

Foremost, I want to convey my heartiest gratitude and thankfulness to my advisor/ Head of the Department Mr. V.Sivahar, for the exceptional support given to me by guiding me to accomplish this goal. The enthusiasm and the motivation given by you are priceless and without your lead, this will not be a success. Furthermore, I would like to thank Professor R.G.N.De.S. Munasinghe, for the excellent guidance given in initialing this research work and providing useful comments, remarks throughout the learning process of this MPhil thesis. Also I would like to thank senior lecturer Mrs. Ravindi Jayasundare and to the Department of Mathematics for giving the fullest support in thesis work.

My sincere thank should also go the research committee for directing me to the right way till the end. Also I greatly appreciate the assistance that I received from the former head of the department and the academic and non-academic staff of Department of Materials Science and Engineering, University of Moratuwa.

Also, the financial support by SRC/LT/17/24 university research fund is greatly acknowledged.

The outcome of this thesis is a collection of efforts. There are lot of helpful hands behind it's success. I would like to express my gratitude to my parents, husband and all the family members for giving me the strength not only to achieve this goal, but for being with me throughout the entire way of personal, educational and career lives. Your support guided me to climb up the ladder.

Last but not least, I would like to express my warm hearted thanks to my colleagues, relatives and every one whom has supported me in every way to make the MPhil thesis a success.

Piyathilake S.A.K.V.M.

1 INTRODUCTION

Corrosion is a chemical reaction which adversely affects the function of metallic components. It is considered as the main cause of failure in most of the metal structures in coastal areas and negatively affects human lives and the economy of a nation. This is a serious concern which is common for many countries in the world that costs trillions of dollars. For the year 2016, the global cost of corrosion was US$2.5 trillion, which is equivalent to 3.4 % of the global Gross Domestic Product (GDP). The annual cost of damages due to corrosion in the USA is over $1.1 trillion dollars. It is over 6.2% of the GDP of the United States and damages due to corrosion is one of the largest single expenses in the US economy even though **(**and yet) it rarely receives the attention it deserves [1]. Hence, it is very important to find effective methods to either eliminate for some extend or drastically reduce the corrosion in metals in order to minimize possible failures of metal structures and avoid consequential catastrophic disasters.

The metallic corrosion can be broadly categorized based on the environment where the metallic components are placed during service i.e. corrosion in atmosphere (atmospheric corrosion), corrosion in liquids such as in fresh and sea water, and corrosion in soil etc. All of these types can have a significant effect on the reliability and failure of structures. Therefore, the main objective of most of the research work worldwide is to detect the extent of corrosion to find possible solutions to minimize the corrosion of steel. The danger and the severity of this phenomenon lies in the fact that it degrades the material's properties drastically and unexpectedly.

Considering all the above, it is essential to understand the real time corrosion behaviour of steel even though it is not possible to prevent it completely. Currently, there are many 'destructive' methods to evaluate corrosion in steel as well as in the other metals. However, cutting or removing a sample from a load bearing structure for testing is not prudent as it can create an initiation of another unnecessary failure. Therefore, a new era

of corrosion estimation has been developed in recent decades under nondestructive estimations. In this research we are basically trying to develop/investigate a methodology to detect the extent of the degree of corrosion in steel using ultrasonic non-destructive evaluations. This research is basically focusing on that challenge which is targeting the detection of the extent or the degree of corrosion in steel using ultrasonic non destructive evaluations. Such evaluation methods are important since these methodologies can be used in in-situ applications. If the extent of corrosion can be detected, the remaining life-time can be predicted by developing a necessary correlation. Also the correlation can be modelled using mathematical modeling software.

During this research work steel samples with known chemical compositions were subjected to corrosion in a corrosion chamber which has the capability to accelerate the corrosion process artificially in a salt spray environment. The rate of corrosion of steel in this artificial environment depends on many factors such as temperature, humidity and chloride iron content and they were controlled according to the standard ASTM B117-11. The experiments were run keeping time as a function. The mechanism of the corrosion process in the chamber was closely monitored and well-studied targeting uniform corrosion, pitting corrosion and corrosion penetrations. Then the variation of ultrasonic attenuation parameter of the samples placed in accelerated corrosive environment was measured. In addition, the degree of corrosion of those samples was measured using destructive methods such as mass loss and microscopic investigations to estimate the penetration attack due to corrosion. The correlation between the ultrasonic attenuation and the degree of corrosion was then developed and this relationship was mathematically modeled to investigate the validity of the outcome of this research work. The developed relationship can be expressed as a function of the degree of corrosion as weight loss per unit area, corrosion rate and the penetration depth of corrosion.

The developed co-relation was refined by adding correction factors expanding the scope of the research. Since the attenuation of a material would vary with the major impurities and the grain structure, the correction of these factors should be added to the co-relation

that would generalize the co-relation. Therefore the attenuation variation of corroded plain carbon steel samples with various carbon contents and the attenuation variation of plain carbon steel with different grain structures were experimentally quantified and evaluated. Carbon is a major constituent in plain carbon steels which affects its corrosion behaviour because of its microstructure. Ferrite is rich with iron while the pearlite forms a galvanic couple of cementite and ferrite. (Herein we also experimentally studied how Ferrite and Pearlite can affect the corrosion rate and the attenuation of ultrasound waves)[2].

Expanding the scope further, the change of mechanical properties such as tensile strength (load bearing capacity) of the corroded samples with the degree of corrosion was measured and the load bearing capacity could be predicted accurately. This section of the research focused on the attack of the general corrosion layer and the corrosion beyond the general attack (pits / penetrations).

It was also observed the depth of penetration of corrosion into the virgin metal in the forms of inter-granular or trans-granular through the grain bulk. This work is significant since it takes into account the full extent of corrosion. It also helps to explain the difference between theoretical prediction and experimentally obtained residual strengths of mild steel members. This deviation from the expected residual strength is due to traditional service life calculations focusing only on the progress of the general attack, once the layers of rust are washed off and the “virgin/healthy” metal is uncovered.

Over the course of the literature survey, it became apparent that the research carried out on the corrosion of mild steel did not cover the penetration of corrosion beyond the general attack. Perhaps this is due to the fact that any kind of penetration is swiftly followed by the coverage of bulk uniform corrosion. Nevertheless, it seemed logical that the existence (or absence) of significant penetrative corrosion and its effect on the mechanical strength of mild steel ought to be studied in detail. This is because the true load-bearing section of a corroded member would be reduced if such penetrations

existed. The findings of this section of the research could lead to the safety factors associated with remaining service life being optimised.

One of the main objectives of this study therefore, was to gather results that could be used to the industrial applications regarding the effect of penetration of corrosion on the load-bearing capacity of mild steel. It aimed to show that said effect is significant enough that it cannot be neglected in residual strength calculations pertaining to corroded load-bearing members.

Finally, the developed relationships of ultrasound attenuation and the degree of corrosion which were refined with the correction factors were co-related with the findings of the mechanical property experiment results.

2 LITERATURE REVIEW

An intensive literature survey was carried out to summarize the current research in this field. Upon investigation of the previous work, we were able to identify and narrow down areas that needed further study which helped us to contribute to the challenges in the field.

In the literature survey, it was mainly focused on the previous research that was carried out on the corrosion behaviour of low and medium carbon steels, grain size, ultrasonic parameters of steels, and the mechanical properties of corroded steels etc.

Since the objective was to develop an experimental model for corrosion, the research was mainly focused on identifying factors that affect corrosion (especially accelerated corrosion). Also research regarding the possible types of corrosion in steel has been studied. In addition, there are also studies on the inter-granular and trans-granular corrosion and corrosion penetration. From the literature survey it was possible to learn about the composition of the corrosion layers, morphology and their behaviour since these factors directly affect the propagation of ultrasonic waves. The destructive methods of the corrosion assessments were also studied, since they are required to evaluate and correlate against the non-destructive parameters. The literature survey in this category has to be extended further on studies with traditional and advanced characterization techniques.

The literature survey was further extended based on the studies in the ultrasonic parameters and corrosion. It could be found only a few studies that investigates the ultrasonic parameters in corrosion of (especially) mild steel and corrosion penetration of the grain boundary attack. But there were similar investigations that had carried out modelling ultrasonic parameters for stimulated corrosion in mild steel. Stainless steel and ultrasonic parameter related research were also considered here.

The summarized literature is mentioned below under some specific areas which can be classified as the major sub-topics of this research.

2.1 Studies performed in the field of corrosion of steel

Research related to the atmospheric corrosion in different types of steels [including carbon steel (0.18 % of C) Figure: 2.1) in marine environments was carried out by Sei J. Oh. The main aim of their research was to characterize the corrosion behaviour as a function of the type and composition of steel and the environmental conditions. They have analysed corrosion components by X-ray diffraction and Raman spectrometry and found that α-FeOOH (Goethite), γ-FeOOH (Lipidocrosite), β-FeOOH (Akaganeite), γ-Fe_2O_3 (Maghemite), α -Fe_2O_3 (Hematite) were present in the corroded samples[3].

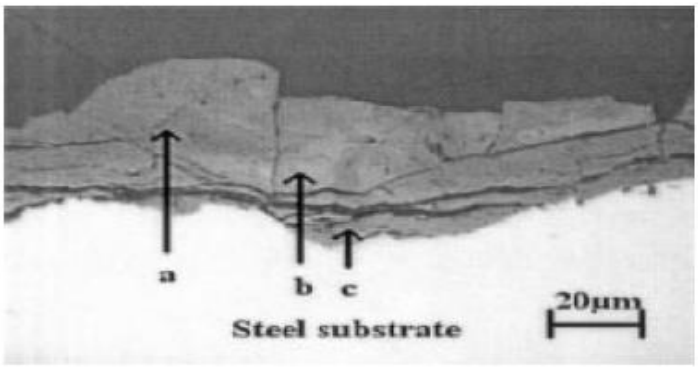

Figure 2. 1 : Corrosion layers formed in coating of the carbon steel exposed at marine site showing regions: (a) Goethite, (b) Superparamagnetic Maghemite plus Goethite, (c) Superparamagnetic Maghemite

A lot of research has been done in marine environments similar to the above-mentioned work. In those research, the types of corrosion products have been identified in different extends under different conditions [4].

Many researchers have attempted to develop empirical relationships between corrosion rate and environmental parameters. The effects of meteorological variables and contaminants such as SO_2, Cl^- on atmospheric corrosion were taken into account in these types of studies[5][6][7].

S. Palrajand et al. have studied atmospheric corrosion of mild steel at 16 different locations in the east coastal areas in India over a period of two years. Atmospheric pollutants such as salinity and sulphur dioxide were estimated in those 16 sites and they were correlated with corrosion rates. The environmental characteristics and corrosivity categories in these sites have been discussed. Their research also proved that the nature and rate of atmospheric corrosion of a metal or alloy depend on the level and type of gaseous pollutants present in the atmosphere. The duration of their action on the metal surface also affects the rate of corrosion. Furthermore, they have strongly suggested that the corrosivity data were essential for the development of specifications to optimize corrosion resistance in manufactured products [8].

M. Morcillo et al. has done a review on atmospheric corrosion in mild steel. The nature of the atmospheric corrosion products, their dependence on the environmental conditions, morphology, mechanisms of atmospheric corrosion, rust formation mechanisms and advanced techniques that can be used to identify corrosion behavior (SEM/EDX, TEM, back scattered electron imaging, Micro-Raman Spectroscopy) have been thoroughly reviewed [9]. The same research team has performed characterization of rust formed on mild steel surfaces which were exposed to marine atmospheres for 6 months (Specimen A in Figure 2.2) and 12 months (Specimen B in Figure 2.2). They have used XRD and SEM/Micro-Raman spectroscopy and identified layers of the rust (Figure 2) [10].

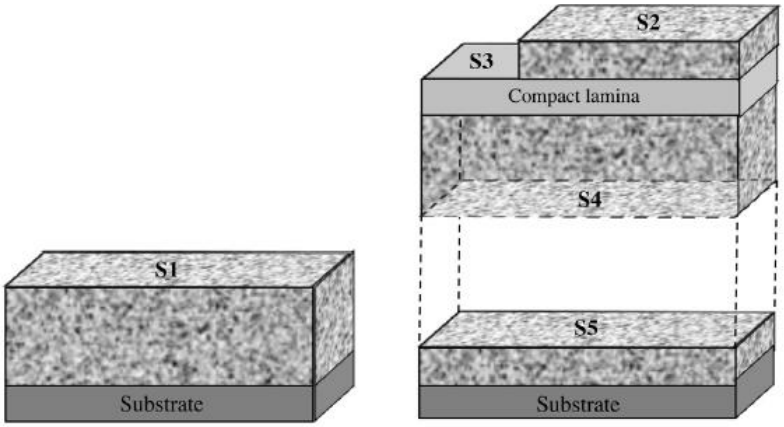

S1: outermost surface of consolidated rust layer
S2: outermost surface of exfoliated rust layer
S3: surface of the internal compact lamina within the exfoliated rust layer
S4: innermost surface of exfoliated rust layer
S5: rust layer on the remaining steel base

Figure 2. 2 : Corrosion layer types in two specimens A and B [10]

The formation of these kinds of layers directly affects to the attenuation of ultrasound waves passing through the corroded sample. The amount of the reduction of the ultrasound energy can be mapped with the amount of corrosion and thereby the degree of corrosion could be predicted through an ultrasound attenuation parameter. P.Dilmann and his colleagues have carried out a similar study to the above mentioned research to investigate the atmospheric corrosion of iron. Composition, structure and porosity of the rust were analyzed by different advanced methods and extracted parameters were used for modeling the corrosion in that given time period. A part of the graphical modeling is given in Figure 2.3 [11].

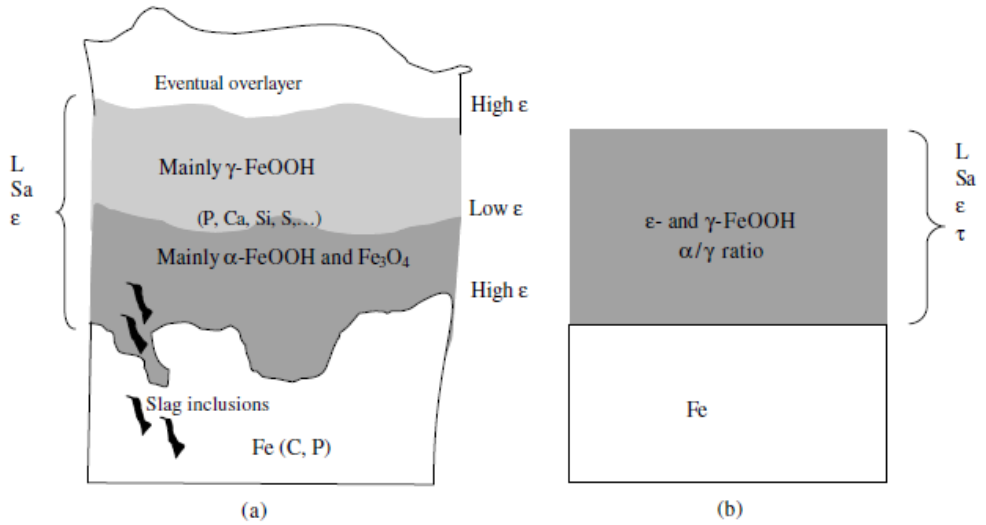

Figure 2. 3 : Cross section of (a) corroded sample (b) model [11]

2.1.1 Intergranular corrosion (IGC) and stress corrosion cracking (SCC)

The research conducted into the intergranular corrosion and stress corrosion cracking of mild steels is decidedly meagre. Both references involved a special set of circumstances that provoked this condition in mild steels, resulting in the passivation of the mild steel surface [12][13]. The work of Parkins [12] is of particular interest, since the Clarke's solution (concentrated Hydrochloric Acid, Stannous Chloride and Antimony Trioxide) used to initiate intergranular corrosion is the exact same chemical solution used in this project to remove corrosion products in order to perform a mass-loss analysis. Vivid details of this regard are mentioned in chapter 3.

2.1.2 Exposure conditions affecting corrosion

Morcillo [14] published a review in 2013 focussing on assorted atmospheric corrosion data of low alloy steels and how different exposure conditions give rise to varied effects of corrosion. Through an extensive review of the available bibliography, they have reached several important conclusions like one given below:

"Continuously moist exposure does not allow the formation of protective rust layers due to the lack of the necessary wet/dry cycles. Furthermore, as in indoor exposure, WS (Weathering Steel) corrosion is not so different to that experienced by CS (Carbon Steel), and thus the use of WS is not justified."

This is an important observation for the purposes of this research since the steel specimens (though not made of weathering steel) will in fact be subjected to continuous moist exposure in the salt spray corrosion chamber. Therefore, it could naturally be assumed that a protective rust layer will not form, and significant corrosion could be achieved. Their work goes on to show the immense amount of literature found on the subject, the limitations of previous work and the body of results that could be manipulated to show patterns and correlations.

In a journal article more specifically related to this research, Yuantai Ma [15] studied the effect of chloride ions as a constituent of the corroding atmosphere on the corrosion of low carbon steels. Their research is important to this project because of the accelerated corrosion conditions encountered inside the salt-spray cabinet used to corrode the mild steel specimens. While concluding that the presence of a high amount of Cl^- ions changes the corrosion products formed nearest to the virgin metal interface, they also verified the application of the following well known wet cycle half reactions (equations 1-4):

$Fe \rightarrow Fe^{2+} + 2e$ (Anodic Reaction) (1)

$Fe^{2+} \rightarrow Fe^{3+} + e$ (Anodic Reaction) (2)

$O_2 + 2H_2O + 4e \rightarrow 4OH^-$ (Cathodic Reaction) (3)

$(Fe^{2+}, Fe^{3+}) + Cl^- + OH^- \rightarrow FeOCl + HCl$ (Total Reaction) (4)

2.1.3 Methods of determining the degree/extent of corrosion

The most heavily researched modes in determining the extent or degree of corrosion are interrelated, and have been expounded below. They are the analysis of mass-loss and the measurement of the depth of corrosion and its penetrations. It must be explained that the "corrosion penetration" alluded above is merely the depth to which the uniform attack has penetrated into the steel, and does not encompass any further incisions beyond the said attack. Refer to Figure 2.4 for an illustration of the difference between the two measurements.

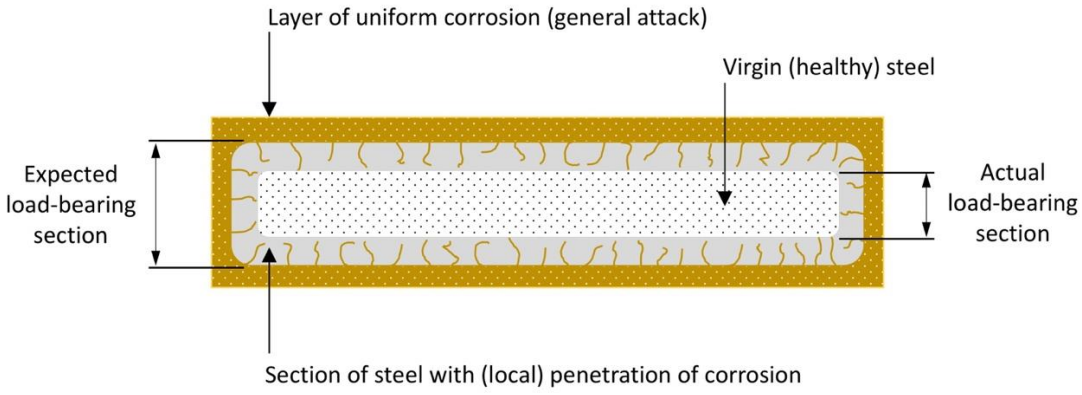

Figure 2. 4 : Cross-sectional view of a corroded member illustrating the penetration of corrosion

2.1.4 Weight loss/ Mass loss analysis

Mass-loss analysis is the one of the methods in determining corrosion rate and is heavily quantitative. The most useful aspect of this method is the prediction of corrosion loss over long and short periods of time. Panchenko of the Russian Academy of Sciences has published two separate research papers [16][17] on this subject accompanied by two

different research teams that propose a power function and a linear function for predicting corrosion mass-loss in structural metals across the world. The salient part of this work is the determination of coefficients to go into the predictive functions, so that they retain an empirical character. The widely used power function that his team manages to modify is shown here (equation 5):

$$K_t = A.t^n \quad (5)$$

where K_t represents the corrosion losses after a time 't', A is a coefficient (constant) of corrosion losses over the first year and n is a constant coefficient that characterizes the protective properties of corrosion products.

The quantified measurement of weight loss analysis was conducted according to ISO 8407 international standard and conditions in the environment were analysed by following EN 12500-2000, EN ISO 9224, EN ISO 9225, EN ISO 9226, etc [18].

2.1.5 Depth of penetration of corrosion

This is the way of measuring the extent of corrosion which involves some form of SEM and X-Ray analysis. This method of measurement is of direct importance to this research work and the work of Zhong [19] , while being more oxidation than corrosion related, offered perspective into the depth of penetration of oxygen along grain boundaries of an alloy system in supercritical water. This study shows that there is scope for the measurement of penetration of corrosion products into the virgin steel, in order to provide a "depth of penetration."

A significant part of this research's methodology, Scanning Electron Microscopy (SEM) is an extremely well researched area by itself, especially in the field of metallurgy where it plays an important part in analysis and characterisation. When it comes to research publications, many papers could be found that utilized SEM imaging for the corrosion detection and measurements.

Avci et al.[20] studied a practical method of determining pit depths in carbon steels subjected to pitting corrosion using X-Ray attenuation and EDX spectra. His thesis focuses on deep and narrow pits that cannot be measured by conventional means.

Girão et al. [21] in a journal published in 2019, focussed on the many applications of SEM – EDS analysis in spheres of analytical chemistry, particularly in microplastics. Though this may seem anomalous in a survey on steel corrosion, the paper offers insight into sample preparation and equipment operation which is invaluable to this research project.

Returning to a more specific study, Zhou and Zuo [22] offer a specific study of intergranular corrosion of mild steels through passivation in a special solution using SEM analysis. This study shows us how SEM imaging technique can be used to study interfaces. Ye et al.[23] has done SEM analysis of high temperature corrosion of Hastelloy alloy in molten fluoride salts, with elemental mapping to help characterise the phases and elements at the interfaces, and de la Fuente et al.[10] endeavour to characterise rust surfaces formed on mild steels using SEM techniques among others.

These varied studies of corrosion or corrosion related processes through SEM analysis show the versatility of the Scanning Electron Microscope as an analytical instrument.

2.2 Effect of the composition of steel on corrosion

Composition of steel is a salient factor that affects the corrosion behaviour. When it comes to plain carbon steel, carbon is the main constituent and that would be the main consideration in this regard. Therefore, the amount of carbon present in the plain carbon steel is a major factor that affects the corrosion. It is said that Pearlite in steel is harmful for corrosion resistance. The lamellar structure of cementite and ferrite in pearlite forms a galvanic cell with the presence of electrolyte. Even moisture is an electrolyte for this. Hence when increasing the carbon content of steel, the corrosion increases [24].However, ferrite phase (α) of iron is more active than austenite phase (γ). Thus, the

formation of austenite tends to decrease the corrosion than in ferrite. Corrosion penetrates in bulk material consuming the ferrite phase surrounding austenite grains until their detachment [25]. Researchers have found that when increasing the ferrite percentage, the resistance to pitting corrosion decreases [2]. Presence of iron in one of its phases prefers general corrosion rather than any intermetallic compound of iron. Hence a combined effect of general, pitting and galvanic corrosion affects steel that contain ferrite and pearlite microstructures.

2.3 Effect of corrosion on the mechanical properties of steels

The effect of corrosion on the weakening of mechanical properties of steels is a fairly old area of research. This is of particular importance in the area of constructional steel research, since the residual strength of corroded steels has a major impact on the service life of steel structures (including concrete reinforcement) susceptible to corrosion. This fact has been highlighted well in literature and those discussed in this section have roots in the construction sector.

Almusallam [26] assessed the effect of degree of corrosion on the mechanical properties of reinforcing steel bars and found that the degree of corrosion resulted in the gradual decrease of breaking load and dictated the nature of eventual material failure under tensile testing. His definition of "the degree of corrosion" was centred on a gravimetric weight-loss analysis, performed using chemical corrosion removal in order to determine the percentage of virgin steel lost due to corrosion. This shall be the basis of the weight-loss analysis to be performed as a part of this research as well. Furthermore, he pointed out that the "ultimate tensile strength" of the steels he tested did not show a significant drop from the stated values prior to the onset of corrosion. What drops is only the "breaking load", since the "tensile strength" itself is a material property independent of the effective load-bearing cross-section.

Lee and Cho [27] centred their work around almost the same principles as Almusallam [26], but branched out to an analysis of both pitting corrosion under chloride attack and

general corrosion under an electrical current. They were also able to conduct a Finite Element Method (FEM) analysis to better predict the remaining service life under reinforcement corrosion. There is an important point to be found in the summary of this research paper:

"There was a very high correlation between the degree of reinforcement corrosion and the mechanical properties of reinforcement. The mechanical properties of reinforcement corroded by chloride induced damage are lower than those of reinforcement corroded by electric method, even if the rates of mass loss by corrosion are the same."

Does that mean the traditional methods of estimation of residual strength for corroded members do not apply to chloride induced damage? This question is directly related to the scope of their research. Furthermore, both Almusallam and Lee [26][27] fail to explain the disparity between the breaking loads that are anticipated from mass-loss analyses, and those actually obtained. This means that there must be some factor that acts to reduce the expected load even further. Most importantly, this provides evidence that the conventional gravimetric weight loss analysis is not giving the complete picture or the value of the degree of corrosion. The degradation due to formation of the pits/ penetrations of corrosion should be added to this value to obtain a comprehensive understanding.

Apostolopoulos and Papadakis [28] studied the consequences of steel corrosion on the ductility of reinforcement steel, which was once again a similar work to the two mentioned above. They distinguish their work from that of the others by focussing on the durability of mechanical strength of steel under corrosive attack simulated through accelerated corrosion in the laboratory, thereby better predicting service life of steel members used as reinforcement bars. Their work is comprehensive in the correlation of the degree of corrosion with the remaining service life of load-bearing members. This is once again based only on general corrosion calculations through corrosion mass-loss measurements. The authors do imply, however, that the expected service life may not be reached to the safety factors not being universally

agreed upon. This conclusion supports the need to perform this research, in order to help to bridge the gap in knowledge where the residual strength of corroded steel is concerned.

Zhang et al. [29] published a similar study focussing on both the tensile and fatigue properties of corroded rebars. They used their research to deliver a comparison of the strength characteristics of corroded steel in actual field use and through laboratory simulated accelerated corrosion. An interesting paragraph which was found in this research paper is as follows:

"The degree of corrosion of the rebars was quantified based on gravimetric mass loss, i.e. the average loss of cross-sectional area of the corroded rebars, and was calculated as the ratio of the difference between the mass of the rebars before and after corrosion to the original mass of the rebars, i.e. before corrosion. This corrosion measurement method may not be able to reflect the influence of local corrosion pits; however, it is of practical significance considering the fact that in engineering practice it is very difficult to measure the local corrosion pits, i.e. the minimum cross-sectional area of corroded rebars."

This paragraph explains why the traditional means of analysing the residual strength of corroded steel members does not take into account the "minimum cross-sectional area". The current research, however, does intend to take the influence of the "local corrosion pits" into account, and indeed that is what is referred to as "pits/penetration of corrosion" throughout the research.

In a recent research, Ohga and his team [30][31] sought to optimise existing models for the calculation of remaining service life of corroded structures, using plates from a 100-year-old Japanese bridge. They have focused on the "representative effective thickness" of a corroded load-bearing member, and proposed an equation to relate that value to the original thickness of the component. That was the first attempt that could be found in literature which has given the attempted to bridge the gap between the expected and actual breaking loads of a corroded load-bearing member. Their literature survey in

turn, refers to 3 other such methods of calculating representative effective thickness of a corroded part, which they then try to optimize using their own formula.

In a review paper encompassing steel plated structures subjected to marine corrosion damage, Yikun Wang et al. [32] sought to fully document various publications on both general and pitting corrosion in marine atmospheres and how they have individually attempted to enhance the service life calculations for marine structures and vessels using mathematical and computational modelling techniques.

To round off this subsection on the effect of corrosion on the mechanical properties of steel, a daring work must be cited. Youde Wang et al. [33] sought to predict the residual strength and deformability of corroded steel using a 3D morphology mapping model. That represents the closest research which has gotten to achieving a truly accurate model that encompasses local pits and the minimum load-bearing cross section for a corroded part.

When it comes to the other important mechanical property, which is the fatigue life of the members, Weber published an article on the effects of surface corrosion damage on the fatigue life of 6061-T6 aluminum alloy extrusions (in 2017). They stated that the fatigue crack initiates from the deepest corrosion pits [34].

"Hence there are conflicting results in the literature on whether fatigue cracks are initiated at deepest corrosion pits."

According to the statement of Weber et al, the importance of finding the relation between the topography and the corrosion pit shapes were discussed. Furthermore, Weber stated that the effect of corrosion damage on fatigue life is predominant at the beginning of the corrosion.

"It is evident that corrosion damage that led to reduced fatigue life took place predominantly in the early stages"

Although the statement was made for Aluminum alloy, this study suggests determining if there is a significant effect for the low carbon steel.

It appears that determination of an exact location where the cracks initiate is unpredictable. Therefore, Xin-Yan et al. published a paper on Effect of corrosion pits on fatigue life and crack initiation in 2013 to review the pit formation and its effect on fatigue life [35].

Xin-Yan states that, *"cracks do not necessarily initiate from the bottom of the pits, for the reason that there were many cracks with a depth smaller than that of the corresponding pit"* Since crack initiation does not occur at a corrosion pit, does that mean whether there could be other governing factors which influence small cracks apart from what is discussed? Do corrosion topography and the equivalent shape of the corrosion pits influence the fatigue crack initiation/growth? These questions have to be answered in future research.

Pedro et al. published an article in 1990 focusing on evaluating the remaining fatigue strength of corroded steel beams in a aqueous environment [36]. They have considered three factors which contribute to the loss in fatigue life. Pedro further states as follows,

"The total reduction in fatigue strength exhibited by the beams tested in the aqueous environments is attributed to (a) the loss in cross-sectional area due to corrosion in plane of crack, (b) the aqueous test environment, and (c) the stress concentration effect of the rust pits."

Mohamed R. Bayoumi et al. [37] published a technical note in 1995 focusing on the effect of surface finish on fatigue strength. Although it is a fairly old publication the conclusions remain valid up to date. They compared the fatigue life-time of aluminum alloy specimens with different surface roughness acquired by polishing. Fatigue phenomenon is very sensitive to surface state. Thus fatigue life is strongly influenced by the surface finish and surface treatment. They have represented the flow strain curves for surface finishes which shows us the variation of fatigue crack initiation period with varying surface roughness. The most related and vital

observation here is, the crack initiation period decreases with increasing surface roughness. In addition, the overall fatigue life and fatigue limit decreases with increasing surface roughness.

"The strain behavior obtained represented the fatigue integrity and indicated clearly that the fatigue life is separated into three stages of crack initiation, crack propagation and final structure. Also, results showed that the endurance stress is greatly affected by the surface finish conditions".

According to the literature survey, there are many evidences that it is certain that the surface condition greatly affects the crack initiation period and the overall fatigue life of a corroded specimen.

2.4 Ultrasonic evaluation and metallic corrosion

There were only a handful of studies that had used ultrasonic waves for the evaluation of corrosion. There has been a few articles that utilized waves in the recent years as mention here in the literature study.

N. Jothilakshmi has researched on the assessment of Inter-Granular Corrosion (IGC) attack in austenitic stainless steel using ultrasonic measurements. She has used longitudinal wave and the mode converted shear wave for the detection of surface corrosion and intergranular corrosion. Figure 2.5 shows one of the wave patterns she obtained. Further, ultrasonic measurement involved in longitudinal mode, longitudinal to shear velocity ratio, sound attenuation measurements, and spectral analysis were also done. Elastic modulus measurement has also been obtained using a nano-hardness tester [38].

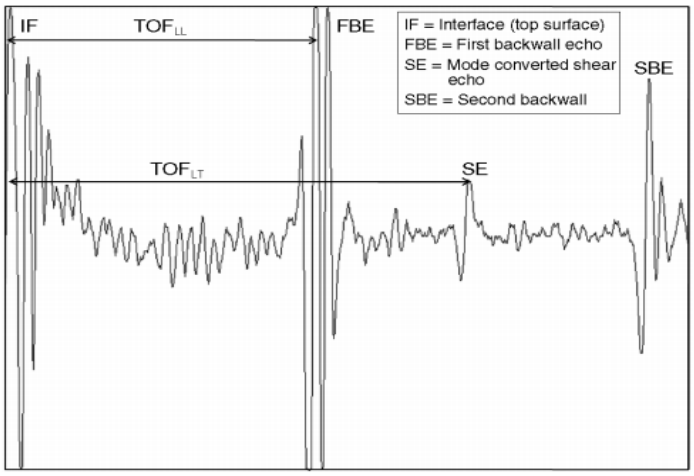

Figure 2. 5 : Ultrasonic Velocity Ratio Measurement for IGC Detection in Austenitic stainless steel

A similar research under the application of ultrasonic methods for early detection of intergranular corrosion in austenitic stainless steel has been done by JIAO Jingpin [39]. He has studied ultrasonic techniques for the early detection of intergranular corrosion in austenitic stainless steel (super 304H). Two methods, including acoustic attenuation and nonlinear parameter measurements, have been utilized to assess the degrees of IGC in five pipes made of super304H.

Karl R.Olsen, (a PhD student in Washington State University) has studied on ultrasonic detection of simulated corrosion in one inch diameter steel tieback rods which were buried in soil. In his research he has artificially made edges in different depths in a way of stimulated corrosion and the effect of transitions of the ultrasonic signals were detected according to the depth. Furthermore, the effect of the depth of the corrosion on the ultrasonic signal and the effect of soil on tieback rod signal attenuation have been measured successfully. He also developed a normalized amplitude method for assessing attenuation in transition of stimulated corrosion. Most importantly, he also has suggested in his thesis, to investigate the detestability of actual corrosion in steel rods on the

ultrasonic signal using accelerated corrosion in salt spray chambers for inducing corrosion which is very much closer to this research objectives [40].
All of the above research studies are useful in understanding the ultrasonic wave behaviour in corroded steel and those are really helpful in the first stages of the detection of corrosion.

In a previous research work that myself and a research team carried [41], it was possible to analyse the extent of corrosion in reinforced rebars in concrete, after subjecting to accelerated corrosion. The evaluation was done by using ultrasound waves through the concrete. It could be concluded that ultrasonic wave velocity measurements can be used to analyse the extent of corrosion of the embedded reinforcement bars in concrete qualitatively as well as quantitatively by establishing a proper correlation between them. This clearly shows that the ultrasound waves can be used to investigate the corrosion in steels.

2.5 Ultrasound and grain size of steel

Grain size is an important parameter in characterizing the microstructure of metals and it also has a great effect on properties of metals such as yield strength, plasticity, toughness, fatigue strength, creep strength and corrosion resistance [42]. Therefore, grain size can influence most of the mechanical properties and hence it can be used for materials characterization. There are two methods to measure grain size manually as outlined by ASTM E 112 standard.

I. Area method

A geometrical figure with known dimensions is marked on the microstructure of the sample. The number of grains in the area is then counted and taken to be equal to the number of grains lying entirely in the figure, plus one-half of the number intersecting the perimeter. Specimens are polished and etched sufficiently to reveal the grain

boundaries before observing under the microscopic investigations [43]. Average grain size diameter can be calculated using below equation (6).

$$\mathbf{d} = \frac{\mathbf{2}\boldsymbol{X}}{\mathbf{M}\sqrt{\boldsymbol{n\pi}}} \qquad (6)$$

Where,

X - Length of the side of the square
M - Magnification used
n - No. of grain in the area
d - Mean diameter of the grains

II. **Linear intercept method (Hen's technique)**

The mean linear intercept is determined from the number of grains or grain boundaries (N) intersecting a line of length L. The most convenient method is to use a line ruled on an eyepiece graticule at a magnification sufficient to give 5-10 intersections per field and count the number of grains on the line for about 50 fields [43]. Average grain size diameter (according to ASTM E 112) can be calculated using below equation (7).

$$d = \frac{N}{LM} \qquad (7)$$

Where,

d - Mean diameter of the grains,
L - Length of the line,
N - Intersecting No. of grains or grain boundaries,
M - Magnification used

Ultrasound waves have been used in many forms to evaluate the grain structures of materials. Hirotsugu Ogi et al. has done a research on Electromagnetic Acoustic Resonance (EMAR) which was discovered to be ideally suited to the non-destructive evaluation of ultrasonic attenuation [44]. They have found that, owing to the non- contacting EMATs, it conveniently excludes the interfering effects which occur with the conventional techniques. The diffraction effect can be strictly corrected using the numerical iteration procedure, resulting in an absolute evaluation of the attenuation coefficient. The measurement can be done with great ease and high reproducibility, accommodating rusty or moderately rough surfaces as well.

3 METHODOLOGY

The experiments were carried out under five different subtopics which were later consolidated to provide a comprehensive view on this research title. Those five projects are described in separate sections below.

3.1 Establishing a relationship between the degree of corrosion and attenuation coefficient for a selected composition

3.1.1 Sample selection

Chemical composition

Industrially used, commercially available material was selected to start the initial steps of the research. Therefore, it would be like the base composition of this research. The chemical composition of the metal samples was analyzed using the atomic emission spectroscopy. The composition is shown in the Table 3.1.

Table 3. 1 : Chemical composition

C (%)	Si%	Mn%	Cu%	P%	S%	Cr%	Ni%	Al%	Fe%
0.28	0.26	0.53	0.04	0.02	0.02	0.11	0.03	0.01	~98.6

Carbon content was 0.28 % and the other elements are in insignificant percentages, thus the content of the other constituents made the particular steel a plain carbon steel.

Microstructure

The initial microstructure was examined using optical microscopy after carrying out grinding, polishing and etching (with 2% Nital) procedures. Since the parent sample was bar shaped it was essential to look in to the microstructures in the rolled direction. The rolled direction is referred as the longitudinal direction and the direction perpendicular to that is referred as the cross direction (Figure 3.1). The average grain diameter was

measured according to ASTM E 112-13 standard. Average grain diameter in the longitudinal direction (rolling direction of the sample) and cross-sectional direction was 51 μm and 53 μm (Figure 3.1) respectively.

Average grain sizes of both directions of the reference sample were quite similar. Therefore, the sample can be considered as homogeneous with regard to microstructure.

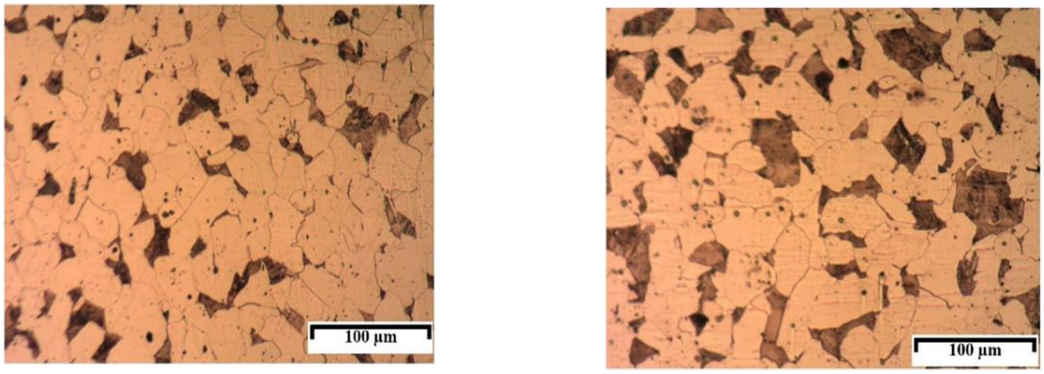

Longitudinal direction Cross direction

Figure 3. 1 : Optical images of the microstructures in the reference sample

3.1.2 Sample preparation

One of the main goals of this research is to correlate the ultrasound attenuation to the degree of corrosion. After establishing the relationship between these aspects/phenomena it will be possible to introduce a fully non-destructive method to measure corrosion that eliminates the need to remove samples from the testing component. However, in order to establish a non-destructive method, it was needed to verify the used technique using existing destructive methods. Therefore, we developed a methodology to test samples using both techniques. Samples were prepared accordingly under the following three categories.

Sample preparation for non-destructive analysis

Two factors were considered while selecting dimensions of the samples for ultrasonic testing specimens: near field value and beam spread angle.

Near field :

A piezoelectric transducer emits spherical ultrasonic waves into the medium. These spherical waves interfere with each other and gives rise to intensity regions of maxima and minima close to the transducer. This region is known as the near field region and it is usually not considered when taking readings. The length of near field can be calculated from the following equation (8):

$$N = \frac{D^2}{4\lambda} \qquad (8)$$

Where:

N : Near field length

D : Transducer diameter

λ : Wavelength

Considering this and the sample cost, the minimum length of the sample was established/estimated to be 16 mm

Beam Spread Angle :

There is always some spreading of the ultrasonic beam in the far field as the waves travel from the transducer. The intensity of the beam is a maximum on the central axis and decreases in proportion to the distance from the transducer. Therefore, the cross section of the sample was calculated keeping positive tolerance to the beam spread area at a distance of 16 mm. The beam spread was calculated using the following equation (9).

$$\text{Sin } \theta = 1.2\ (\lambda/D) \text{ or Sin } \theta = 1.2\ (V/DF) \quad (9)$$

Where:

V : Ultrasound longitudinal velocity is steel

D : Transducer Diameter

λ : Wavelength

F : Frequency of the probe

Beam spread half angle was 12.97^0

After considering above factors, it was decided to use 40 mm x 40 mm cross-section and 16 mm height samples to obtain ultrasound parameters. Three samples were tested per month while each sample was used to take nine readings.

Sample preparation for destructive analysis Weight Loss Per unit Area (WLPA) and the Corrosion Rate (CR) :

These samples were prepared to obtain the weight loss values due to the corrosion and the corrosion rate as a function of time. The procedure was followed in accordance with ISO 8407 international standard. The standard doesn't have constraints about the sample sizes and it is flexible for us to choose any dimension that is good enough to provide an accurate and significant weight loss value. After considering the above and the space in the corrosion chamber, it could finalize the sizes of the weight loss samples to be 10 mm x 10 mm x 6 mm as mentioned before (Figure 3.2). Three samples were tested to obtain each reading.

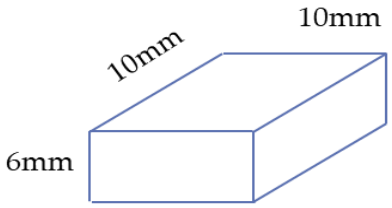

Figure 3. 2 : Sample dimensions for weight loss measurements

Samples to observe the microstructure and the penetration behavior of the corrosion :

To obtain an accurate and comprehensive value for the degree of corrosion it is essential to extract and add the impact of the corrosion penetrations. Hence samples were prepared in such a way that gives us the ability to observe the microstructure after corroding. To this end, the samples were subjected to both the optical imaging and SEM imaging. The same sample size used for the weight loss measurements were used for this as well. One sample was kept aside for each set of readings.

3.1.3 Periodic testing under accelerated corrosion

All the three sample sets; samples for ultrasound testing, samples for weight loss measurement and samples for microstructural analysis were periodically tested over 6 months. All of them were subjected to an accelerated corrosion environment in a salt spray chamber.

Accelerated corrosion

Acceleration of the corrosion has to be done due to the limitation of the time. Otherwise it would take more time to obtain a measurable and significant level of corrosion. a salt spray environment was used to accelerate the corrosion rate.

All the three types of specimens were placed in corrosion chamber. A wooden frame was prepared to keep the specimens as illustrated in Figure 3.3. One surface was kept free for exposure and other surfaces were covered with hard Greece to avoid corrosion.

Figure 3. 3 : Specimens inside the corrosion chamber

According to the ASTM B117-11 standard test, specimens were placed in a specified angle between 15º and 30º as shown in Figure 3.3. All specimens were placed away from each other without any contact to any metallic material or to any material which is capable of acting as a catalyst for corrosion. A gel and grease were applied in between the specimens to avoid the contact of specimens as well as to protect from corrosion. The salt solution which was used to form the fog inside the chamber was prepared by adding sodium chloride to the water. A 99% commercially available salt solution was kept 5% (w/w) as per the standard. pH level and temperature range (25 ^{0}C – 30 ^{0}C) were maintained within the ranges specified by the standard. The pressure in the chamber was 10 psi and humidity was 70-100%. The nozzle was placed to ensure that the spray was not directly focused on the test specimens. All the specimens were stenciled with a defined numbering system and the first set of samples were placed in the top of the set and the final specimen set was placed in the bottom. All the samples underwent the preliminary weight analysis and ultrasound testing prior to putting them in to the chamber.

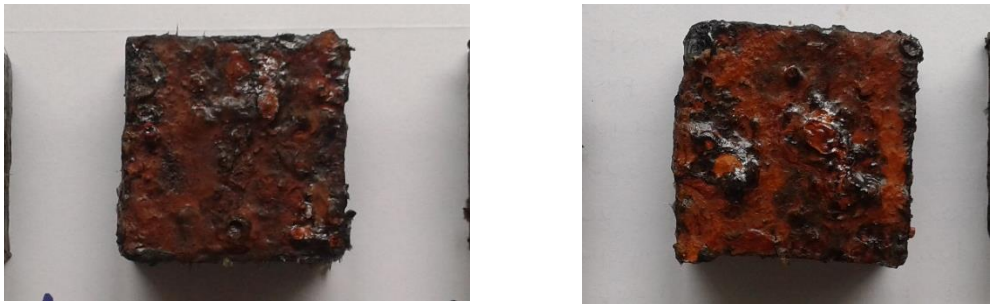

Figure 3. 4 : Two corroded samples after 992 h exposure

Nondestructive measurements:

Non-destructive testing samples were tested for ultrasonic attenuation using EPOCH 600-Ultrasonic Flaw Detector shown in Figure 3.5(a). The machine was used to measure ultrasound attenuation of the samples throughout the research.

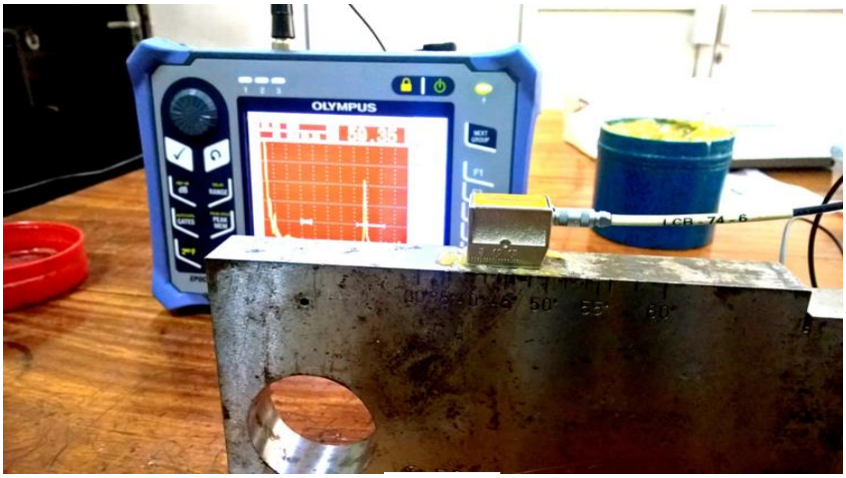

(a)

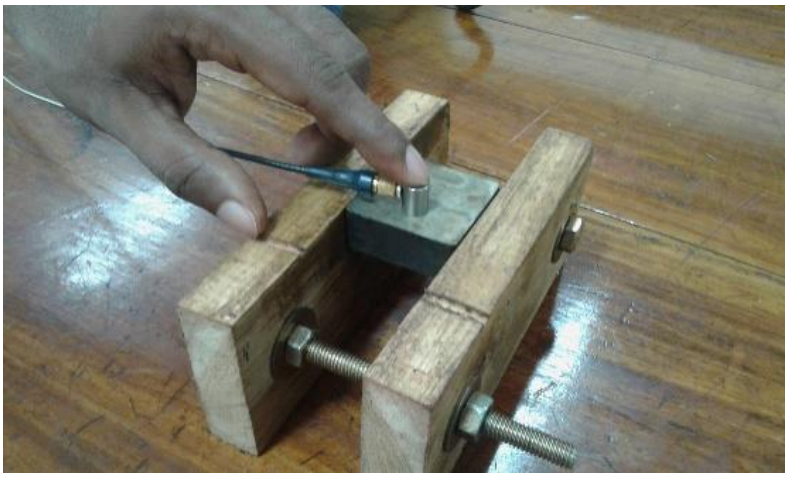

(b)

Figure 3. 5 : (a) EPOCH 600-Ultrasonic flaw detector

(b) Inspections under ultrasound with 5 MHz normal probe

Ultrasound attenuation measurements :

Attenuation is the energy loss due to certain properties of the material, while the energy is passing through it.Ultrasonic attenuation is the energy loss due to the scattering of the wave, absorption by the material and the spreading of the beam. In this case, the beam spread is a constant value since it only depends on the probe that we are using. But the

scattering and the absorption are directly affected by corrosion.

The attenuation was calculated by using following standard equations (10) and (11). 5 MHz normal probe was used throughout the research work (Direct method).

$$\text{Attenuation Coefficient} = \frac{\text{Total Attenuation}}{\text{Travel Distance of the wave}} \quad (10)$$

$$\text{Attenuation Coefficient} = \frac{\text{Gain of the } 4^{th} \text{ Echo - Gain of the } 2^{nd} \text{ Echo}}{16 \text{ mm x } 4} \quad (11)$$

The interface of the ultrasound machine is shown in the Figure 3.6. Second and fourth back wall echoes were taken for the calculations . The gain values of the second and the fourth back wall echoes were taken when they are in the 80% of the full screen height (Figure 3.6). By that the attenuation coefficient of the uncorroded reference samples were calculated prior keeping the samples inside the chamber.

First set of samples were taken from the chamber after 192 hours and measured the second and fourth echoes as per the above-mentioned method. The same procedure was carried after 360 hours, 528 hours, 688 hours, 840 hours and 992 hours. To observe the penetration behavior as a function of time samples were again subjected to ultrasound testing after corrosion removal (washing).

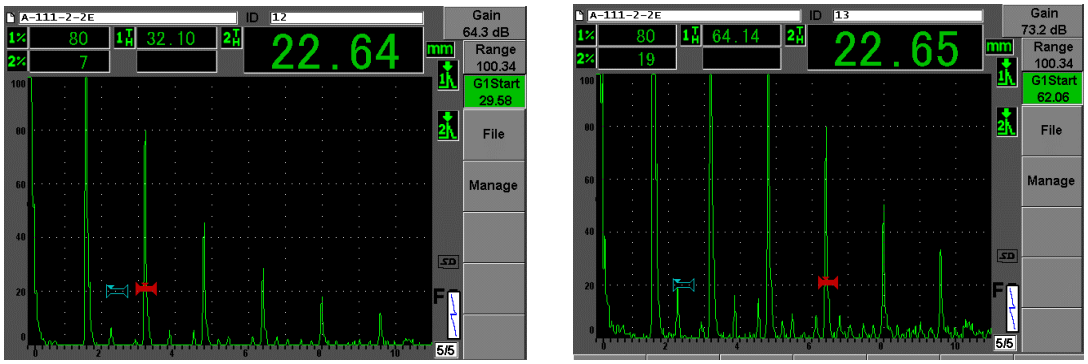

(a) (b)

Figure 3. 6 : Machine interface during ultrasonic attenuation measurements
(a) Second echo to 80 % gain (b) fourth echo to 80% gain

Destructive measurements :

Weight Loss Per unit Area (WLPA) :

ISO 8407:1991(E) standard was used to calculate the WLPA. These measurements were also taken from 6 mm x 10 mm x 6 mm samples. The initial weight of all the samples was measured prior to the accelerated corrosion. Three samples were taken out for each time period and the corrosion layers were removed using standard chemicals and the standard methodology (ISO 8407). Since the initial weights of the samples were known the weight loss due to corrosion can be calculated after removing corrosion layers and measuring the samples.

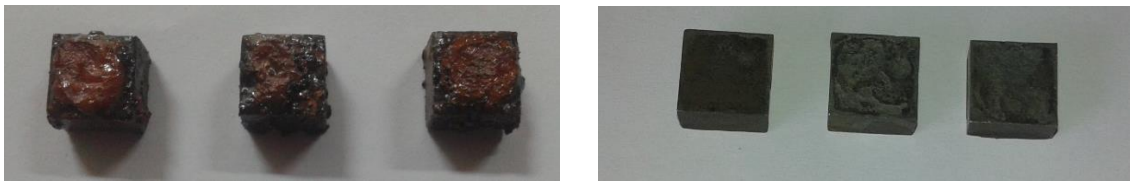

Figure 3. 7 : Weight loss samples before and after the washing of corrosion

In order to analyse the weight loss, the corrosion products formed on the surface of the specimens had to be cleaned. The method of removal could be mechanical, chemical or electrolytic. Chemical removal was chosen because it provides the best balance of economy and accuracy.

The details of the technique is outlined below

- Standard Employed : ISO 8407
- System Designation : C.3.1
- Chemicals Used : 1000 ml HCl (ρ=1.19 g/ml)
  (per 1000 ml) : 20 g Sb_2O_3
  : 50 g $SnCl_2$
- Temperature : Room Temperature
- Time of Washing : 15 – 25 minutes

The weight loss specimens were washed using the recommended solution in accordance with the stated parameters. Afterwards the relevant mass was recorded and the percentage loss calculated. The calculated and analyzed values of Weight Loss Per Area and the Corrosion Rate will be discussed in results and discussion chapter (Chapter 4).

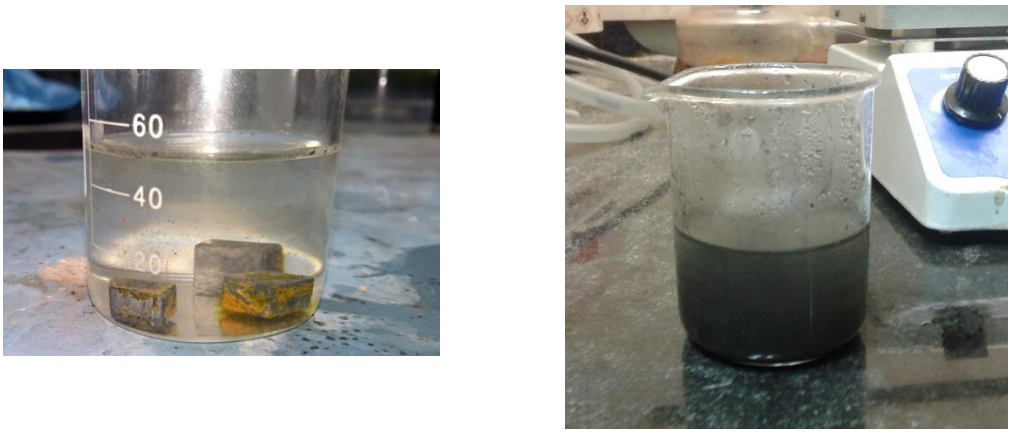

Figure 3. 8 : Corrosion removal with the chemical solution

Microstructural observations :

Weight loss is the most widely used parameter in the industry to estimate and predict corrosion behavior of a structure. But in order to get a complete idea about the accuracy of that parameter, microscopic analysis was carried out on the corroded samples.

Samples had to be prepared for microscopic examination to verify and measure the general corrosion and the penetration of corrosion beyond the general attack. The final sample was prepared in such a way that the SEM would be able to view the mounted steel samples at a high resolution.

The samples were prepared for microscopic analysis under following steps. First a cross-section of the chosen specimen was carefully removed using a precision cutter (Figure 3.9) while making sure not to flake off any corrosion products during the cutting process. But due to the adhesion of the lubricant from the precision cutter onto the cut sample, it had to be washed. This was performed by immersing the cut section in ethyl alcohol until the lubricant was removed. Then sample was dried and placed on the stage of the mounting press where the appropriate amount of Bakelite powder was poured.

Next press is tightened to apply mounting pressure and the sample was ready for grinding after applying heat and pressure.

The mounted sample was then subjected to a full grinding cycle with perpendicular switches of grinding orientations between the wet grinding papers. All four papers were used from coarsest to finest finish: 1200, 600, 400 and 240 grading. Then the sample was polished to a mirror finish using a water-based diamond suspension (5-micron size) on polishing fabrics for approximately 20 minutes. Optionally, depending on the features to be observed, the sample would then be etched with a 2% Nital solution.

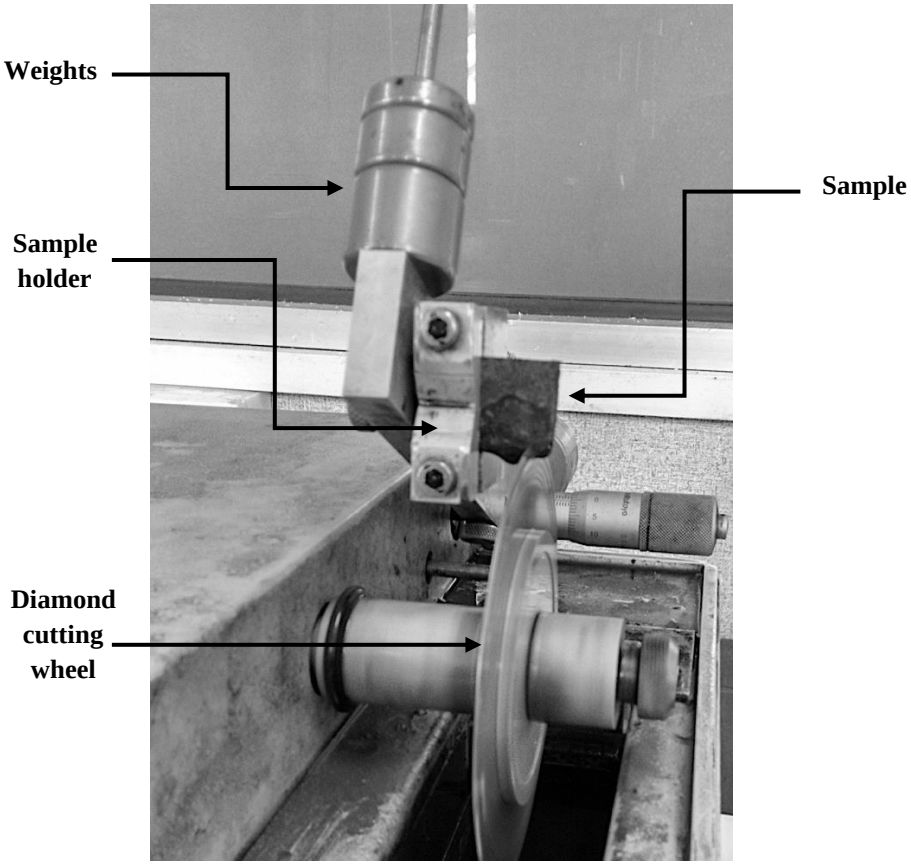

Figure 3. 9 : Precision cutting instrument in operation

Figure 3. 10 : Samples for microstructure observation after cutting and mounting

After sample preparation they were checked under the optical microscope. Optical microscopy was used as a preliminary analytical tool in order to observe the general layer and identify potential regions of interest which could then be studied extensively under the SEM. Optical microscopy, however, is not good enough to investigate pits/penetrations due to the magnifying constraints. Figure 3.11 shows an image obtained from the optical microscope, displaying the interface between the virgin steel, the general corrosion layer and the mounting polymer.

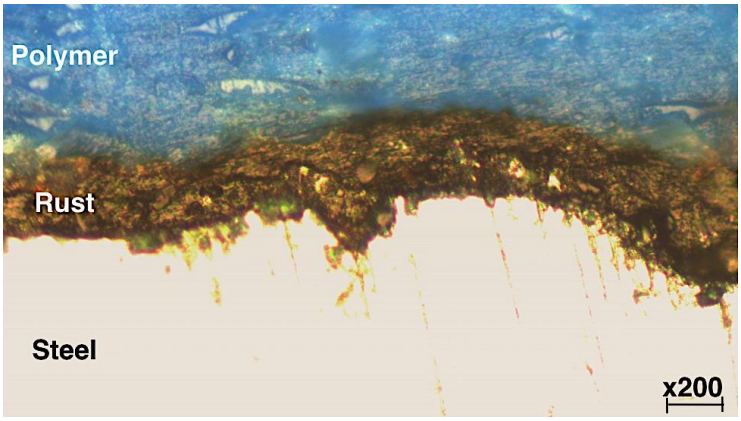

Figure 3. 11 : Optical microscope image showing the metal-corrosion interface

Following the observations under optical microscope, the sample was studied under the SEM for further investigations. It was used as a measuring instrument and also as an analytical instrument (to characterise corrosion) using EDS.

The details of the SEM and the average working conditions are listed below.

- Instrument : Carl Zeiss Evo 18 Research
- Normal Working Distance : 8 – 12 mm
- Operating Voltage Used : 20 kV

Samples were analysed at the minimum magnification (x48) to confirm the presence of sites located through the optical microscope. Sites of corrosion penetration were located and a clear image was obtained at a magnification that could encompass the entire penetration depth. This image was subjected to EDS analysis to verify that the feature observed was indeed a penetration of corrosion into the steel (Figure 3.12 (b)). In an area of penetration corrosion, it was expected to find traces of Magnetite (Fe_3O_4), Hematite (Fe_2O_3), and Iron Hydroxides which are compounds of oxygen. EDS provides the capability to identify and map the elements in different colour maps (Figure 3.12 (b)). For example, green colour denotes oxygen in EDS which can be used to identify the presence of oxygen and study the penetrations. Then the depths of the features were also measured. These measurements were entered into data tables.

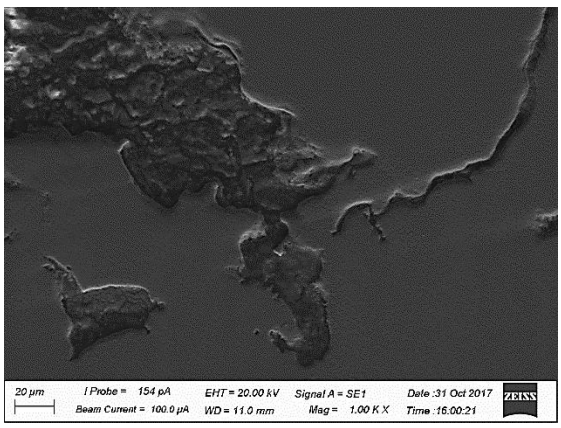

(a)

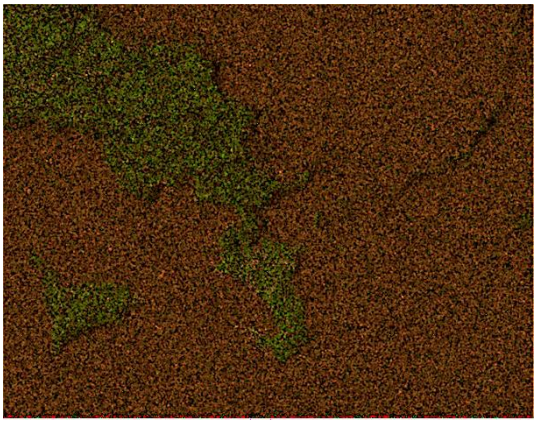

(b)

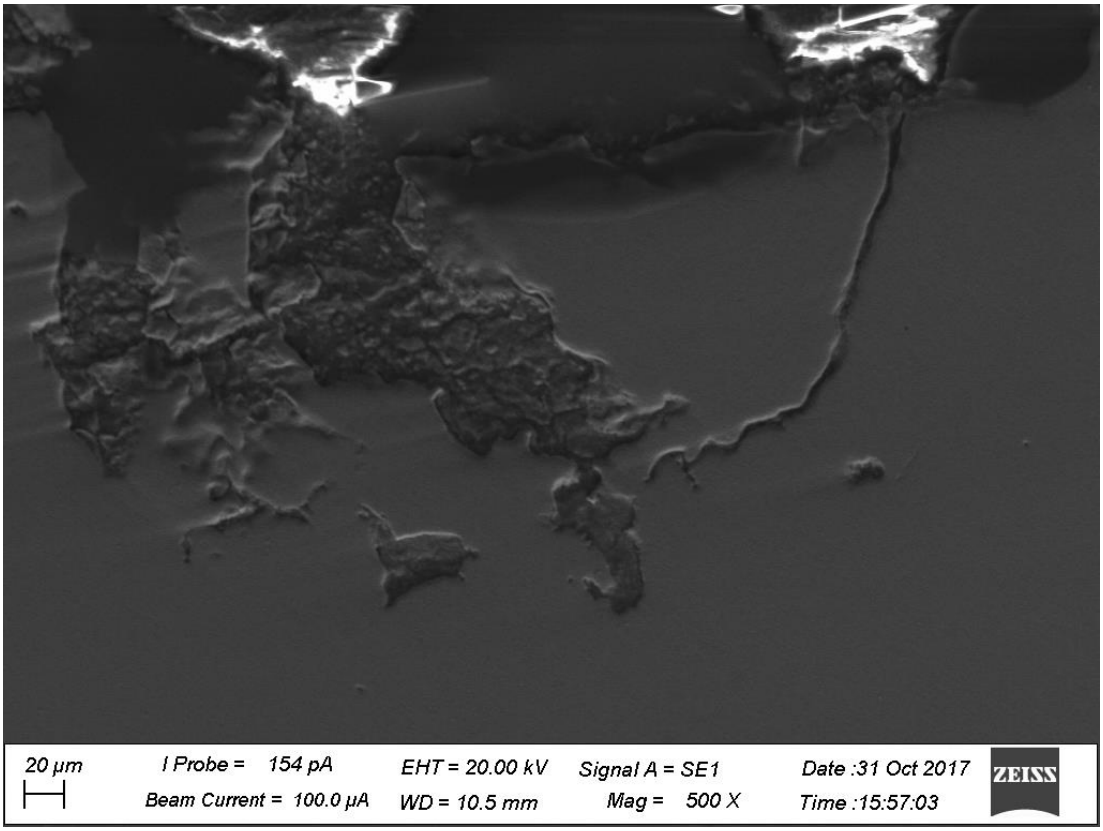

Figure 3. 12 : Identification and verification of penetration of corrosion using SEM; a) Secondary Electron mode and b) EDS elemental mapping (O in green, Fe in red)

After methodically completing the process steps and analyzing the results relationships were developed between the degree of corrosion and ultrasound attenuation that is discussed in the next chapter. However, since it is known that the attenuation (thus the attenuation coefficient) is dependent on the grain size and the impurity content (mainly the carbon content), this developed relationship is only valid for a particular material type with a given grain size. Therefore, to derive a universal relationship two correction factors have to be introduced in to the developed equation. In order to obtain a more comprehensive understanding this study was further extended to evaluate the effects of grain size and the carbon content on the attenuation of ultrasound waves in steel samples.

3.2 Experiments for the correction factors

3.2.1 Carbon content

Carbon is the main constituent in plain carbon steel which mainly affects the attenuation. To develop the correlation between the degree of corrosion and the ultrasound attenuation a steel sample with the following chemical composition was used (base composition as mentioned in the previous section).

Table 3. 2 : Composition of the base/reference steel

C%	Si%	Mn%	Cu%	P%	S%	Cr%	Ni%	Al%	Fe%
0.28	0.26	0.53	0.04	0.02	0.02	0.11	0.03	0.01	~98.6

To find the effect of carbon, three different compositions were used in this experiment. Compositions are given in Table 3.3. Since carbon is the major impurity (Mn, Si,P contents at the minimum ranges and nearly the same in every sample), it was tried to keep the amount of other impurities equal among the samples so that the influence due to the other impurities on ultrasound attenuation would be considered to be similar. The carbon percentage of the sample ranges from 0.21 – 0.53; therefore, the series represents

a section of low carbon steel and a section of medium carbon steel. It was very difficult to go beyond a carbon content of 0.53 % since steel becomes alloyed steel as the carbon composition increases. Therefore, the search for high carbon plain steels in the market was not successful. 0.26 % carbon steel was used for the validation of the developed relationship.

Table 3. 3 : Compositions of steel samples used for the experiment

C%	Si%	Mn%	Cu%	P%	S%	Cr%	Ni%	Al%	Fe%
0.21	0.22	0.59	0.01	0.07	0.03	0.01	<0.003	<0.002	~98.8
0.42	0.18	0.58	0.09	0.03	0.01	0.02	0.003	0.03	~98.4
0.53	0.24	0.65	0.12	0.03	0.04	0.12	0.05	0.01	~98.1

To analyze the effect of the carbon content, the other factor – the influence of the grain size - should be kept constant. Therefore, the grain sizes of the above three sample sets were brought to the same level of the base composition by heat treatment.

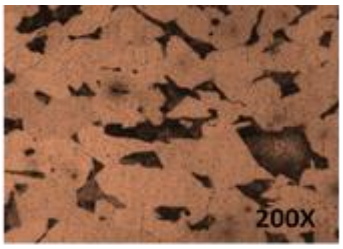

0.21% plain carbon steel

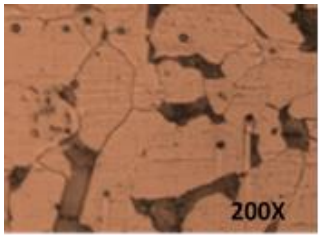

0.28% plain carbon steel

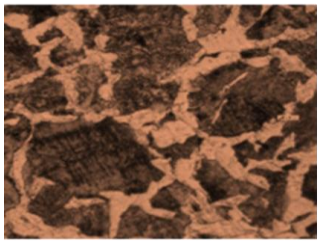

0.42% plain carbon steel

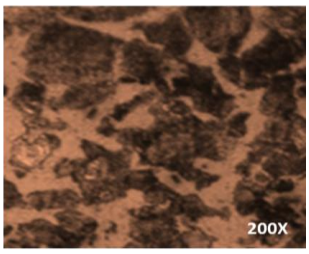

0.53% plain carbon steel

Figure 3. 13 : Optical microscopic images of the expermented steel samples -200X

The average grain diameters of the above sample sets are given in the Table 3.4.

Table 3. 4: Initial grain diameters of the steel samples

Carbon Content (%)	Average Grain Diameter (Area Method /mm)	Standard Deviation
0.21	0.049	0.0015
0.28	0.051	0.0012
0.42	0.052	0.0013
0.53	0.050	0.0015

After making the grain sizes equal for all the samples the impact of grain structure on attenuation is equivalent. Therefore, it was possible to check the effect of carbon content on attenuation independent of grain size. To this end, the same methodology that has outlined for the base composition was followed on other three types of carbon compositions.

The accelerated corrosion was achieved under the same conditions. The nondestructive analysis was followed using the same machine, same standards and the methodologies. Under the destructive analysis, Weight Loss Per unit Area was calculated using the same steps discussed before. The microstructural analysis was also carried out for each set of samples for each time domain.

Results were analyzed and how those results would be used to add as a correction factor will be discussed in the next chapter.

3.2.2 Grain size

Size of the grain is the other vital factor that affects the attenuation of ultrasound waves in steel samples. To understand the effect of the grain sizes, a range of grain sizes with the same base composition were subjected to this experiment. As discussed above, the base sample has 0.28 of carbon percentage and the microstructure was varied after treating the sample with heat under controlled conditions.

Sample preparation

The dimensions of the material should be large enough to avoid near field effect of the probe and the beam spread as mentioned in the section 3.2.2.Therefore, in order to be consistent, the same sample size was taken for all the samples.

Heat treatment process

The original grain size which was in the purchased sample was kept as the initial grain size, which was 0.0051 mm in average. Starting from that point, the heat treatment cycles were designed to achieve different grain sizes/structures in the five sets. Prior to the designing of the heat treatment cycles the materials capability on the rate of heat transfer has be understood well. Basically, the combination of the minimum temperature and the minimum soaking time, which would provide the allow to transfer the heat uniformly through out the sample should be practically identified. Otherwise, the center of the material would not be able to grow the grains homogeneously. After trials it could be found that keeping 980 ^{0}C for 40 minutes was the minimum setting to achieve the homogeneous grain growth throughout the sample. It was ensured by observing the microstructure and measuring the grain sizes on the surface and inside the sample in the depths o f 3 mm, 6 mm, 9 mm, 12 mm, 15 mm and 19 mm (depths are measured from

surface). The slicing of the samples for the observations was done as shown in the Figure 3.14.

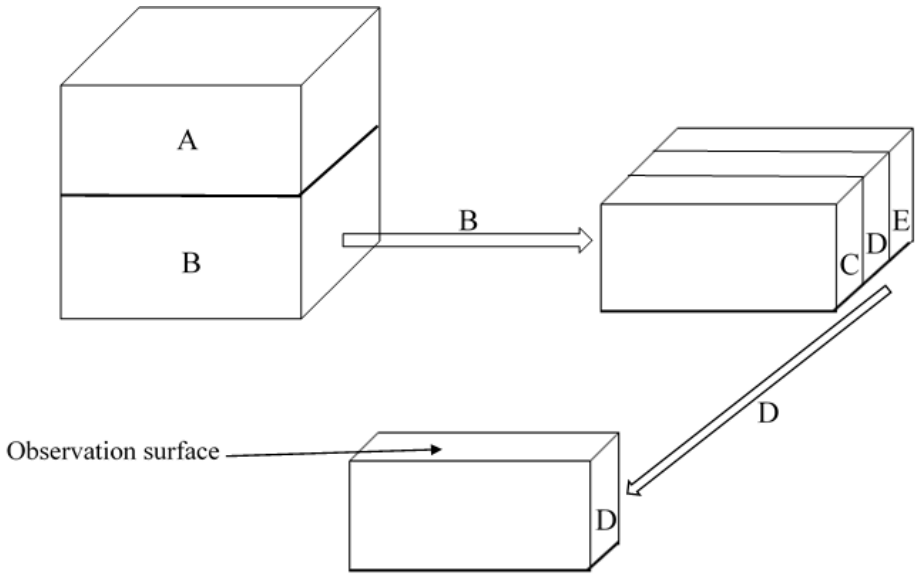

Figure 3. 14 : Slicing of the sample

The microstructures were observed after slicing at the decided depths. All the microstructures are shown in the Figure 3.15 .

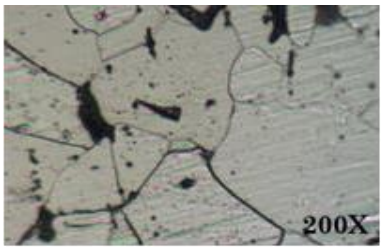

Surfac

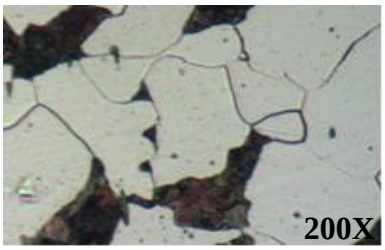

At a 3 mm depth from
the surface

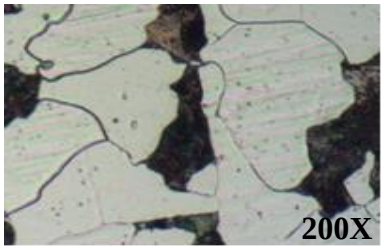

At a 6 mm depth from
the surface

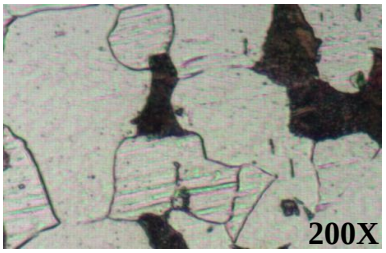

At a 9 mm depth from
the surface

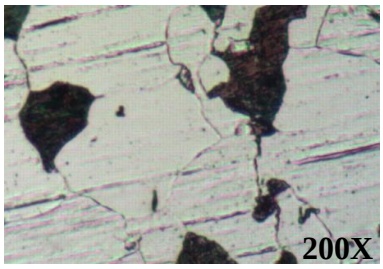

At a 12 mm depth from
the surface

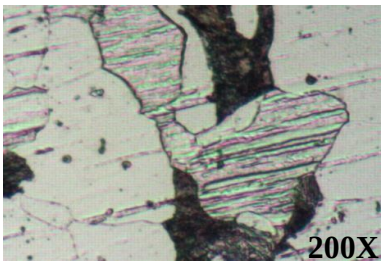

At a 15 mm depth from
the surface

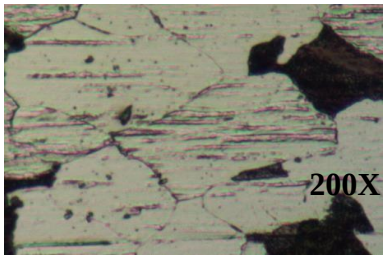

At a 19 mm depth from
the surface

Figure 3. 15 : Microstructures after the heat treatment at decided depths

The dimensions of the grains were extracted/measured using the liner intercept method. They are given in the Table 3.5.

Table 3. 5 : Grain sizes at various depths after the minimum setting of heat treatment

Distance from surface (mm)	0	3	6	9	12	15	19
Average value of grain diameter (mm)	0.117	0.119	0.120	0.115	0.117	0.117	0.116

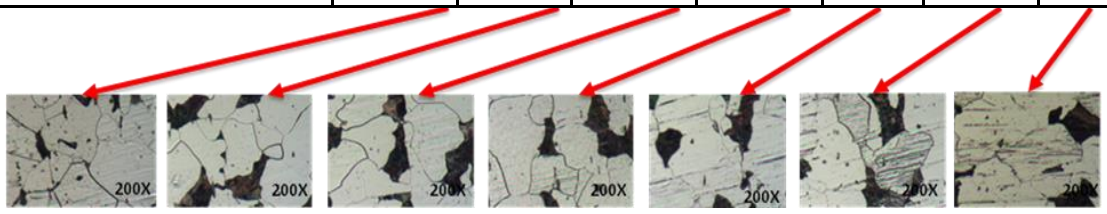

The standard deviation of the above results is 0.0057. Given this small variation it can be assumed that the temperature at the surface and at the center of the sample cube was equal and the grain growth would be homogenous for the heat treatments beyond the above-mentioned minimum settings (980 ^{0}C temperature and the 40 minutes soaking time).

After finalizing the minimum settings, the other heat treatment cycles were designed accordingly (based on the minimum setting). The following equation (12) was used to understand the relationship between the soaking time and the microstructure (grain size).

$$D^2 - D_0^2 = Kt \quad (12)$$

Where,

D - Actual grain size after the heat treatment

D_0 - Initial grin size

K is the proportionality constant that depends on absolute heating temperature, and activation energy. t is holding time at the heating temperature.

Soaking times were calculated according to the above equation to get a series of average grain sizes as given in the Table 3.6. Initial grain size of the reference sample was taken as the lower limit of the grain size series.

Table 3. 6: Average grain sizes in different soaking times for 0.28 % C steel

Soaking time	**Avg Grain Size (mm)**
References	0.052
40min	0.117
1hr	0.150
2hr52min	0.180
4hr25min	0.196
6hr10min	0.210

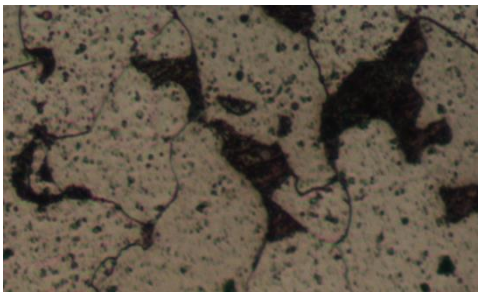

40 min soaking

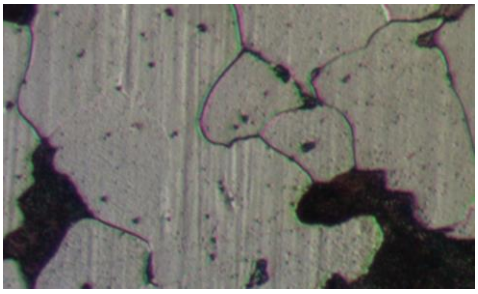

1 hour soaking

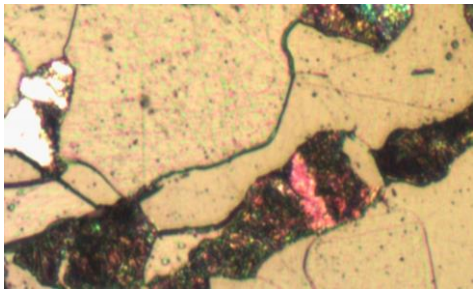

2 h 52 min soaking

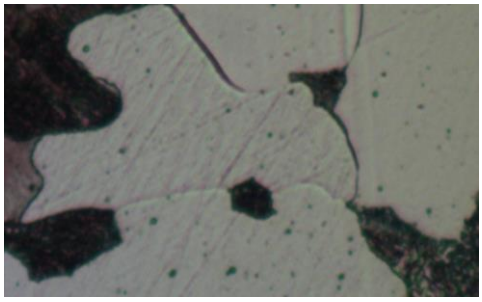

4 h 25 min soaking

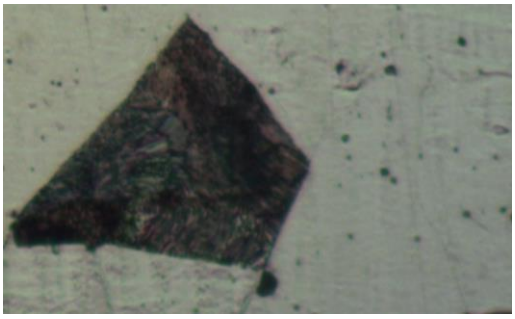

6 h 10 min

Figure 3. 16 : Microstructures in different soaking times

After completing the sample preparation, ultrasound attenuation measurements were taken from each sample set (9 readings from 3 samples per each grain size). The results were analyzed and used to introduce a correction factor in to the main correlation.

3.3 Establishing a relationship between the load bearing capacity and the degree of corrosion

Corrosion degrades the material. In previous sections the degree of the corrosion and its effect on attenuation coefficient of the ultrasound waves, are discussed. In addition, it is also important to understand and asses how the corrosion degradation effects the mechanical properties of steel. It is obvious that as mechanical properties get weaker, structures are more susceptible to failures, that can be catastrophic in some cases.

After considering the failure effects on the structures the scope of this research was further extended to evaluate the mechanical properties of corroded steel as well. Tensile strength (load bearing capacity under tension) is one of the main and important properties which is frequently tested in most of the structural components. Therefore, it is of utmost importance to understand the impact of corrosion on tensile strength and gain knowledge to predict tensile strength using ultrasound waves as an accurate and reliable non-destructive technology. An evaluation regarding the affect of corrosion on the tensile strength, accuracy and the reliability of the present industrial method and the benefit of ultrasound predictions are to be analyzed based on the methodology mentioned in this section.

The steel samples placed in an aggressive atmosphere (approximately over 840 hours) and subjected those to periodic tensile testing and corrosion mass-loss (weight loss per unit area) analysis. Also the samples were examined under optical and scanning electron microscopy to observe the penetration behavior of the corrosion layers. All the procedures are given below in this section.

3.3.1 Sample selection and preparation

Specimen used for tensile testing is usually machined from a sheet material or might be cylindrical. Depending on the specifications followed by the tensile testing machine in the Materials Science department, it was decided to use sheet material (steel in the range of low carbon) and to machine flat samples. After taking in to account the time duration of corrosion in an accelerated environment, it was decided to use samples with 4 mm thickness for this experiment. After inquiring for samples in the selected thickness range, decided to use low carbon range sheets since they were readily available in the market. After purchasing, samples were duly prepared and tested.

Samples were prepared under three sets; one for corrosion weight loss (mass–loss) analysis, another for microstructural analysis and the last for tensile testing. They were machined from the same steel plate for accurate cross-relation of results after corrosion. The weight loss specimens had cross sections of 30 mm x 30 mm and thicknesses of 4 mm. The tensile specimens were machined in accordance with dimensions given in the British Standard BS EN 10002-1:2001. Figure 3.17 represents the tensile specimen.

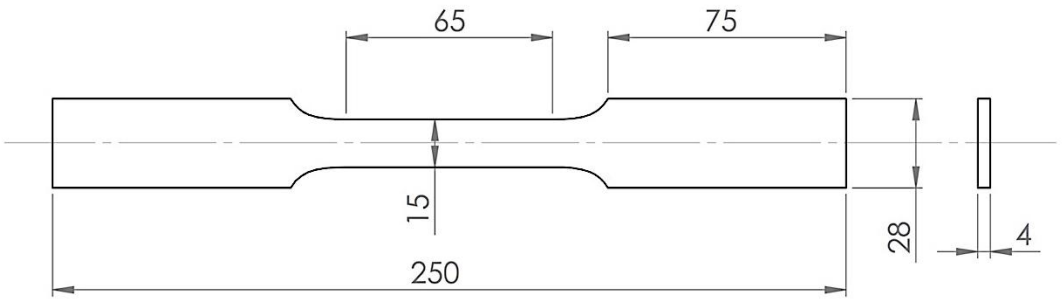

Figure 3. 17 : Plan view of tensile specimen (measurements in mm)

Figure 3. 18 : Tensile specimen

After preparation, specimens were coded based on the duration of corrosion. This way sample removal and subsequent testing could be studied appropriately based on their corrosion duration in the aggressive environment. All specimens were cleaned, weighed, measured thickness and width and subsequently placed in the corrosion chamber.

3.3.2 Accelerated corrosion

The same accelerated corrosion environment was used for these two sample sets as well. During placement in the chamber, samples were aligned at an angle (30^0 according to the standard), to reduce/eliminate pitting corrosion due to local salt-water stagnation. Figure 3.19 shows the arrangement employed for tensile testing specimens. To achieve uniform corrosion among all samples, all specimens were flipped (top to bottom and side to side) once every two weeks.

Figure 3. 19 : Tensile specimen in side the corrosion chamber

The testing required for the reference samples were completed in the initial stage and tensile, weight loss and microstructure samples were taken out for testing at increasing time intervals: 192 hours, 360 hours, 528 hours, 688 hours and 840 hours.

3.3.3 Tensile testing

After taking samples out from the accelerated environment, tensile testing was performed on corroded specimens. Reference (stock) specimens were tested initially to establish an average material strength that could then be used in later residual strength calculations. For every sample set inside the corrosion chamber, 4 samples were tested for their residual strength. The particulars of the equipment and the process are given below:

- Instrument : Universal Tensile Testing Machine (100S-0147)
- Max. Load Rating : 50 kN
- Clamping : Manual
- Rate of Extension : 30 mm/minute
- Standard Employed : BS EN 10002-1:2001

In order to prevent slippage at the clamp the shoulder of the sample had to be filed to remove the corrosion products. Prior to the tensile test being carried out, the gauge length of the specimens was marked. The breaking load was provided on screen. The extension was calculated manually using the gauge length before and after testing. The specimens were then relabeled and placed in the desiccators.

3.3.4 Weight loss analysis

The same procedure described in section 3.2.3. was used to perform the weight loss analysis.

In order to compare and verify that the weight loss specimens and the tensile specimens provide the same corrosion weight loss readings, samples of the latter were subjected to chemical corrosion removal process for the first three months. Based on the readings it could be concluded that the results were homogenous enough to obtain the weight loss readings from the designated samples as valid for the tensile sample set as well.

3.3.5 Microstructure analysis

The microstructural samples were cleaned prior to observations using the previously mentioned cleaning procedure. Then they were subjected to the same observation procedures under optical, SEM and EDS as discussed under microstructural observations in section 3.2.3.

The above sections outline all the methodologies followed in this research. In addition to the above experiments two other experiments were run to verify the obtained relationships and to identify the effect the corrosion penetrations on the fatigue strength on steel. These experiments will be discussed in the next chapters (Results and Discussion & Further Improvements) in detail.

3.3.6 Fatigue Experiments

The experiments were done regarding the fatigue strength under the area of mechanical properties of steels in corrosive environment.

Some experiments up to a certain extent were carried under this area and it is briefly described below. Main focus was to determine the effect of corrosion on fatigue life of steel. Jaap Schijve has said “In the crack initiation period, fatigue is a material surface phenomenon [45]. Corrosion penetrations/pits effects for the initiations of the cracks and also their depth, geometry and the distribution also matter.

To study regarding this phenomenon, first experimental fatigue testing and the measurements of the degree of corrosion were done. Then the topographical reconstruction of corrosion surfaces were developed using a 3D surface constructing software - MountainsMap®. The developed topology of the surface was used to model the pit geometries in corroded specimen and Finite Element Modelling was used to model the pits in the samples. Those were subjected to and fe-safe fatigue analysis. The experimental and the modeled values were compared then.

For the experiments AISI 1005 low carbon steel was selected with the thickness of 0.9 mm (the thickness which is allowable for the fatigue machine). 6 samples were tested per each set of experiment.

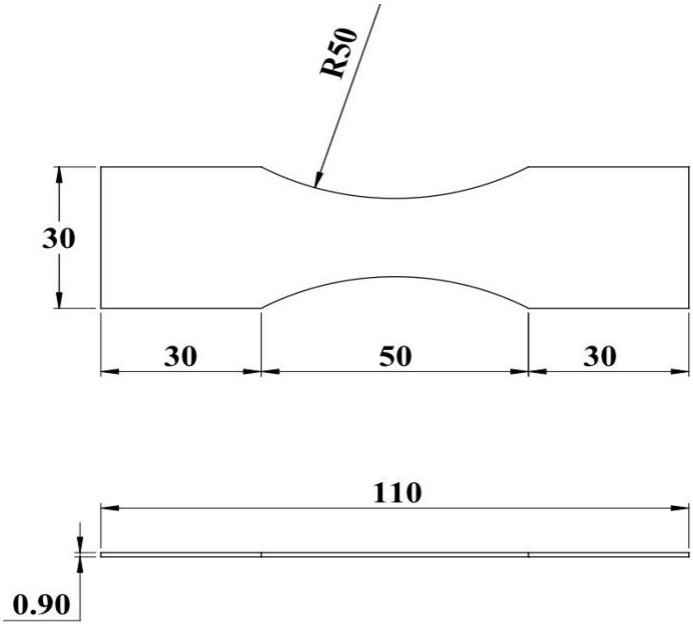

Figure 3. 20 : Fatigue specimen

Initially samples were kept in the same corrosion environment which the other sample sets were kept. But it was not successful since the sample was too thin (0.9 mm) and that thickness was not sufficient enough to keep for the required time period. They were pierced after around 192 h. Since the thickness of the sample is a constraint of the fatigue machine, the alternative solution was taken as to change the corrosive environment. The corrosion environment was change to atmospheric conditions which is under the category C4-C5 (according to the environmental categories – (Table 4.1).

Table 3. 7 : Environmental categories under C4 – C5

ISO 12944	Impact	Interior	Exterior
C3	Middle	Buildings for production with high atmospheric humidity and some air	Urban and industrial areas, moderate sulphur dioxide

		pollution such as food manufacturers, breweries, dairies and laundries.	pollution. Coastal areas with low salt content.
C4	High	Chemical manufacturers, swimming baths and ship- and boatyards by the sea.	Industrial areas and coastal areas with moderate salt impact.

High cycle fatigue (> 10^4 cycles) experiments were carried out.

(a) (b)

Figure 3. 21 : samples – placed in Angulana coastal area (a) initial conditions (b) after one week

Figure 3.21 shows how the samples were placed in the Angulana coastal area. The samples were flipped in every one week time to equalize the exposure of the samples to the wind direction.

Figure 3. 22 : Even corrosion in environmental conditions

Samples were taken in two weeks duration.

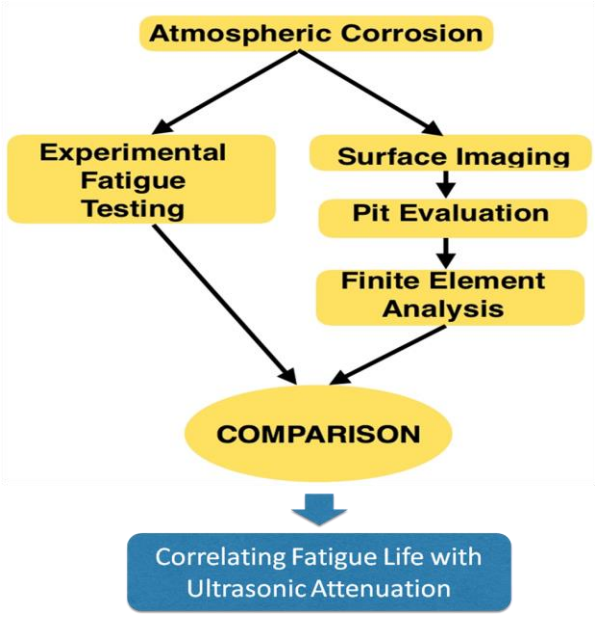

Figure 3. 23: Methodology for the fatigue analysis

Figure 3.23 shows the procedure followed to conduct the fatigue analysis.

Figure 3. 24: Shimadzu UF-15 fatigue machine

- Type of Fatigue : 4 point bending
- Mean Stress : 0 MPa
- Cyclic Stress : 236MPa- 260MPa
- Frequency : 30 Hz

4 RESULTS AND DISCUSSION

In this chapter all the results obtained from experiments and the findings will be accumulated, analyzed and discussed. The steps which were followed to obtain the final relationship and the validation are also outlined in detail. The experiments and results are presented and discussed in different sub-sections here. Finally, all of them were combined to develop the final equations. The results are presented in the same order as the experimental methodology presented in chapter 3.

4.1 Establishing a relationship between the degree of corrosion and ultrasonic attenuation coefficient

The results related to this section are the basis of this research. The main step is the establishment of the correlation between the degree of corrosion and the ultrasonic attenuation coefficient for 0.21% C,0.28% C, 0.42% C and 0.53% C composition steels.

The steel samples for destructive and non destructive testing were kept in the corrosive environment for 992 hours period.

4.1.1 Weight Loss Per unit Area (WLPA)

Weight loss measurements were taken in accordance with the ISO 8407 standard and the calculated Weight Loss per unit Area was plotted as shown in the Figure 4.1.

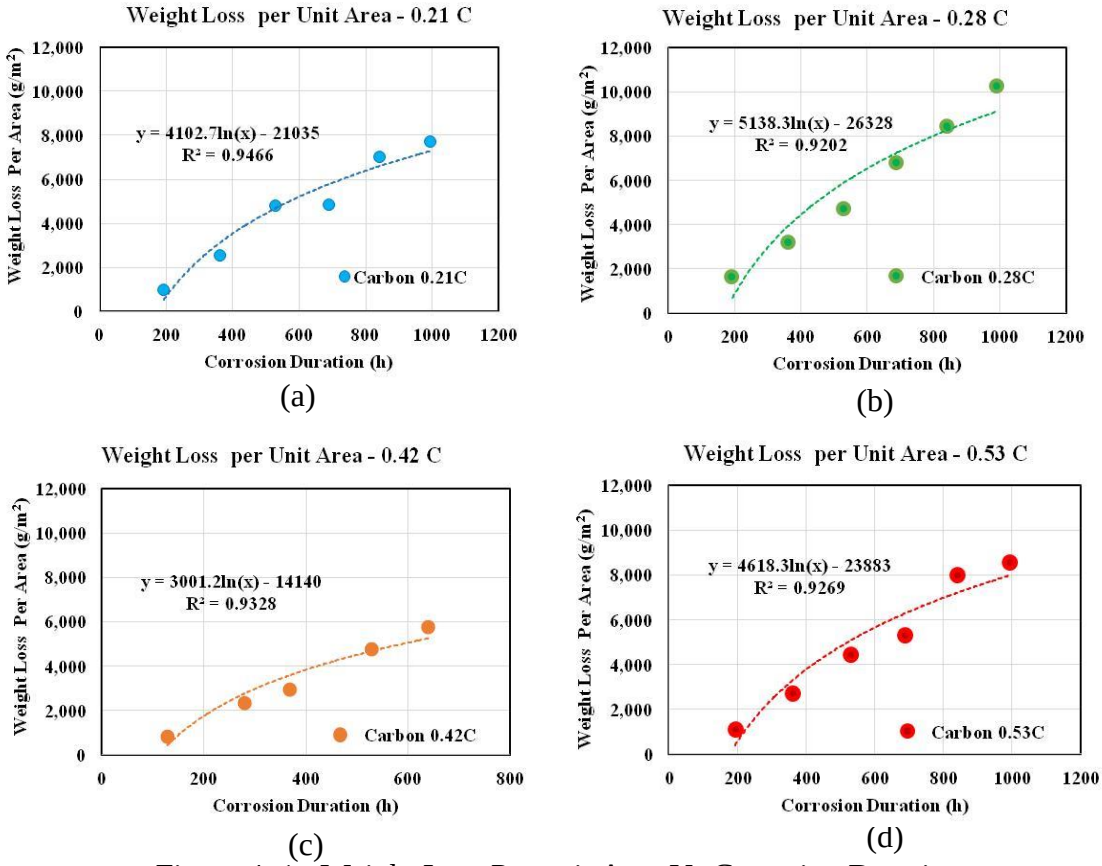

Figure 4. 1 : Weight Loss Per unit Area Vs Corrosion Duration

(a) 0.21% C (b) 0.28% C (c) 0.42% C (d) 0.53% C

The fits are logarithmic relationships. Normally logarithmic relationships present decremented increments. According to the theory, the surface corrosion rates of metals are also increasing with a function of time, but in a decreasing manner. This is due to the passivation layers created by corrosion. Metals need oxygen to oxidize. But as the oxidized layers are formed on top of the metal, they prevent the diffusion of oxygen into the healthy metal through the layers which in effect reduces the corrosion rate. This behavior is shown by the all compositions. For the readings see Appendix I).

(It was not possible to obtain 992 h reading for steel sample with 0.42% C composition due to the limitations in the sample availability.)

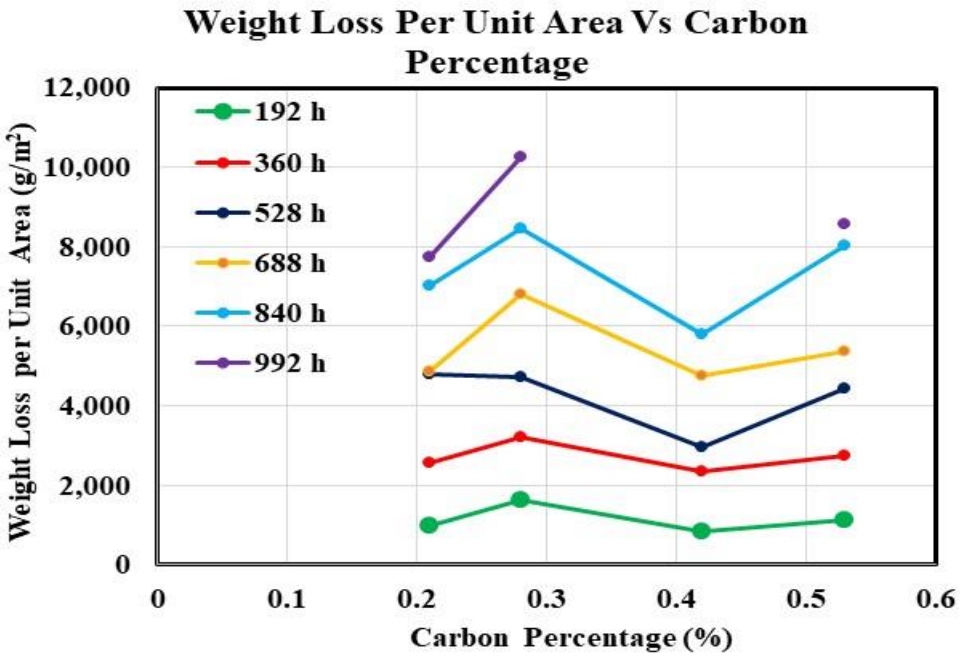

Figure 4. 2 : Weight loss per unit area vs carbon content for 192 h, 360 h, 528 h, 688 h, 840 h and 992 h

Figure 4.2 shows the behavior of WLPA as a function of carbon percentage which shows a non-linear pattern for different corrosion times. WLPA is directly proportional to the extent of corrosion. It was a novel observation; the degree of the weight loss is a maximum at 0.28 % of carbon.

A separate analysis with a focus on steel morphology and carbon content was conducted to understand the reasons behind this observation. Steel consists of two phases, ferrite and iron carbide (cementite - Fe_3C). In steels up to 0.8% C, the microstructure is formed of ferrite phase and a combined form of ferrite and cementite, which is referred to as pearlite (cementite and ferrite is arranged in a lamellar structure). Higher carbon percentages form more pearlite. Table 4.1 provides details regarding ferrite to pearlite ratio for the samples used in this study.

Table 4. 1: Ferrite pearlite fractions of the tested samples

C %	Ferrite %	Pearlite %	Ferrite: Pearlite
0.21	75.64	24.36	3.11
0.28	66.67	33.33	2.00
0.42	48.72	51.28	0.95
0.53	34.62	65.38	0.53

Ferrite and pearlite both are responsible for corrosion in steel. In literatures it is clearly shown that ferrite improves the general corrosion and pearlite leads for the corrosion penetrations since its lamellar layers can induce the galvanic nature [2]. Therefore, following those findings, it can be concleded that total corrosion behavior of plain carbon steels is a combined effect of ferrite and pearlite. From the results it can be identified that the optimum ferrite to pearlite ratio is 2.00 which gives rise the maximum extent of corrosion (for the given composition range). Therefore, the degree of corrosion does not simply improve with the carbon content as it depends on the ratio between ferrite and pearlite microstructure.

The plot of Figure 4.3 provides the evidences for the above conclusion. The WLPA shows a maximum value when ferrite to pearlite ratio is 2.

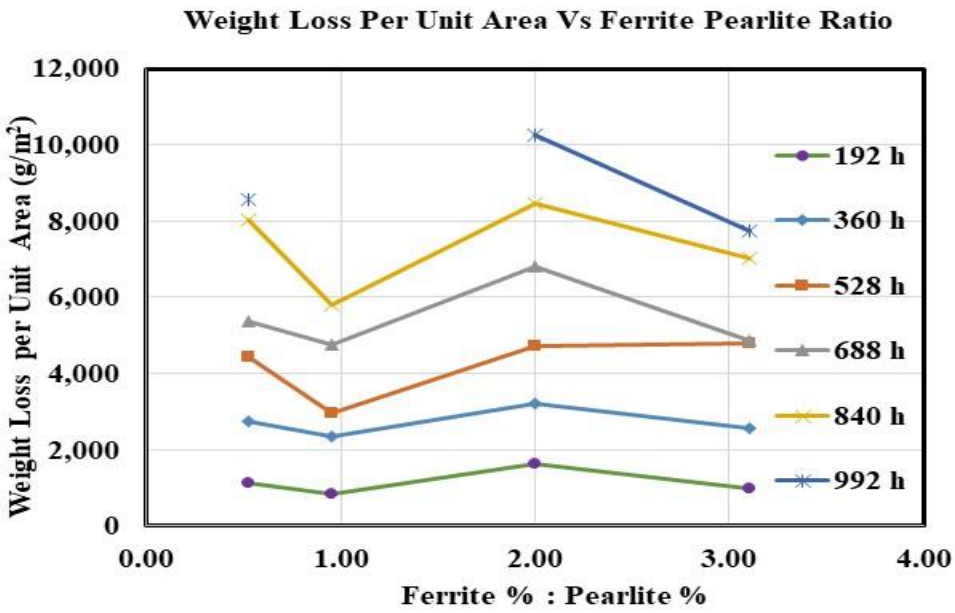

Figure 4. 3 : Variation of WLPA Vs Ferrite to Pearlite

4.1.2 Corrosion rate (CR)

Corrosion rate was calculated using the equation (13).

$$\text{Corrosion Rate} = \frac{87.6 * W}{D * A * T} \qquad (13)$$

Where; W = weight loss /mg

D = density of steel /g/cm^3

A = total area of corrosion /cm^2

T = corrosion time / hours

Rate of corrosion is also a measurement which gives a better understanding regarding the degree of corrosion. The corrosion rates for 0.21% C, 0.28% C, 0.42% C and 0.53% C are shown in the Figure 4.4.

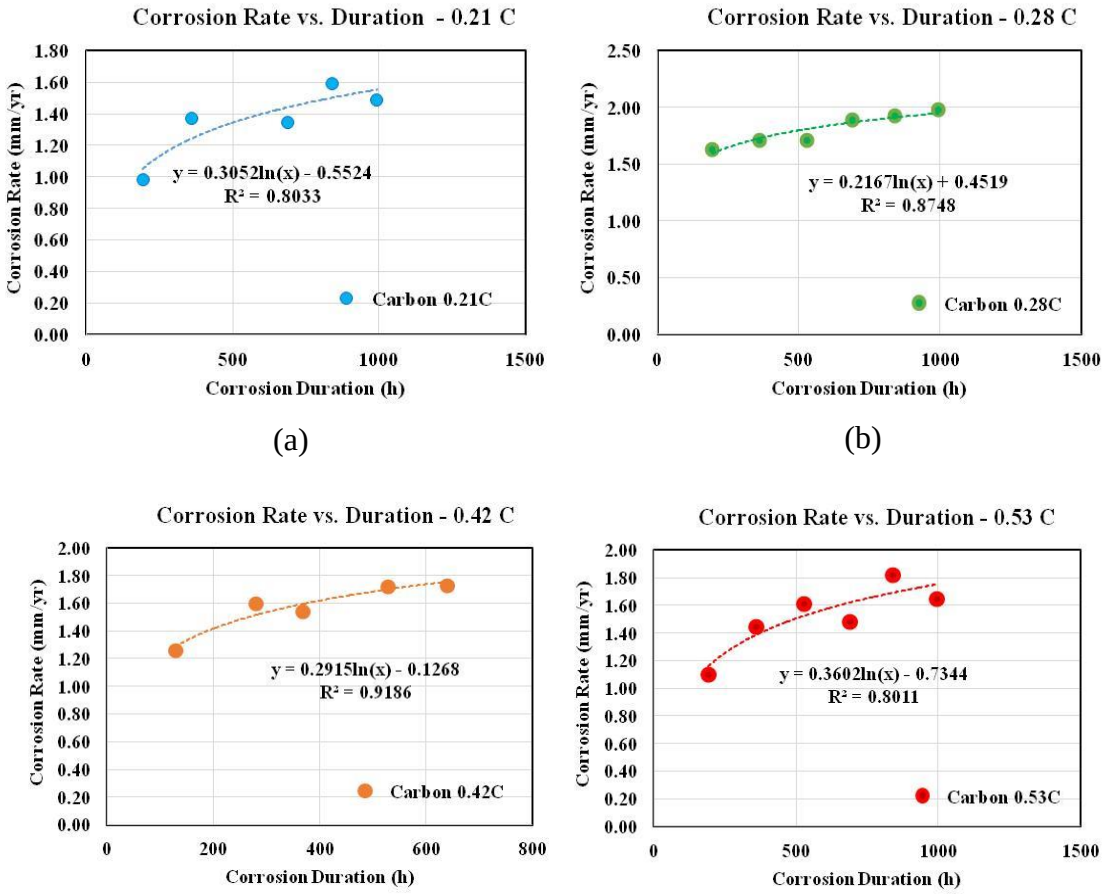

Figure 4. 4 : Weight Loss Per unit Area Vs Corrosion Duration

(a) 0.21% C (b) 0.28% C (c) 0.42% C (d) 0.53% C

The WLPA and the CR both follow a similar pattern. Even though it seems like the corrosion rate should be plateau after some time, it doesn't happen practically. One of the reasons is the instability of the corrosion layers due to the environmental factors. Due to the external factors the layers could be damages and removed. Another reason is the formation of Iron Hydroxides such as FeO (OH) or Fe(OH)3 which form in the outer layers in time. Most of the crystalline iron oxides, such as Fe_2O_3 /Fe_3O_4 get converted to

hydroxides and they tend to peel off easily. Therefore, the saturation of the corrosion rate is not considered to be practical.

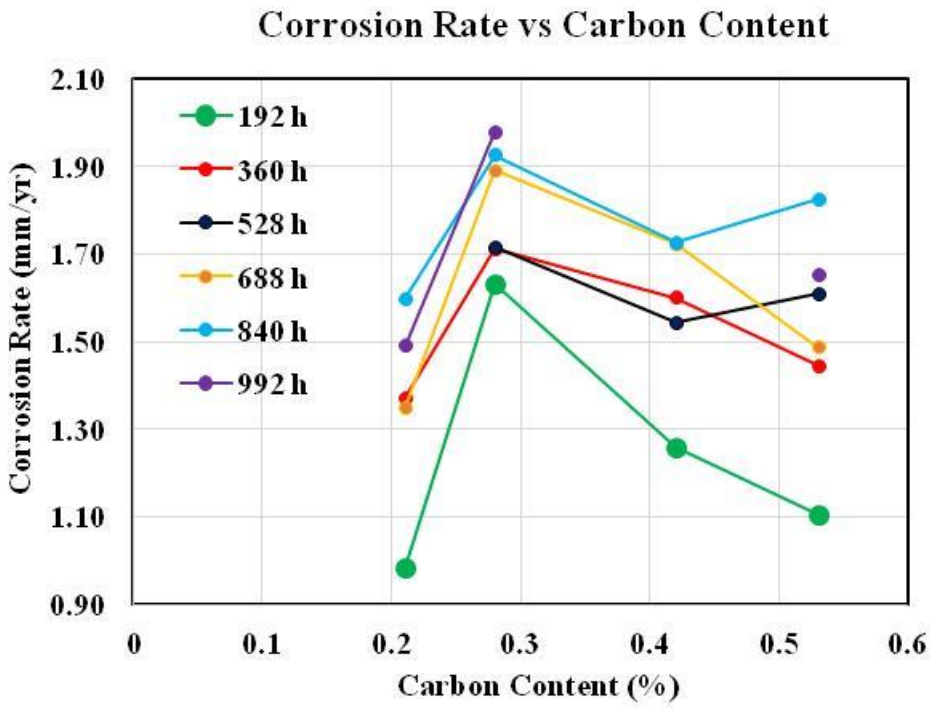

Figure 4. 5 : Corrosion rate Vs carbon content for 192 h, 360 h, 528 h, 688 h, 840 h and 992 h

The maximum corrosion rate occurs at 0.28 % C (Figure 4.5). Thus it is evident that the highest corrosion behavior occurs in steel with 0.28% carbon composition. Figure 4.6 shows the same information as a function of ferrite to pearlite ratio which further makes this clear.

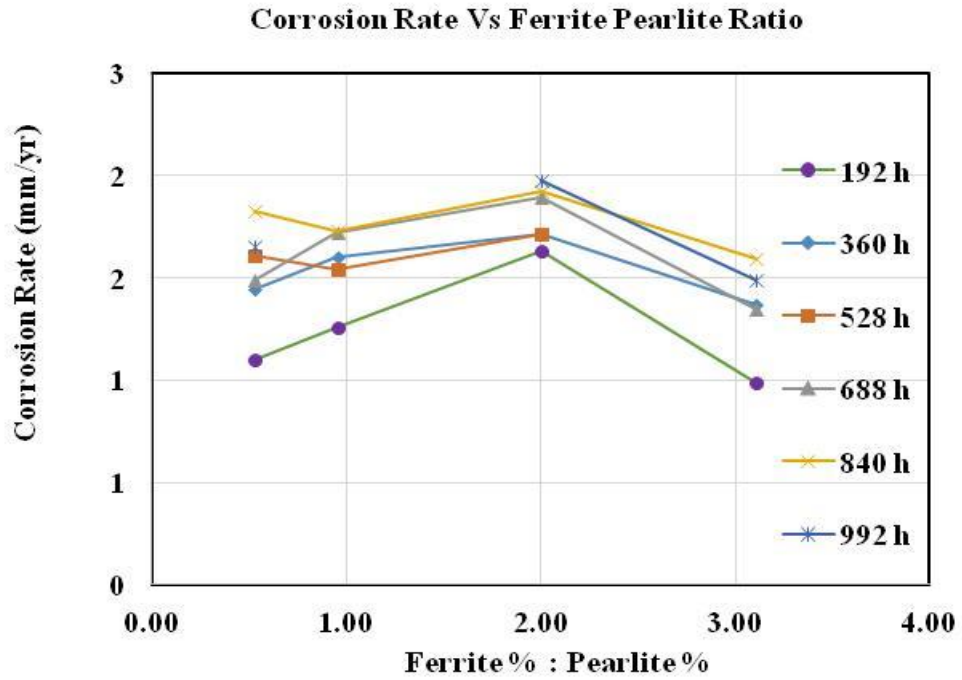

Figure 4. 6 : Corrosion Rate vs percentage of Ferrite : percentage of Pearlite

Two is the optimal ferrite to pearlite ratio that provides the highest corrosion rate in the experimented range.

4.1.3 Penetration Depth of Corrosion (PDC)

This is the third type of parameter that indicates the degree of corrosion. The readings of this parameter were limited to 0.28 % and 0.53% C steel due to the limitations of sample availability and the allocation of SEM/EDS facility. The samples were kept up in the same accelerated environment up to 992 hours for corrosion.

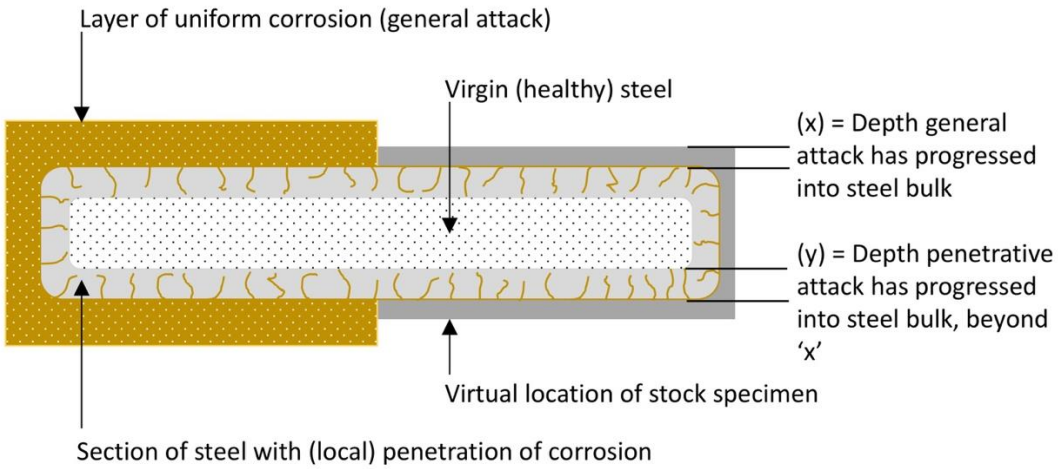

Figure 4. 7 : Representation of corrosion attack inside a specimen

The nature of corrosion attack in to the material is shown in the Figure 4.7. Material loses its properties due to both the general corrosion attack and the penetration attack. (a detailed discussion has done under the section 4.3.). Therefore it is important to study the propagation of ccorrosion in to the material and how the material has degraded due to the corrosion. SEM and EDS analysis was carried out for the characterization of the corroded specimens. Prior to the measurements the corrosion layers were characterized using EDS as mentioned in the section microstrutural observations under 3.2.3..Then the images were taken to determine the average depth of corrosion for both general corrosion and corrosion pits. Observations are as follows (Figure 4.8).

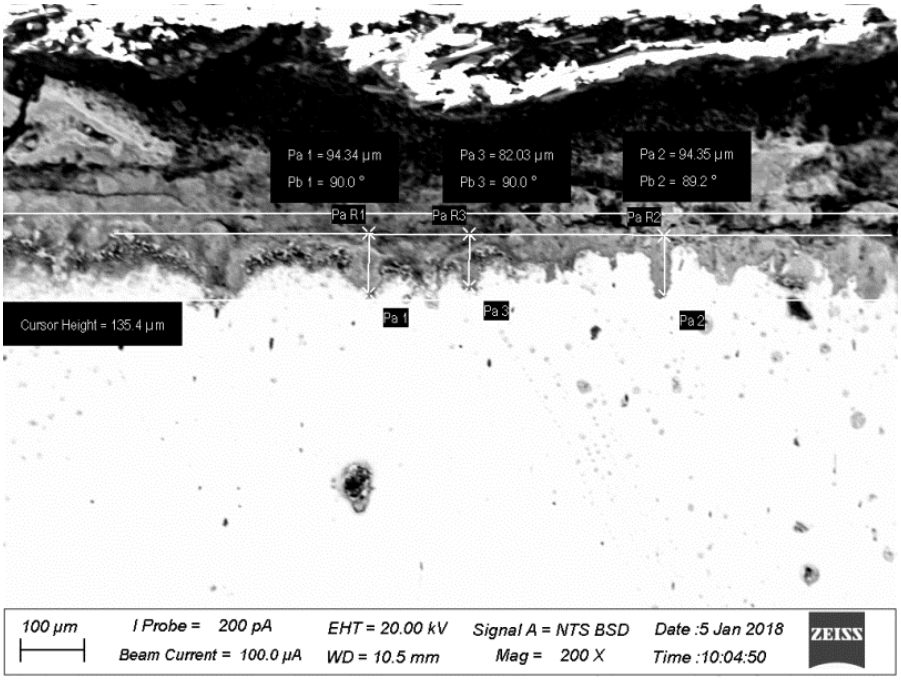

Figure 4.8 (a)

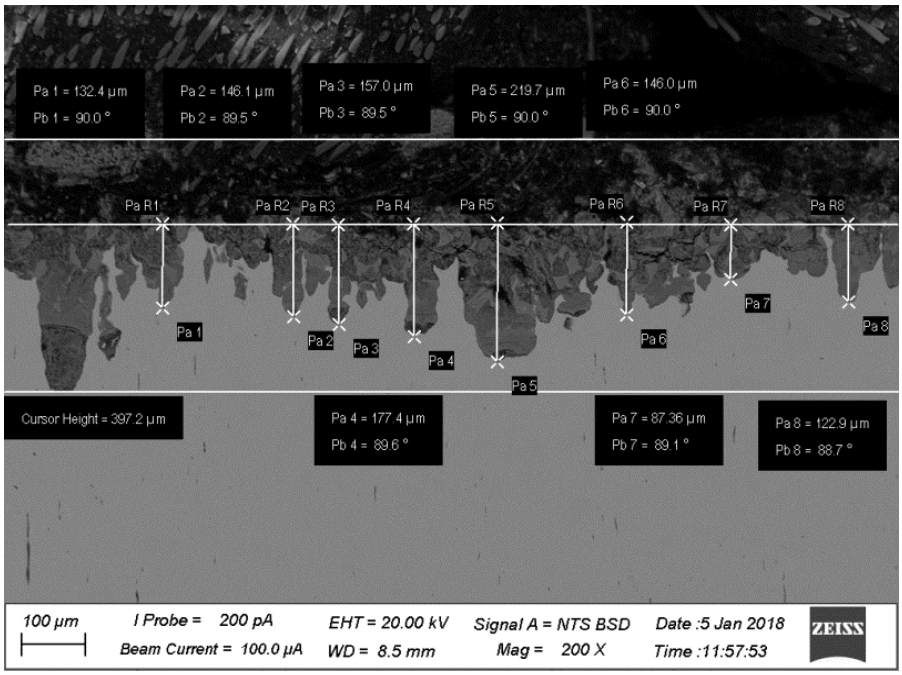

Figure 4.8 (b)

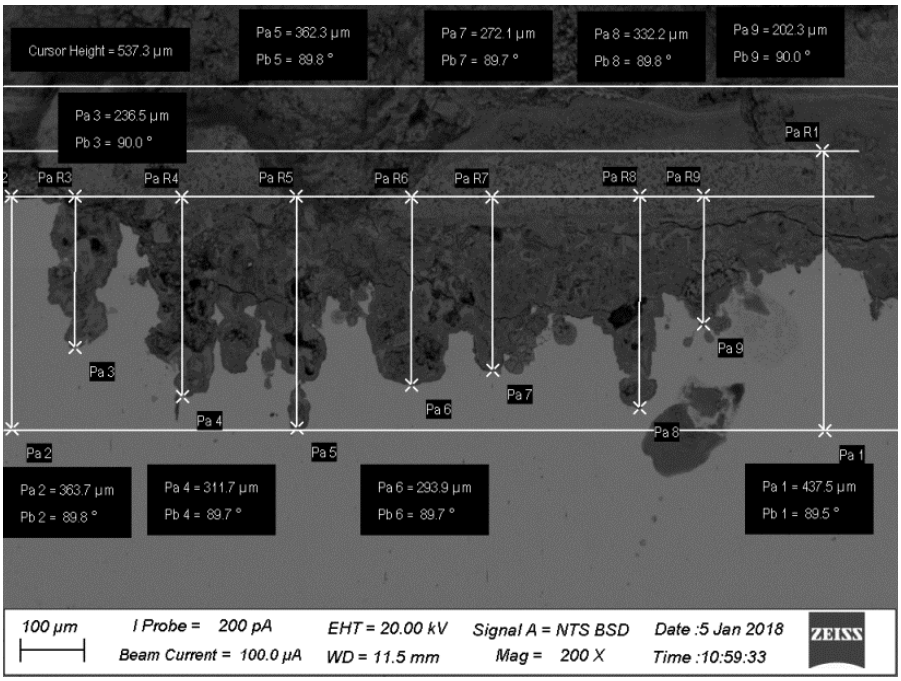

Figure 4.8 (c)

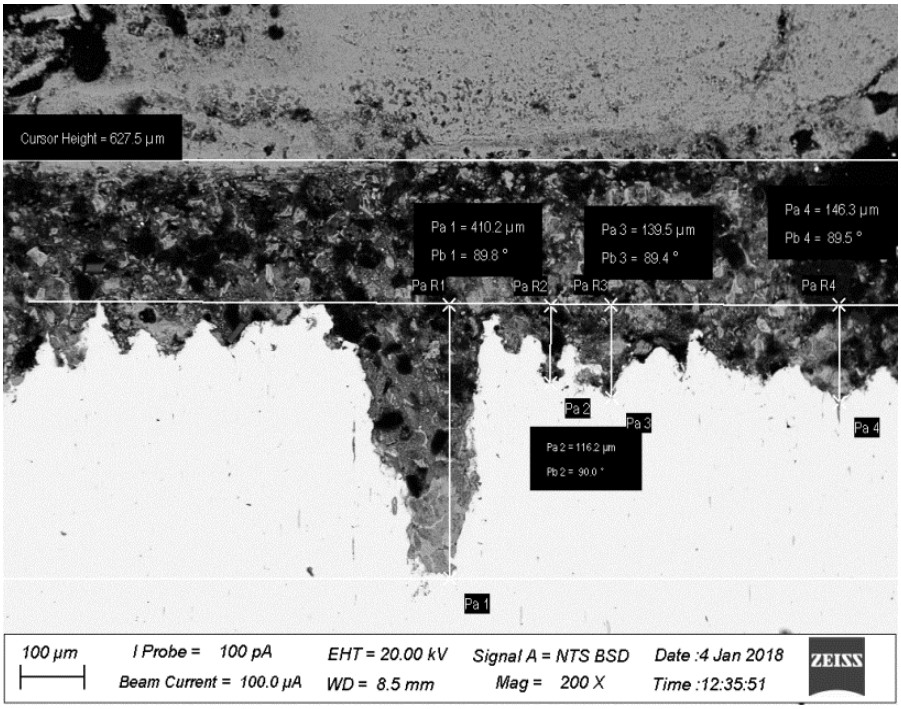

Figure 4.8 (d)

Figure 4. 8 : SEM images for the cross sections of the corroded samples after (a) 192 hours (b) 360 hours (c) 528 hours (d) 688 hours in 0.28% C steel

Table 4. 2: Total depth of corrosion for 0.28 % C and 0.53 % steels

Corrosion Duration (h)	Depth of corrosion (µm) 0.28% C			Depth of corrosion (µm) 0.53% C		
	General corrosion	Penetration of corrosion	Total penetration depth of corrosion	General corrosion	Penetration of corrosion	Total penetration depth of corrosion
192	90.47	112.45	202.92	5.09	12.17	17.26
360	50.56	265.86	316.42	35.12	35.00	70.12
528	257.60	163.00	420.60	25.30	55.52	80.82
688	297.93	184.19	482.12	99.00	131.11	230.11
840	364.20	306.80	671.00	161.73	233.67	385.4

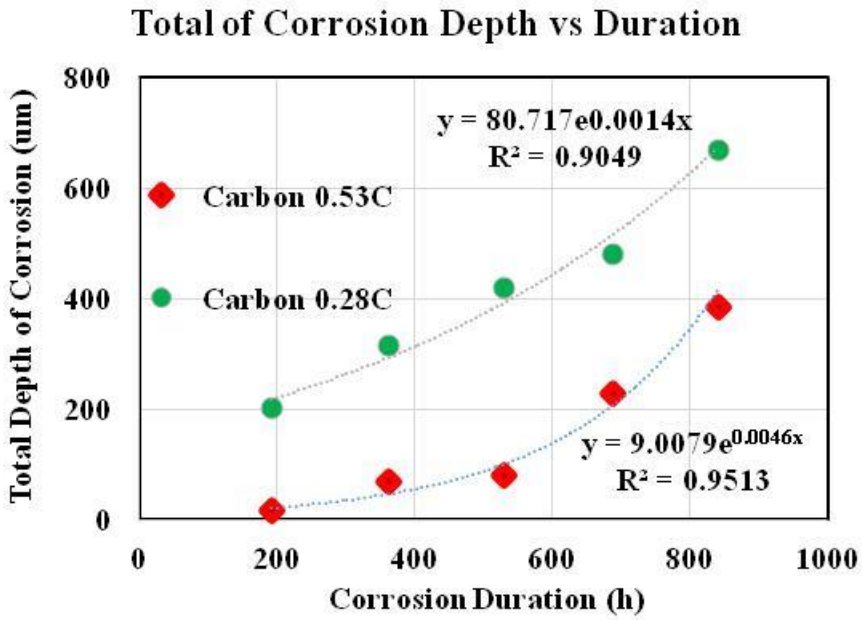

Figure 4. 9 : Total depth of corrosion Vs Duration for 0.28% C and 0.53% C

These results clearly show that the depth of the total corrosion penetration inside the material can be fitted in an exponential manner with a good regression value (Figure 4.9).

These are the three main destructive measurements which provide information regarding the degree of corrosion in a corroded sample. The goal of the research is to map these three parameters and compare them to ultrasound attenuation, which is a non-destructive parameter.

4.1.4 Ultrasound Attenuation

The results for carbon compositions of 0.21%, 0.28%, 0.42% and 0.53% are given in the Figure 4.10.Ultrasound Attenuation coefficient was calculated using the attenuation value (with corrosion durations of 192, 360, 528, 688, 840 and 992 hours) were calculated using the equation mentioned in the section 3.1.3.The calculated attenuation coefficients for the above mentioned time periods are plotted in the Figure 4.10 (For the readings see Appendix 1).

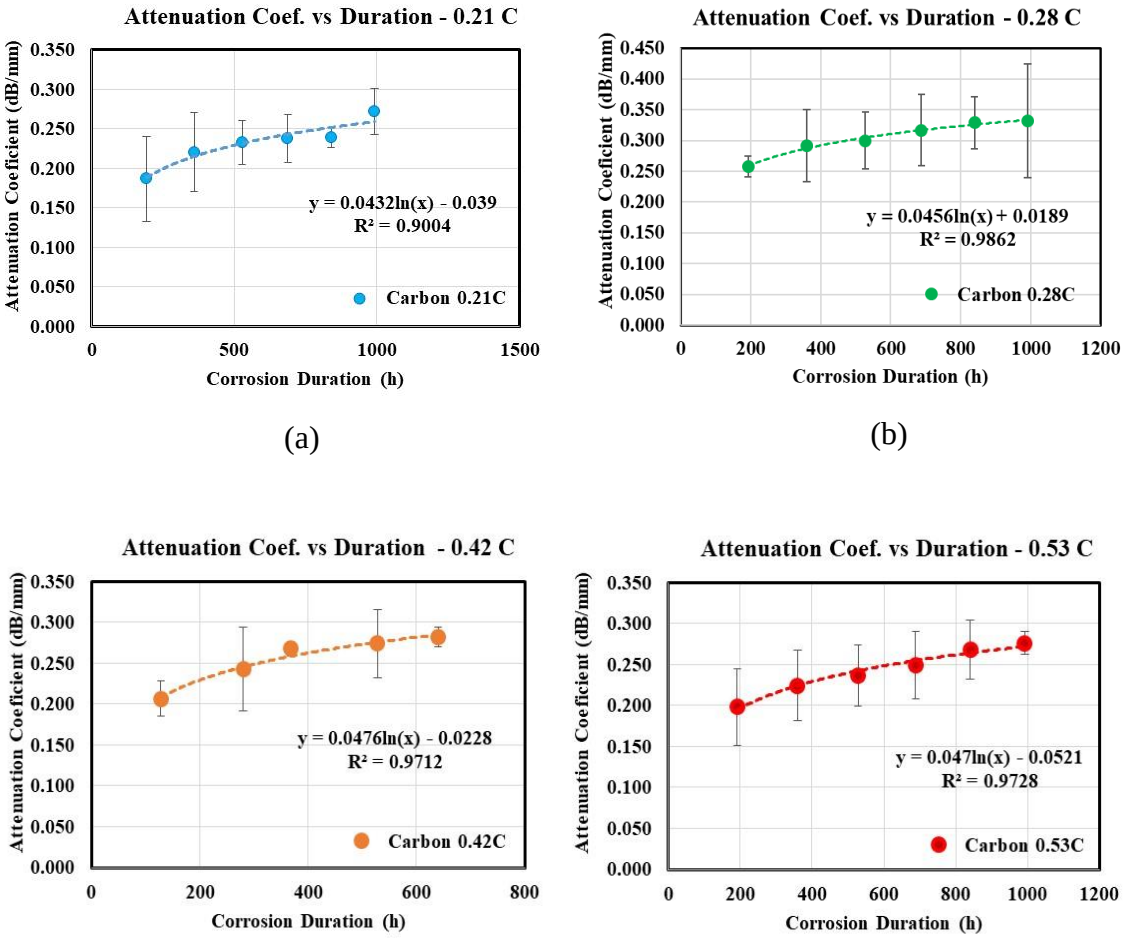

Figure 4. 10 : Attenuation Coefficient Vs Corrosion duration of carbon contents

(a) 0.21% C (b) 0.28% C (c) 0.42% C (d) 0.53% C

The energy loss in the ultrasound waves increase logarithmically. The logarithmic patterns usually present decremented increments. The amount of energy loss increases with the formation of the corrosion layers. When the rate of formation of corrosion layers reduces in time, it also slows down the increase of the ultrasound coefficient.

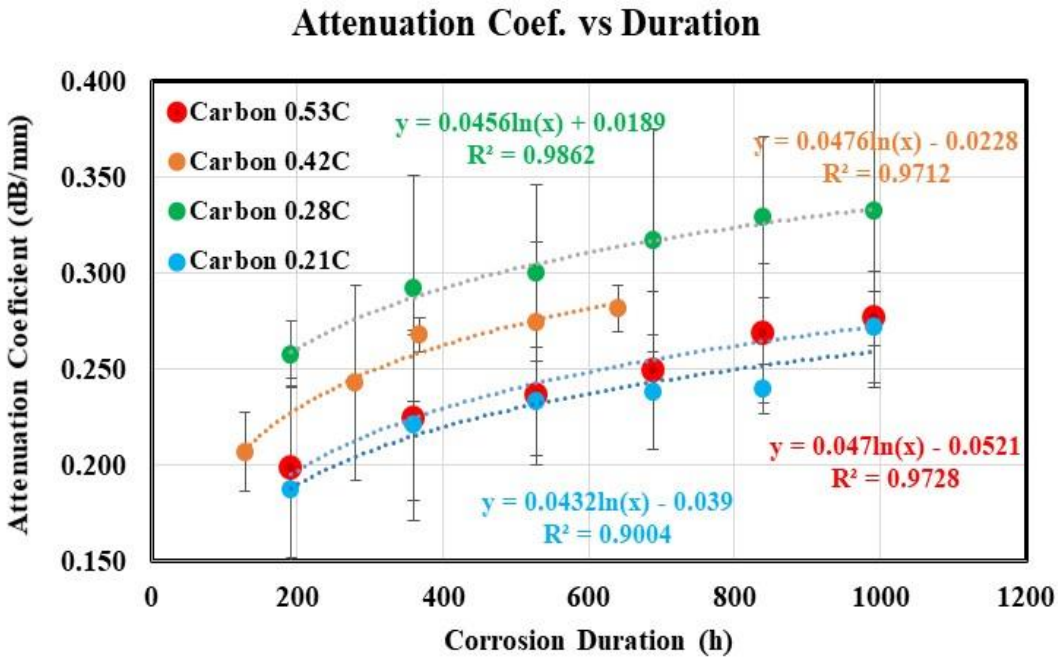

Figure 4. 11 : Attenuation coefficient Vs. Corrosion duration
(All data)

Attenuation coefficient is always led by 0.28% C for the every duration value. This can be clearly observed from Figure 4.11, Figure 4.12 and Figure 4.13. This is similar to our observations on weight loss per area and the corrosion rate as well. The attenuation coefficient is unique for a given material due to inherent its properties such as scattering, absorption and the beam spread. When there is a corrosion layer inside the material it behaves as a different medium from the parent material with higher acoustic impedance. This will lead to an increase in the attenuation coefficient and it will keep increasing with higher degrees of the corrosion.

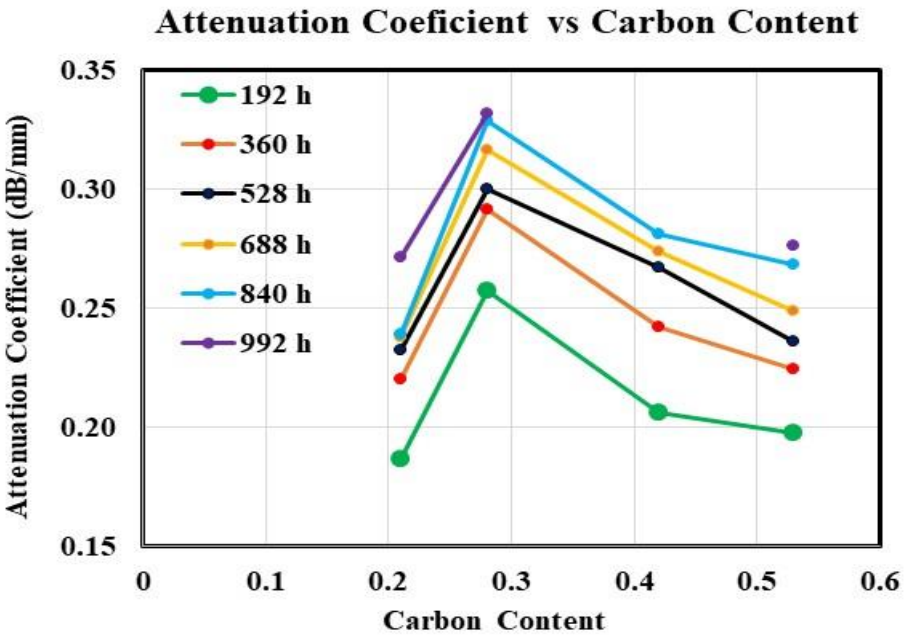

Figure 4. 12 : Attenuation coefficient vs Carbon content

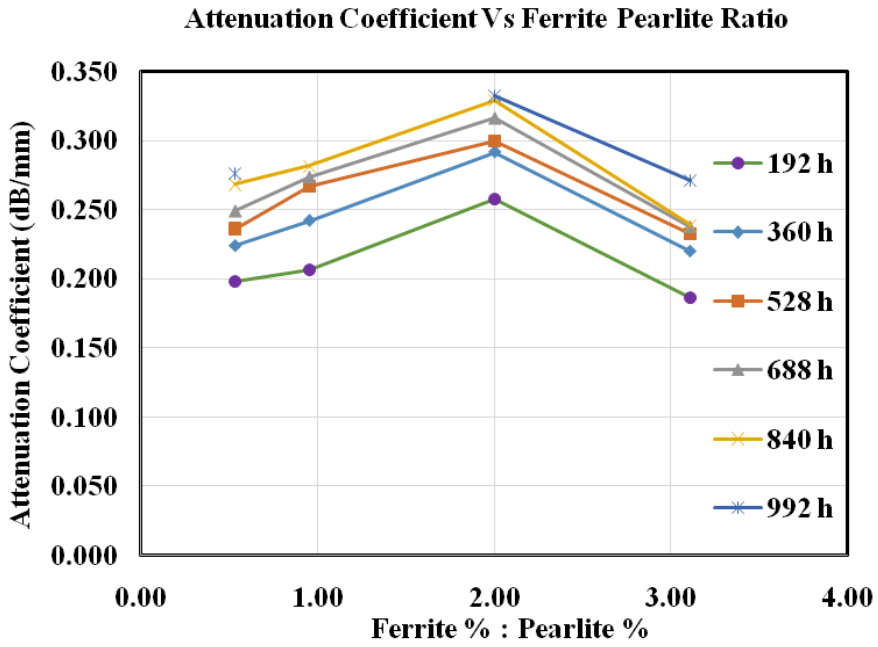

Figure 4. 13 : Attenuation Coefficient vs Ferrite : Pearlite

Attenuation coefficient is the main independent variable in this analysis while weight loss per unit area, corrosion rate and penetration depth of corrosion are dependent variables that represent the degree of corrosion. Those three variables were plotted against the attenuation coefficient in Figure 4.14, 4.15 and 4.16.

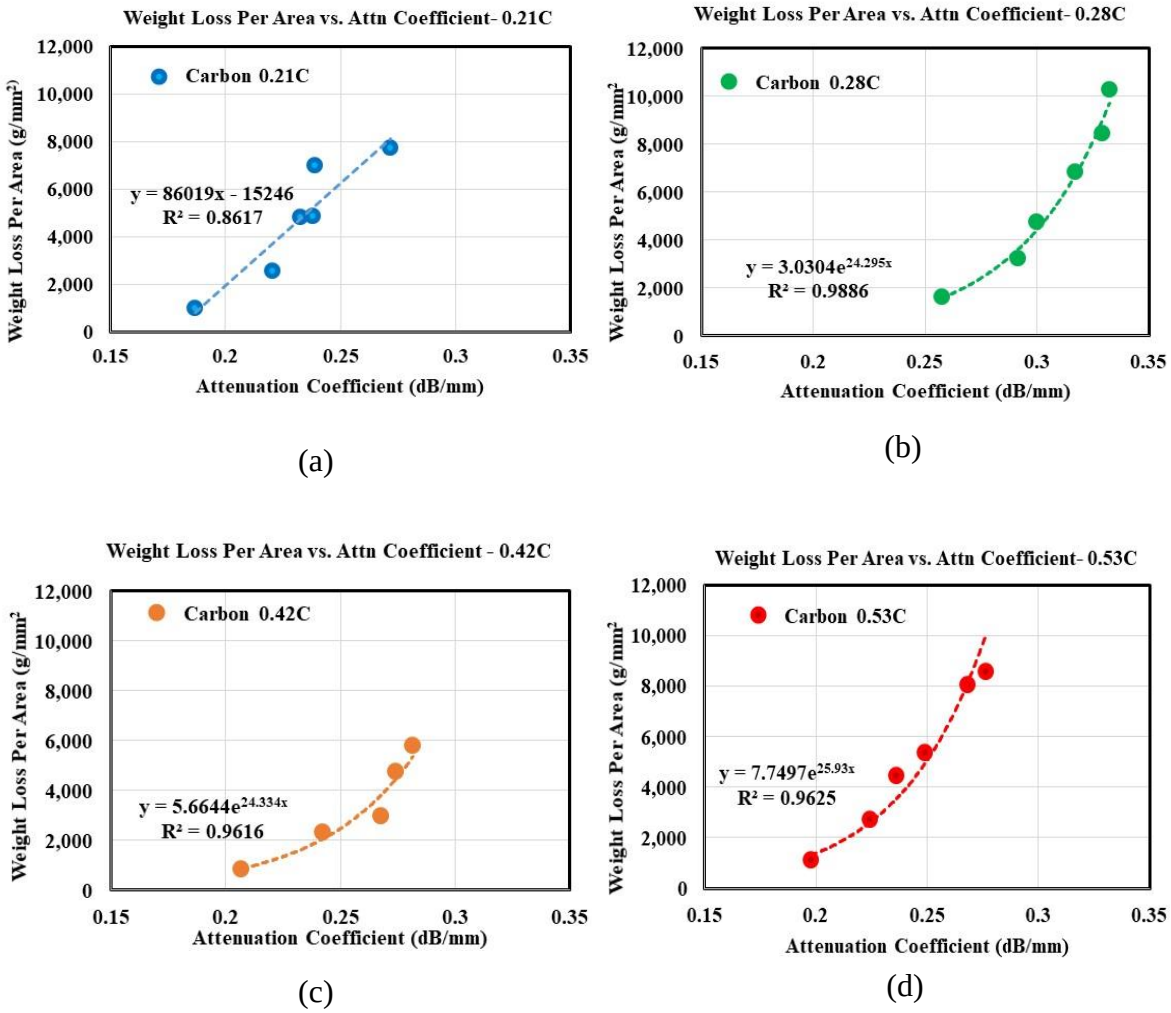

Figure 4. 14 : Weight loss per area vs. Attenuation coefficient
(a) 0.21% C (b) 0.28% C (c) 0.42% C (d) 0.53% C

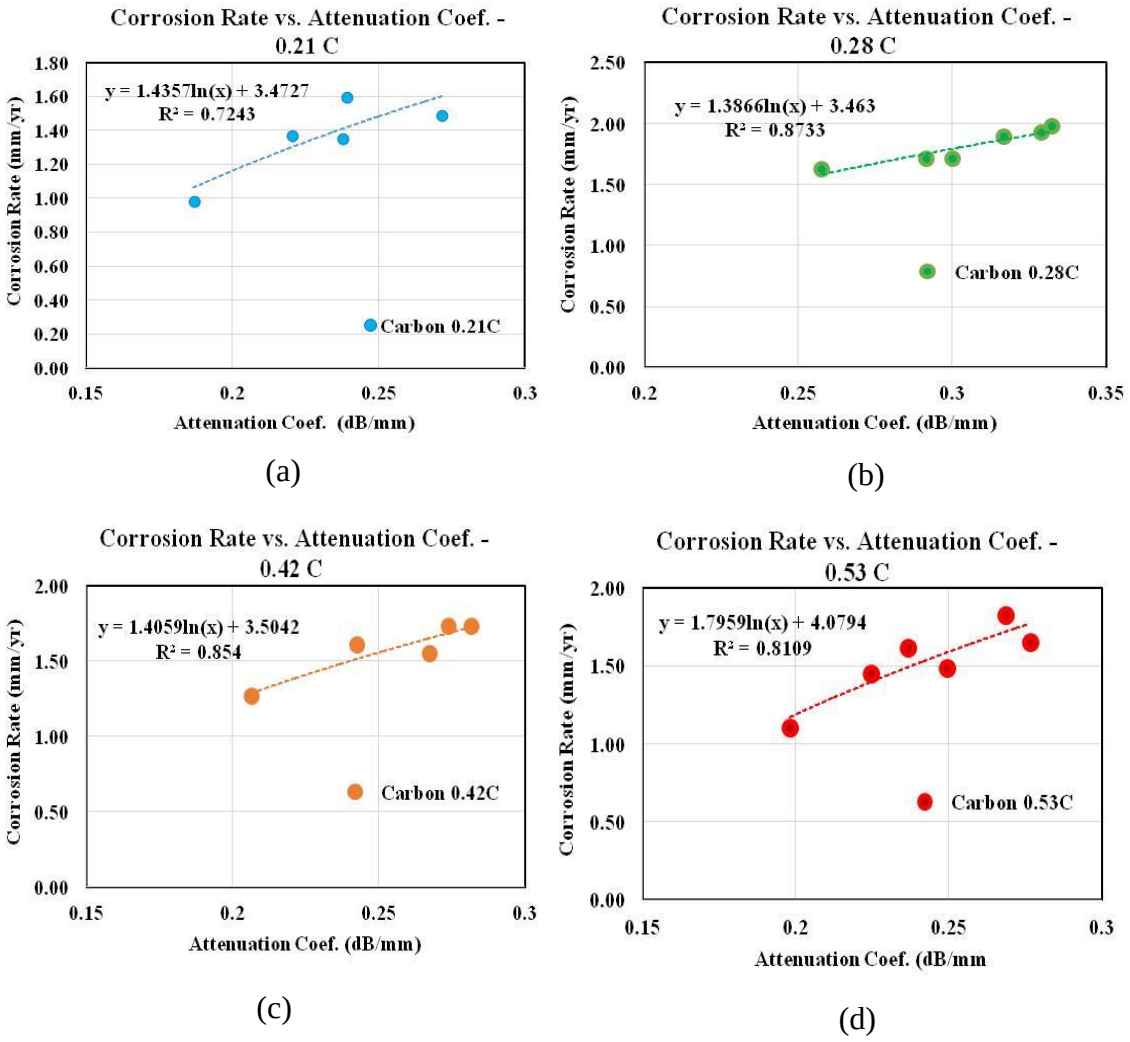

Figure 4. 15 : Corrosion rate vs. Attenuation coefficient

(a) 0.21% C (b) 0.28% C (c) 0.42% C (d) 0.53% C

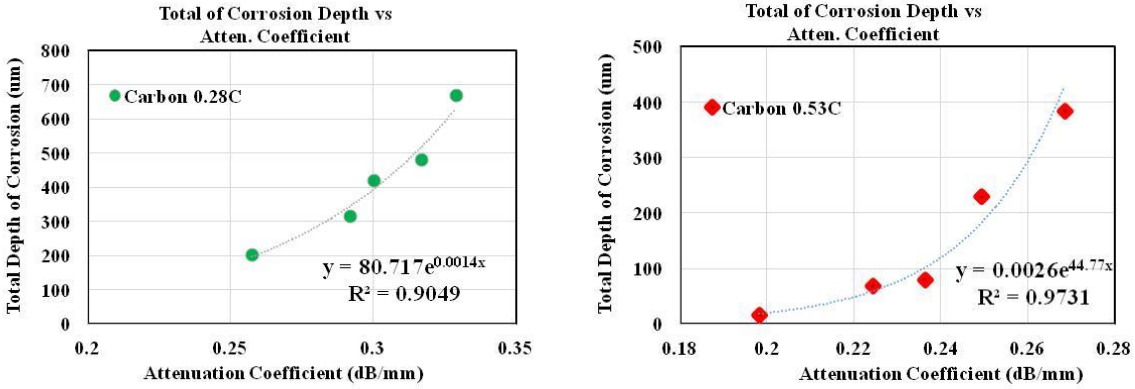

(a) (b)

Figure 4. 16 :Total corrosion depth vs. Attenuation coefficient
(a) 0.28% C (b) 0.53% C

These correlations were used as a set of inputs for the final model.

These attenuation coefficient values are related to a carbon composition of 0.28% and a specific grain size of 0.052 mm. Therefore, the attenuation coefficient is limited to material with these specific values. The experiments were further extended using different carbon compositions and grain sizes to fine-tune the developed relationships. These experiments enabled us to extract correction factors and these factors would make the correlations for a more generic and practical. A detailed discussion can be found in section 4.2.

4.2 Effect of grain size on ultrasound attenuation for plain carbon steel in the selected range

There are three main factors that affect ultrasound attenuation; scattering, absorption and the beam spread of the wave propagation [46]. Beam spread is a probe property and it does not depend on the material. But the other two properties are directly related to the material. The function of scattering is strongly influenced by the size of the grains and the density of the grain boundaries. Since industrially used materials tend to have different grain sizes, the derived relationships with ultrasound attenuation should have a correction factor related to grain size. In essence, the final correlations should be universal after correction factors are taken in to account.

The experiments were carried out for base composition with 0.28% C as mentioned in section 3.2.2. The variation of ultrasound attenuation against the grain size for above sample is shown in the Figure 4.17.

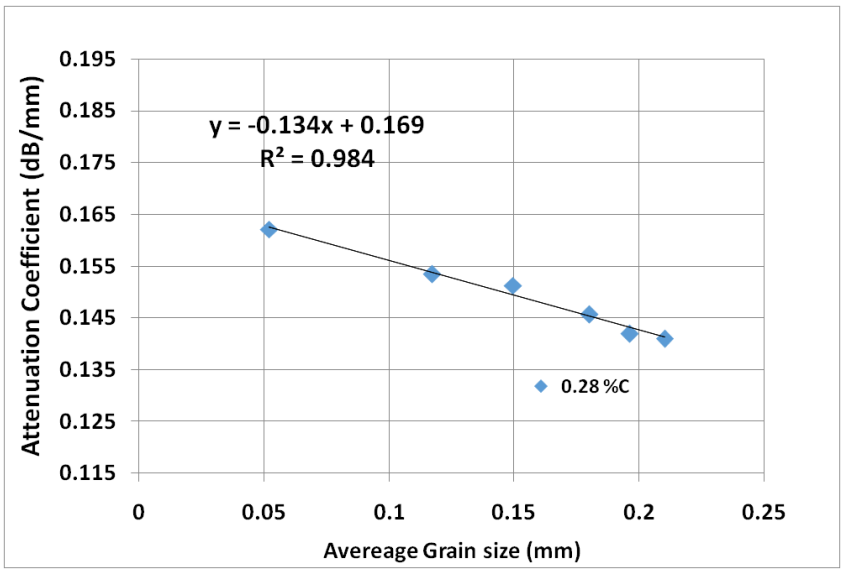

Figure 4. 17 : Attenuation coefficient vs. average grain size of 0.28% carbon content sample

The wave attenuation decreases with increasing grain size. Larger grain sizes also lead to the reduction in grain boundary density. The total area which the atoms are arranged in an order is reduced because of that. The uncorroded grain boundaries would scatter the ultrasound waves more and therefore increase the loss of wave energy or the attenuation. Therefore, our experimental observation is consistent with the theory.

Using these theoretical factors, the developed correlation between ultrasound attenuation and the grain size can be extrapolated to predict the behavior of other plain carbon steels (0.21 % c, 0.42% C and 0.53% C) as well. As mentioned above, the attenuation of a material mainly depends on scattering, absorption and the beam spread.

Beam spread is a factor caused by the probe. Therefore, this factor is common for all our experiments (this research is based on 5 MHz normal probe with a diameter of 8 mm: thus, the same probe has to be used in industrial testing to utilize this study). Since the scattering is mainly dependent on the grain boundary density, the energy reduction of the ultrasound waves should follow the same pattern with the same tangent value of 0.1349. However theoretically the intercept point should not be the same due to the energy loss caused by the absorption. The energy loss due to absorption is an inherent/ unique property for a given material which is related to the chemical composition of that material as discussed in the literature section.

In the selected sample series, we have only varied the carbon content which in effect changes the chemical composition. Therefore, in summary the attenuation coefficient with respect to grain sizes of 0.21%, 0.42% and 0.53% C steel samples should have the same gradient as the 0.28% C sample but with different intercepts depending on the initial attenuation. The initial grain size of all the samples were kept at 0.052 mm and the initial attenuation coefficients of the 0.21% C, 0.28% C,0.42% C and 0.53% C are 0.151 dB ,0.163 dB ,0.173 dB and 0.184 dB respectively.

The derived equations using the base equation and the theory are given in the Table 4.3. The graphs are shown in Figure 4.18.

Table 4. 3 : Correlations of attenuation and grain size

Carbon composition	Relationship between ultrasound attenuation (y) and the grain size (x)
0.28% C	y = -0.134x + 0.1696
0.21% C	y = -0.134x + 0.1576
0.42% C	y = -0.134x + 0.1800
0.53% C	y = -0.134x + 0.1907

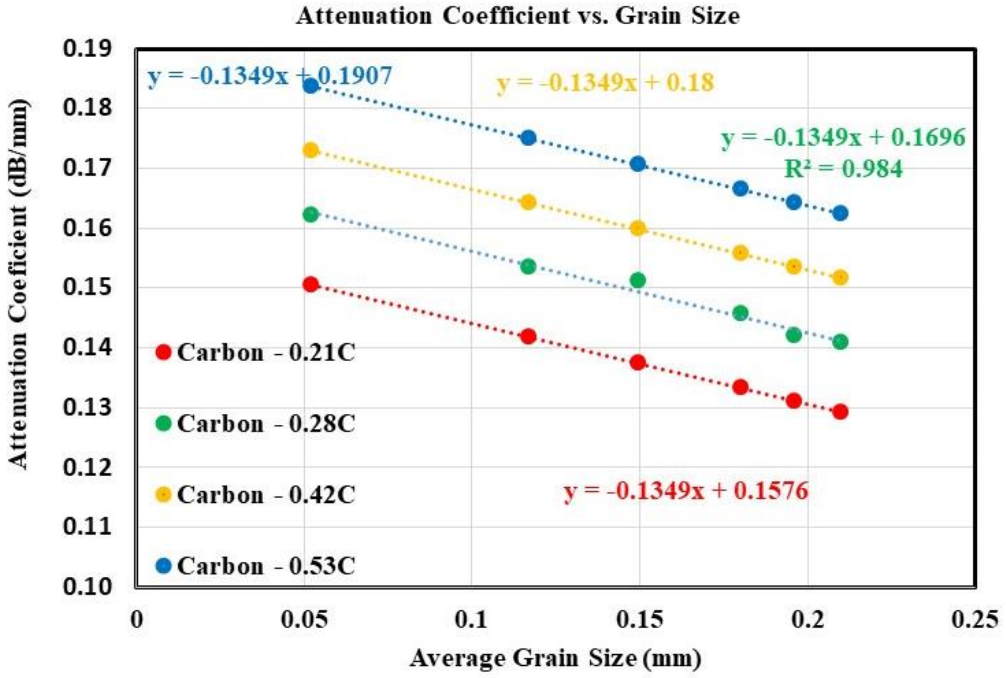

Figure 4. 18 : Attenuation coefficient Vs. Grain size in 0.21% C, 0.28% C, 0.42% C and 0.53% C

The data provided in Figure 4.18 consists of three variables; attenuation coefficient, grain size and the carbon content. These relationships can be mathematically modeled to predict the measurement of uncorroded samples. In other words, data related to these three variables can be used to plot a plane which would provide the inherited or the original attenuation coefficients of low and medium carbon steels with various grain sizes in uncorroded state. This plane can be utilized as the reference or the base condition. The attenuation (coefficient) taken from a corroded specimen is a collective value of the above-mentioned reference attenuation and the attenuation due to the amount/degree of corrosion. The Difference of Attenuation Coefficient (DAC) can be found by subtracting the relevant reference attenuation coefficient from the final/Total attenuation Coefficient (TAC). The mathematical model will be discussed in section 4.4.

4.3 Relationship between the load bearing capacity and the degree of corrosion

4.3.1 Residual strength analysis

Table 4. 4 : Average breaking loads and the relevant weight loss of tensile specimens

Corrosion Condition	Average Breaking Load (N)	Standard Deviation (N)	Average Weight Loss per Area (g/m^2)
Reference/Stock	18100	477.28	-
192 hours	16825	225.00	2004.24
360 hours	15732	883.88	2848.60
528 hours	14838	1255.24	4354.26
688 hours	13800	169.71	5801.60
840 hours	11575	1549.46	7720.45

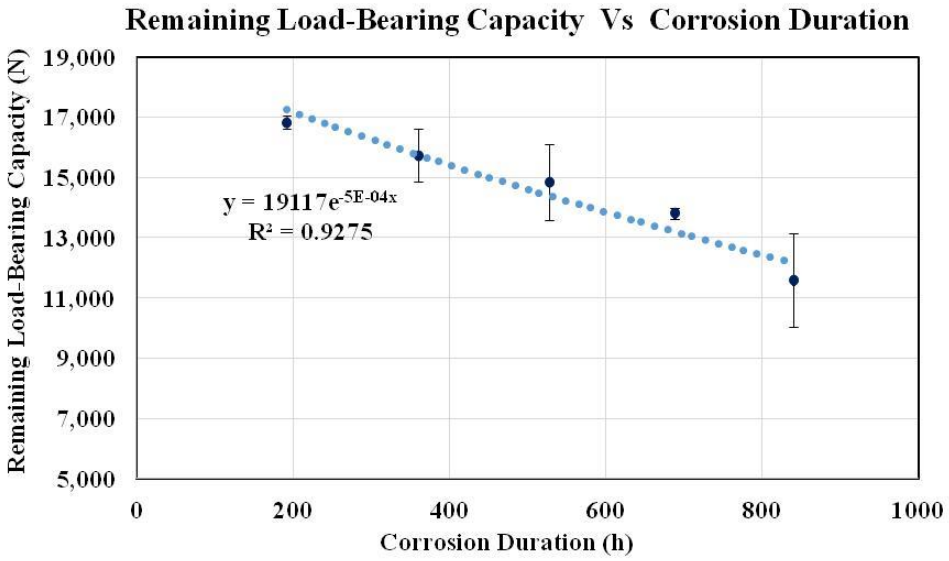

Figure 4. 19 : Remaining load bearing capacity Vs Corrosion duration

The practical load bearing capacity of the tensile specimen over the corrosion duration is plotted in Figure 4.19. The load bearing capacity decreases with corrosion as expected (as the cross section decreases). In the industry, the remaining load bearing capacity is calculated using an in-situ weight loss analysis. The loss of weight due to corrosion is measured from a sample that is removed from the test structure, and that weight loss due to corrosion is used to calculate the remaining thickness of the sample. The corrosion penetrations are not taken in to account in this method. Therefore, the predicted theoretical value is higher than the practical values shown in Figure 4.20 below.

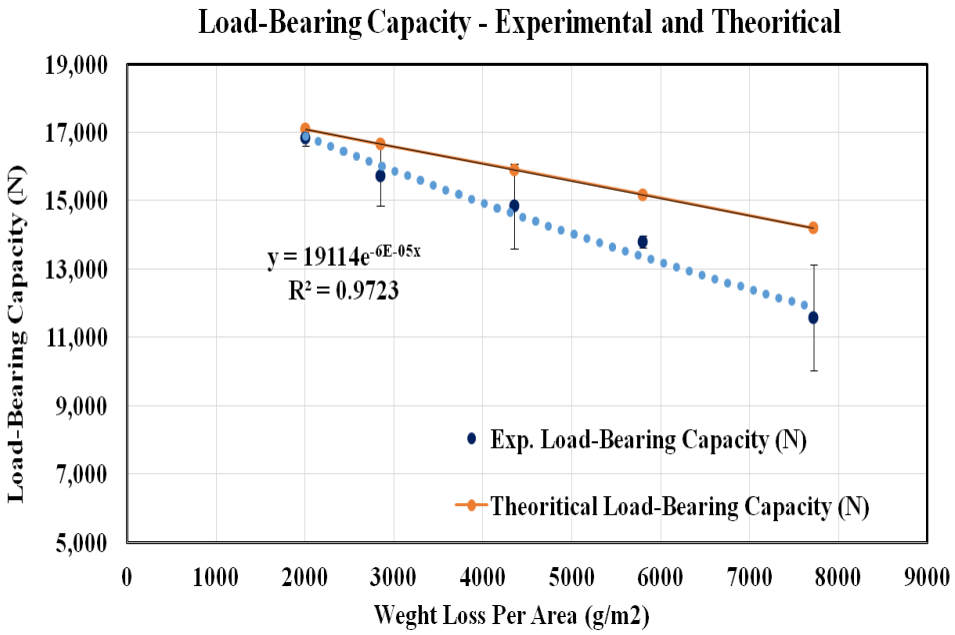

Figure 4. 20 : Theoretical and practical load bearing capacity of the corroded tensile specimen Vs Weight loss per area

The disparity between theoretical and practical load bearing capacities increase with time as shown in Figure 4.21.

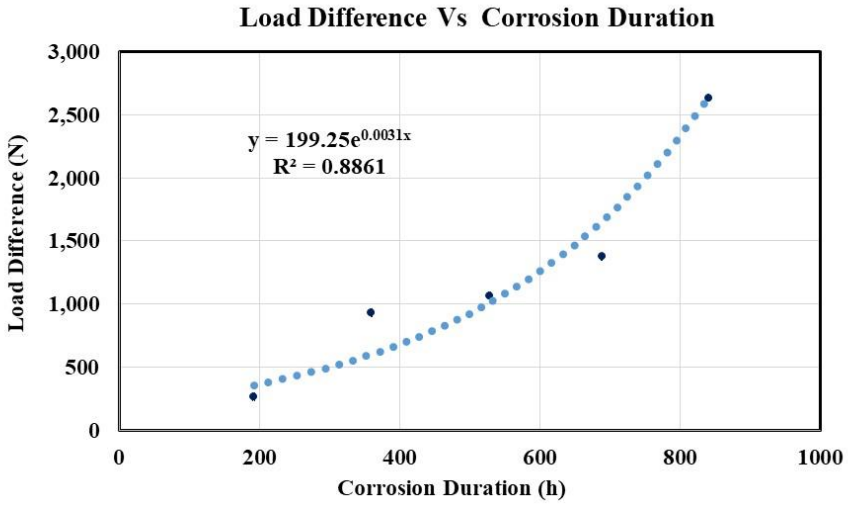

Figure 4. 21 : Load difference vs Corrosion duration

Increasing disparity in load bearing capacity is not a simple issue. This could lead to serious problems due to wrong calculations/estimations. Therefore, more attention should be given to available and existing methods of corrosion estimation and these methods should be updated with more accurate methods such as ultrasound investigations.

The remaining load bearing capacity can also be plotted against the relevant total corrosion penetration as shown in Figure 4.22.

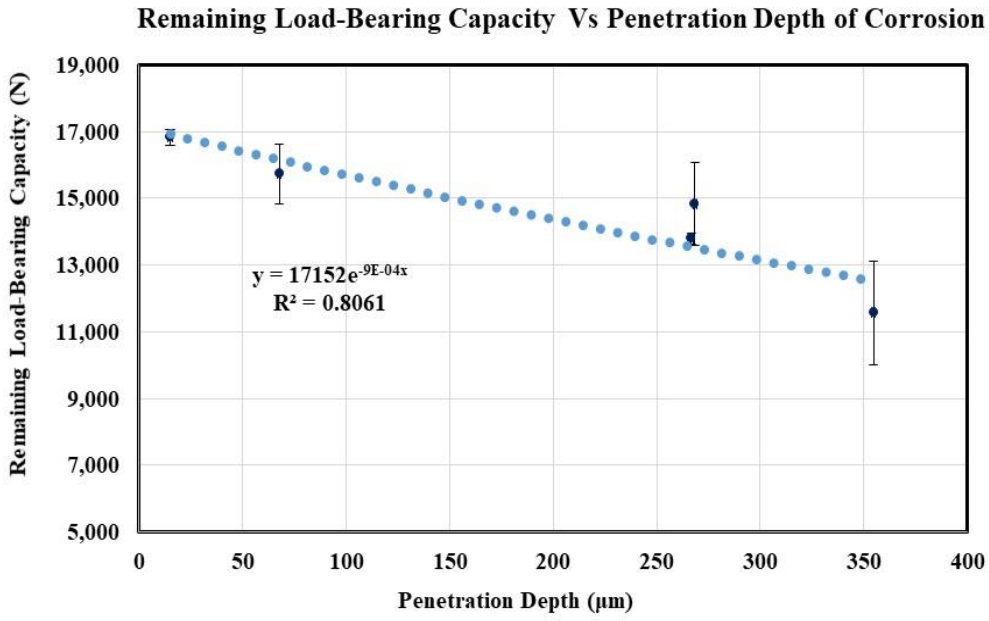

Figure 4. 22 : Remaining load bearing capacity vs penetration depth of corrosion

Since the attenuation coefficient is the dependent variable, the remaining load bearing capacity should be mapped with the attenuation coefficient and should be able to trace through the dependable variable. Following the analysis, the extracted parameters from this section were used to develop final mathematical models.

4.4 Development of the mathematical model

The correlations obtained under the above-mentioned experimental sub sections are collected together and a final mathematical model has been developed. MATLAB (2016) and SPSS mathematical software were used for this purpose.

When analyzing all the raw data it was complex since there were many independent and dependable variables. Carbon content, time duration under corrosion, attenuation coefficient was taken as the independent variables while weight loss per area (represents the degree of corrosion), corrosion rate (represents the degree of corrosion), penetration depth of corrosion (represents the degree of corrosion) and remaining load bearing capacity (denotes mechanical properties) were taken under dependable variables. As for the first step the baseline correction should be done as described in the following section.

4.4.1 Development of MATLAB models/plots

4.4.1.1 Baseline correction

Carbon content is available to be known in specs and records, while the attenuation coefficient is to be measured and the relevant grain size of the test piece or the structure is unknown. thus there should be a way to determine the grain size since the particular material has its inherited attenuation confident depending on the grain size. attenuation confident as discussed above in the section 4.3, the attenuation coefficient measured from the corroded test piece, which is referred as Total Attenuation Coefficient (TAC), is a summation of attenuation coefficients caused by the properties (carbon content and the grain size) of the original material and the corrosion of the test sample. Thus, to determine the attenuation caused only by the corrosion, the initial attenuation coefficient which is inherited to the material should be reduced from TAC. For that, a reference

plane is developed using MATLAB as shown in the Figure 4.28. This is referred as baseline correction.

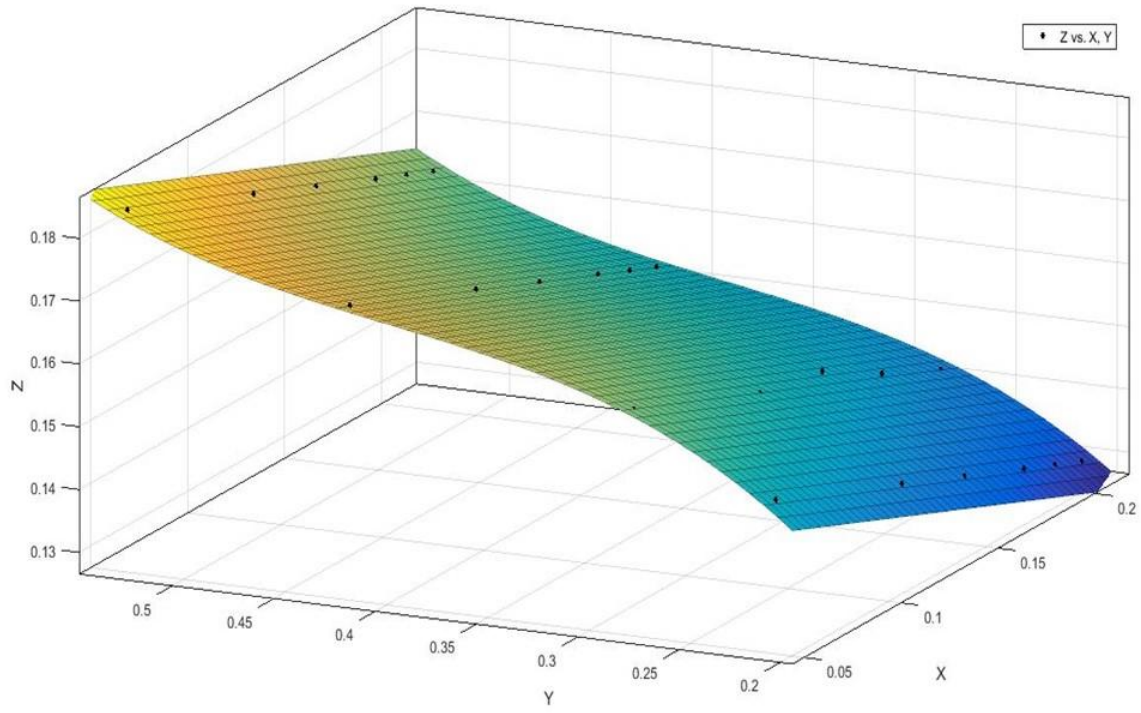

Figure 4. 23 : Baseline correction using MATLAB – grain size (x), carbon content (y), reference/base/initial attenuation coefficient [z – f(x,y)] plane

Polynomial function: Linear model Poly13:
f(x,y) = p00 + p10*x + p01*y + p11*x*y + p02*y^2 + p12*x*y^2 + p03*y^3 (14)

Coefficients (with 95% confidence bounds):

p00 = 0.05204 (0.03759, 0.06648)
p10 = -0.1349 (-0.1885, -0.08142)
p01 = 0.853 (0.7357, 0.9702)
p11 = 0.0002434 (-0.3171, 0.3176)
p02 = -2.03 (-2.337, -1.723)

p12 = -0.0003832 (-0.4265, 0.4257)

p03 = 1.725 (1.457, 1.993)

Goodness of fit:

SSE: 5.137e-06

R-square: 0.9989

Adjusted R-square: 0.9986

RMSE: 0.0005497

This plane with the baseline correction will be used throughout the analysis to determine the Difference of the Attenuation Coefficient (DAC) in corroded samples (Difference in Attenuation Coefficient = Total Attenuation Coefficient – Reference Attenuation Coefficient).

4.4.1.2 Models for the corroded samples against the time function

The same type of models as described above were developed to represent the planes in corroded samples. Corrosion is a phenomenon which occurs with the time function. In the baseline plane the time is considered as 0, since the samples have not been corroded. The rest of the planes were developed after taking the results in 192 h, 360 h, 528 h, 688 h, 840 h and 992 h.

192 h

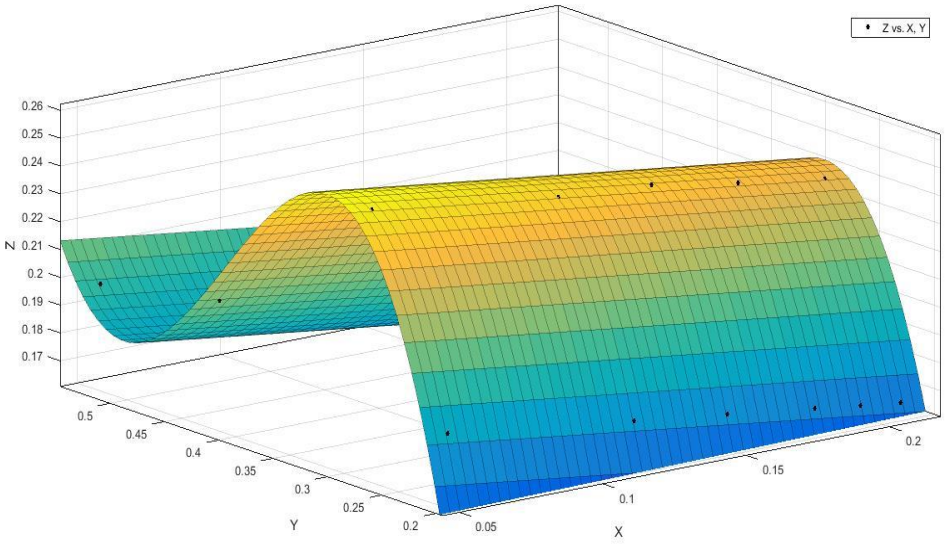

Figure 4. 24 : Plane for 192 h exposure using MATLAB – grain size (x), carbon content (y), reference/base/initial attenuation coefficient [z – f(x,y)] plane

Linear model Poly13:

$$f(x,y) = p00 + p10*x + p01*y + p11*x*y + p02*y^2 + p12*x*y^2 + p03*y^3 \quad (15)$$

Coefficients (with 95% confidence bounds):

p00 = -1.003 (-1.018, -0.9886)
p10 = -0.1414 (-0.1952, -0.08769)
p01 = 10.63 (10.51, 10.75)
p11 = 0.04031 (-0.2783, 0.3589)
p02 = -28.56 (-28.87, -28.25)
p12 = -0.05225 (-0.48, 0.3755)
p03 = 24.15 (23.89, 24.42)

Goodness of fit:
SSE: 5.177e-06
R-square: 0.9997
Adjusted R-square: 0.9996
RMSE: 0.0005518

This plane lies above the reference plane.

360 h

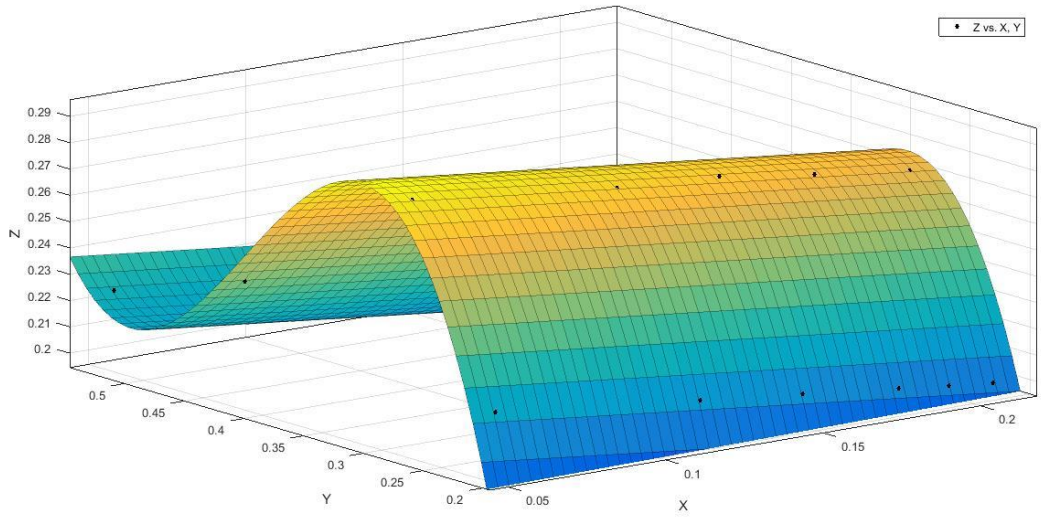

Figure 4. 25 : Plane for 360 h exposure using MATLAB – grain size (x), carbon content (y), reference/base/initial attenuation coefficient [z – f(x,y)] plane

Linear model Poly13:

$$f(x,y) = p00 + p10*x + p01*y + p11*x*y + p02*y^2 + p12*x*y^2 + p03*y^3 \qquad (16)$$

Coefficients (with 95% confidence bounds):

p00 = -0.9388 (-0.9532, -0.9243)
p10 = -0.1349 (-0.1884, -0.08134)
p01 = 10.3 (10.18, 10.41)
p11 = -0.0003488 (-0.3177, 0.317)
p02 = -27.4 (-27.7, -27.09)
p12 = 0.0005671 (-0.4255, 0.4266)
p03 = 22.89 (22.63, 23.16)

Goodness of fit:
SSE: 5.137e-06
R-square: 0.9998
Adjusted R-square: 0.9997
RMSE: 0.0005497

528 h

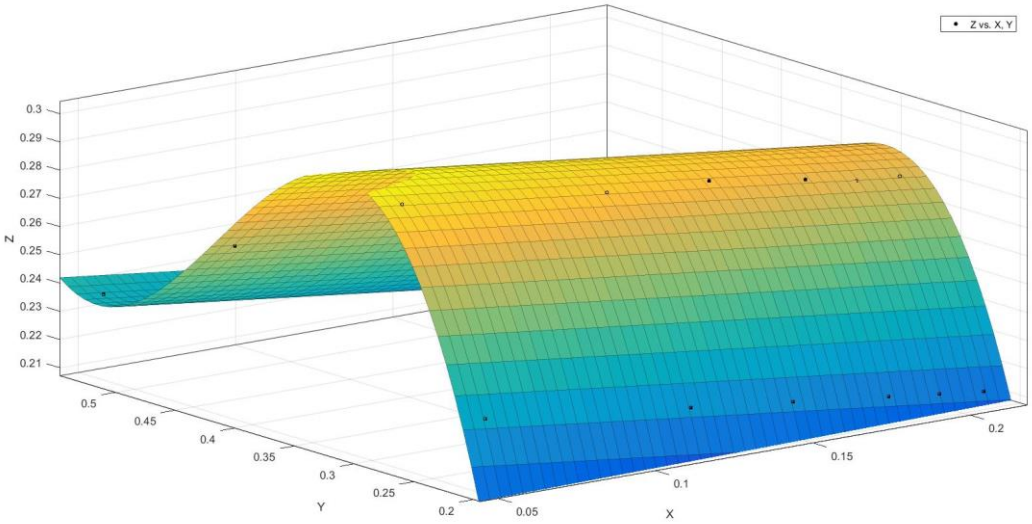

Figure 4. 26 : Plane for 528 h exposure using MATLAB – grain size (x), carbon content (y), reference/base/initial attenuation coefficient [z – f(x,y)] plane

Linear model Poly13:

f(x,y) = p00 + p10*x + p01*y + p11*x*y + p02*y^2 + p12*x*y^2 + p03*y^3 (17)

Coefficients (with 95% confidence bounds):

p00 = -0.727 (-0.7414, -0.7125)
p10 = -0.1349 (-0.1885, -0.08142)
p01 = 8.349 (8.232, 8.466)
p11 = 0.0002434 (-0.3171, 0.3176)
p02 = -21.47 (-21.78, -21.16)
p12 = -0.0003832 (-0.4265, 0.4257)
p03 = 17.3 (17.03, 17.57)

Goodness of fit:

SSE: 5.137e-06
R-square: 0.9997
Adjusted R-square: 0.9996
RMSE: 0.0005497

688 h

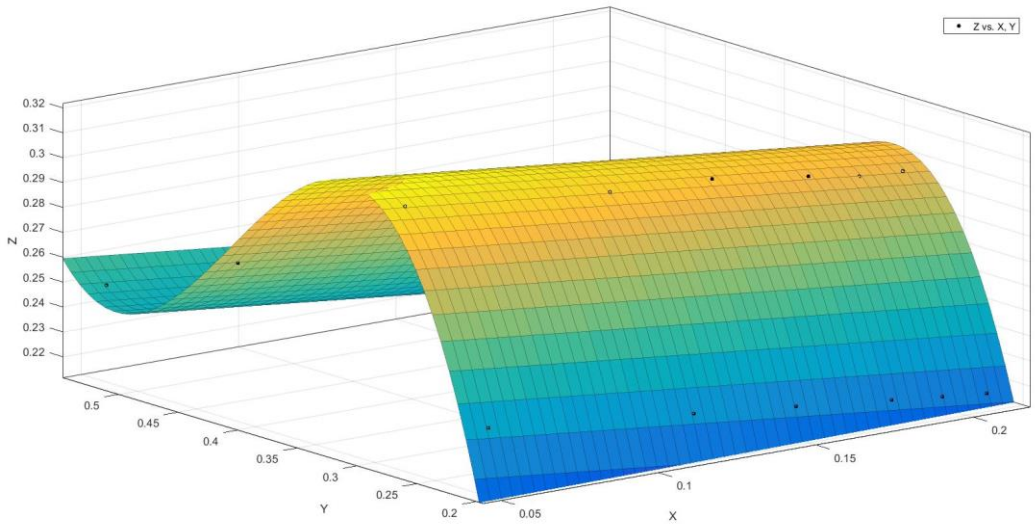

Figure 4. 27 : Plane for 688 h exposure using MATLAB – grain size (x), carbon content (y), reference/base/initial attenuation coefficient [z – f(x,y)] plane

Linear model Poly13:

f(x,y) = p00 + p10*x + p01*y + p11*x*y + p02*y^2 + p12*x*y^2 + p03*y^3 (18)

Coefficients (with 95% confidence bounds):

p00 = -0.9548 (-0.9693, -0.9404)
p10 = -0.1349 (-0.1885, -0.08142)
p01 = 10.47 (10.35, 10.59)
p11 = 0.0002434 (-0.3171, 0.3176)
p02 = -27.4 (-27.7, -27.09)
p12 = -0.0003832 (-0.4265, 0.4257)
p03 = 22.55 (22.28, 22.82)

Goodness of fit:

SSE: 5.137e-06
R-square: 0.9998
Adjusted R-square: 0.9997
RMSE: 0.0005497

840 h

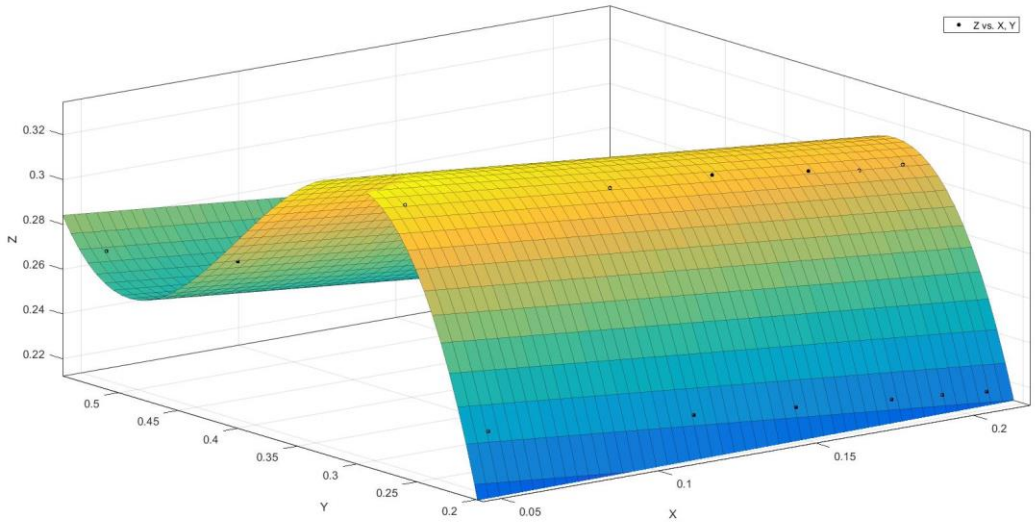

Figure 4. 28 : Plane for 840 h exposure using MATLAB – grain size (x), carbon content (y), reference/base/initial attenuation coefficient [z – f(x,y)] plane

Linear model Poly13:

f(x,y) = p00 + p10*x + p01*y + p11*x*y + p02*y^2 + p12*x*y^2 + p03*y^3 (19)

Coefficients (with 95% confidence bounds):

p00 = -1.152 (-1.167, -1.138)
p10 = -0.1349 (-0.1885, -0.08142)
p01 = 12.28 (12.16, 12.4)
p11 = 0.0002434 (-0.3171, 0.3176)
p02 = -32.46 (-32.77, -32.15)
p12 = -0.0003832 (-0.4265, 0.4257)
p03 = 27.12 (26.85, 27.39)

Goodness of fit:

SSE: 5.137e-06
R-square: 0.9998
Adjusted R-square: 0.9997
RMSE: 0.0005497

992 h

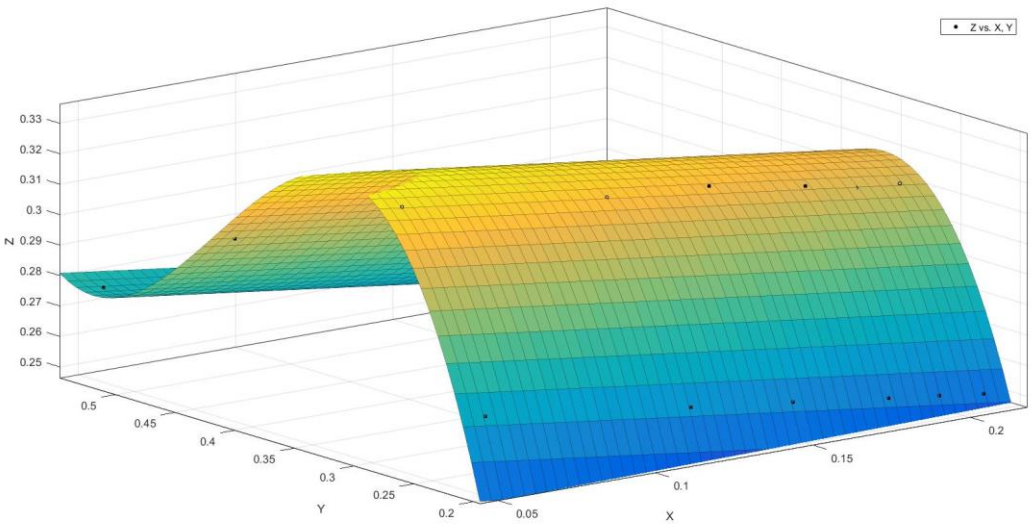

Figure 4. 29 : Plane for 992 h exposure using MATLAB – grain size (x), carbon content (y), reference/base/initial attenuation coefficient [z – f(x,y)] plane

Linear model Poly13:

f(x,y) = p00 + p10*x + p01*y + p11*x*y + p02*y^2 + p12*x*y^2 + p03*y^3 (20)

Coefficients (with 95% confidence bounds):

p00 = -0.5749 (-0.5894, -0.5605)
p10 = -0.1349 (-0.1885, -0.08142)
p01 = 7.344 (7.227, 7.461)
p11 = 0.0002434 (-0.3171, 0.3176)
p02 = -18.77 (-19.08, -18.47)
p12 = -0.0003832 (-0.4265, 0.4257)
p03 = 15.04 (14.78, 15.31)

Goodness of fit:

SSE: 5.137e-06
R-square: 0.9997
Adjusted R-square: 0.9996
RMSE: 0.0005497

All data related to these plots are given in the Appendix II.

Using the above database following relationships also can be developed (Figure 4.35). Those relationships could be used to plot the MATLAB plane for a given exposure time.

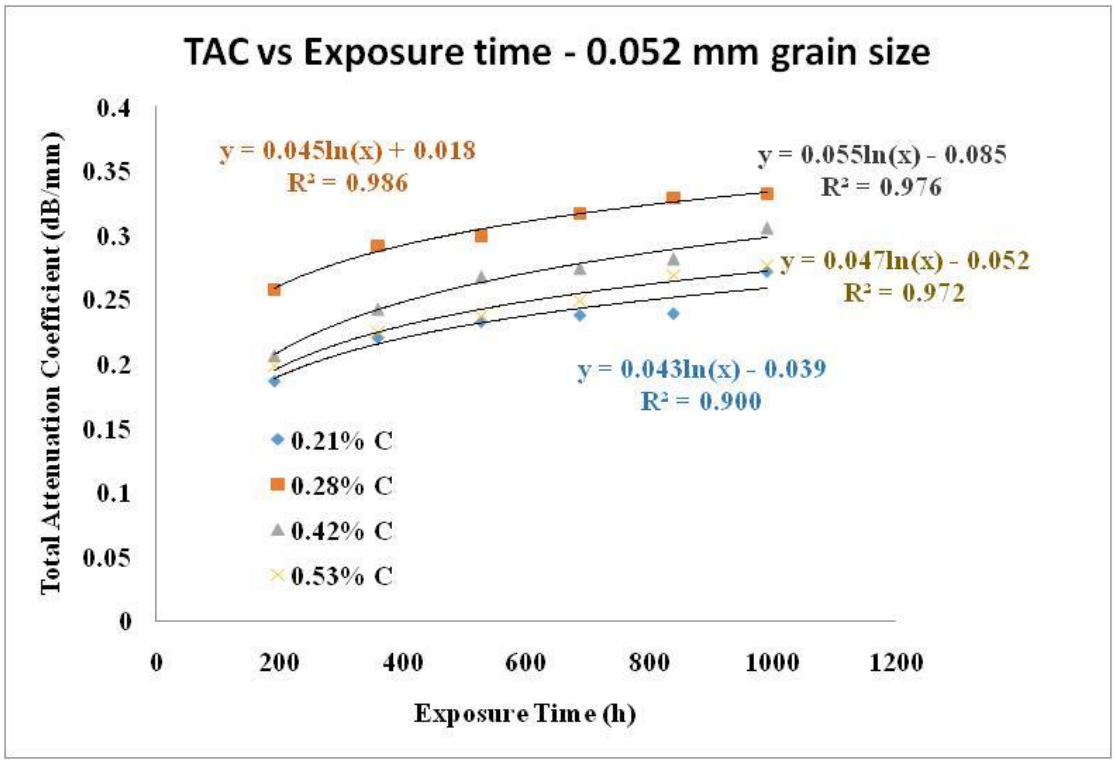

Figure 4. 30 : Total attenuation coefficient vs Exposure time for 0.052 mm grain size in 0.21% C, 0.28% C, 0.42% C and 0.53% C steels

Using these relationships, the Total Attenuation Coefficient of the above mentioned four different carbon contents could be found at a given exposure time. By subtracting the reference attenuation of the 0.052 mm grain size (for that particular composition) from this TAC, the difference of the attenuation coefficient could be found. That difference will be added to the reference values of other grain sizes to find the relevant TAC for them at the given time. Thus, the plane TAC plane related to a give exposure time could be plotted. This would be needed for the analysis described in the section 4.4.2.

4.4.2 Development of the SPSS model

As mentioned above, there are four main functions to be determined to express the degree of corrosion and the mechanical properties. Thus, four main mathematical models were generated to determine four dependable variables.

functions related to Weight Loss Per Area (WLPA), Corrosion Rate (CR), Penetration Depth of Corrosion (PDC) were analyzed using one data base and reaming load bearing capacity was analyzed using a separate data base.

Prior to the analysis and the generation of the models, the correlation among the WLPA, CR and PDC were analyzed since it is important to know the relationship between theses three response variables. According to the analysis it reflects that the three variables are having strong linear relationships. Thus, it has no problem in having three deferent models to talk about the three. since it is proven that they are having a linear relationship between each other.

SPSS analysis provides qualitative values regarding the correlation among these as given in the Table 4.5.

Table 4. 5: SPSS analysis of the correlation among WLPA, CR and PDC

Correlations

		CR	WLPA	PDC
CR	Pearson Correlation	1	.776**	.822**
	Sig. (2-tailed)		.008	.004
	N	10	10	10
WLPA	Pearson Correlation	.776**	1	.707*
	Sig. (2-tailed)	.008		.022
	N	10	10	10
PDC	Pearson Correlation	.822**	.707*	1
	Sig. (2-tailed)	.004	.022	
	N	10	10	10

**. Correlation is significant at the 0.01 level (2-tailed).

*. Correlation is significant at the 0.05 level (2-tailed).

The statistics of the model fit shows that all the coefficients in the model are significant at the t test. Pearson Correlation factors are closer to 0.8 and the significance is closer to 0.000 which are in satisfactory levels.

4.4.2.1 Mathematical Model -Weight Loss Per Area (WLPA)

Then WLPA was modelled (equation 21) it has a linear relationship among the carbon content (C Content), hours and the DAC (Difference in Attenuation Coefficient)

$$WLPA = -7719.656 + 8976.973(\text{Carbon Content}) + 29.821(\text{Hours}) + 58004.066(\text{DAC}) \quad (21)$$

Table 4. 6 : Coefficients related to WLPA model

Coefficients[a]

Model		Unstandardized Coefficients		Standardized Coefficients	t	Sig.	95.0% Confidence Interval for B		Collinearity Statistics	
		B	Std. Error	Beta			Lower Bound	Upper Bound	Tolerance	VIF
1	(Constant)	-7719.656	1684.645		-4.582	.000	-11258.963	-4180.349		
	CContent	8976.973	3134.792	.113	2.864	.010	2391.020	15562.926	.735	1.360
	Hours	29.821	1.585	.836	18.815	.000	26.491	33.151	.585	1.709
	DAC	58004.066	11728.799	.246	4.945	.000	33362.774	82645.358	.467	2.143

a. Dependent Variable: WLPA

Table 4. 7 :ANOVA analysis for WLPA model

ANOVA[a]

Model		Sum of Squares	df	Mean Square	F	Sig.
1	Regression	2096288578	3	698762859.4	282.746	.000[b]
	Residual	44484244.55	18	2471346.919		
	Total	2140772823	21			

a. Dependent Variable: WLPA

b. Predictors: (Constant), DAC, CContent, Hours

Table 4. 8 : Model summary for WLPA

Model Summary[b]

Model	R	R Square	Adjusted R Square	Std. Error of the Estimate	Durbin-Watson
1	.990[a]	.979	.976	1572.05182	2.023

a. Predictors: (Constant), DAC, CContent, Hours

b. Dependent Variable: WLPA

ANOVA table 4.7 shows that the model enough explains the version of data for WLPA. Since the significance values is less than 0.01, it can be said the even at 0.01 (1%) level the performance of the regression model is good. Normally in statistics 5 % is the level of the accuracy, but in this model, it is even lesser that 1 %. Therefore, it can be taken as a very accurate model.

For the model validation (Table 4.8), the model summary was taken. The R Square was analyzed. The R Square shows that 0.976 percent of the total variation of the data is explained by the model.

The histogram of the dependent variable WLPA (Figure 4.31), says that the residuals are normal.

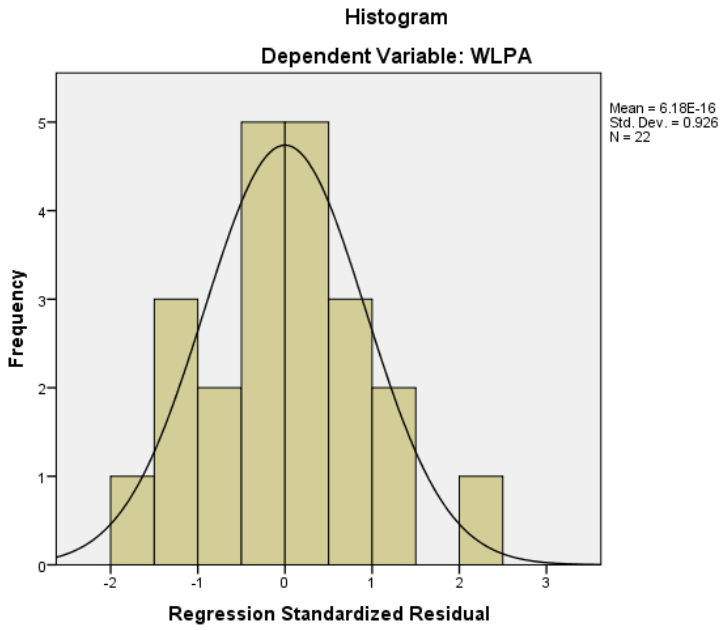

Figure 4. 31 : Histogram of the WPLA

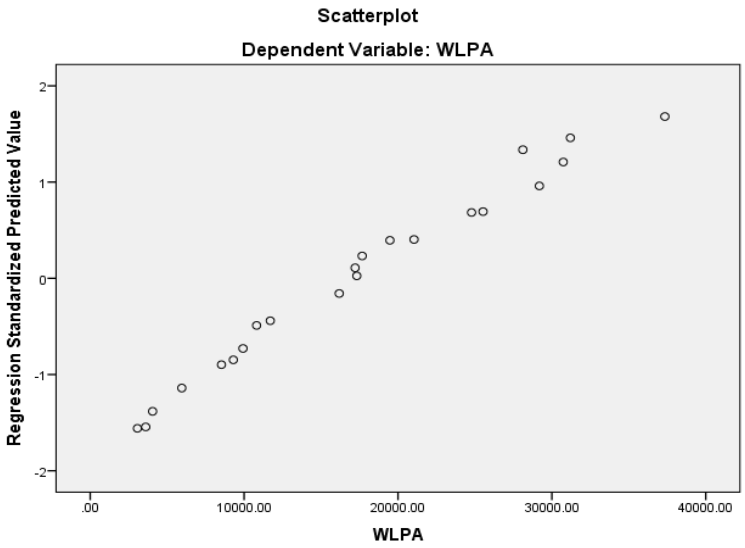

Figure 4. 32 : Regression standardized predicted values of WLPA

Further the models validities were confirmed by the predicted values, the predicted values are also lying along a straight line (Figure 4.32).

Carbon content and the hours (exposure time) could be known while the DAC should be measured. The direct measurement that would be taken in the site is the Total Attenuation (Coefficient). After taking that reading, the DAC should be calculated. For it is needed to be known the Reference Attenuation (Coefficient). RAC is a function of the carbon content and the grain size. Carbon content is known, but the grain size is unknown. To find the grain size, the MATLAB plane should be plotted. As described in the latter part of the section 4.4.1. if the exposure time is known the TAC – carbon content – grain size plane could be plotted. Then, the particular grain size for the particular TAC and the carbon content could be found. From that the relevant Reference Attenuation Coefficient point could be identified from the baseline correction or the reference plane. Thereby the DAC can be calculated and using the equation 21, WLPA could be found.

4.4.2.2 Mathematical Model - Corrosion rate (CR)

The mathematical model to find the Corrosion Rate (CR) was also developed (Equation 22)

Table 4. 9 : Coefficients related to CR model

Coefficients[a]

Model		Unstandardized Coefficients		Standardized Coefficients	t	Sig.	95.0% Confidence Interval for B		Collinearity Statistics	
		B	Std. Error	Beta			Lower Bound	Upper Bound	Tolerance	VIF
1	(Constant)	.675	.107		6.294	.000	.450	.901		
	CContent	.922	.200	.466	4.618	.000	.503	1.342	.735	1.360
	Hours	4.904E-006	.000	.006	.049	.962	.000	.000	.585	1.709
	DAC	6.138	.747	1.042	8.216	.000	4.568	7.707	.467	2.143

a. Dependent Variable: CR

$$CR = 0.675 + 0.922(\text{Carbon Content}) + 6.138(DAC) \qquad (22)$$

Here also the significance values are closer to 0.000 which are in satisfactory levels.

Table 4. 10 : ANOVA analysis of CR model

ANOVA[a]

Model		Sum of Squares	df	Mean Square	F	Sig.
1	Regression	1.156	3	.385	38.427	.000[b]
	Residual	.180	18	.010		
	Total	1.336	21			

a. Dependent Variable: CR

b. Predictors: (Constant), DAC, CContent, Hours

ANOVA Table 4.10 shows that the significance value is less than 0.01.

In the model validation Table 4.11, the R Square was 0.842 which is in an acceptable range.

Table 4. 11 : Model summary for CR

Model Summary[b]

Model	R	R Square	Adjusted R Square	Std. Error of the Estimate	Durbin-Watson
1	.930[a]	.865	.842	.10013	3.101

a. Predictors: (Constant), DAC, CContent, Hours

b. Dependent Variable: CR

4.4.2.3 Mathematical Model – Penetration Depth of Corrosion (PDC)

Equation 23 gives the model to find the Penetration Depth of Corrosion (PDC)

Table 4. 12 : Coefficients related to PDC model

Coefficients[a]

Model		Unstandardized Coefficients		Standardized Coefficients	t	Sig.	95.0% Confidence Interval for B		Collinearity Statistics	
		B	Std. Error	Beta			Lower Bound	Upper Bound	Tolerance	VIF
1	(Constant)	-39.259	45.249		-.868	.414	-146.256	67.739		
	DAC	1363.731	400.562	.703	3.405	.011	416.552	2310.910	.765	1.308
	Hours	.118	.085	.287	1.389	.208	-.083	.319	.765	1.308

a. Dependent Variable: PDC

$$PDC = 1363.731(DAC) \qquad (23)$$

Since the 0.95 % confidence interval for the coefficient values are varying in between plus and minus range for the constant and the hours, they were not included for the model. Only the DAC is under the significant range.

Table 4. 13 : ANOVA analysis of PDC model

ANOVA[a]

Model		Sum of Squares	df	Mean Square	F	Sig.
1	Regression	68900.212	2	34450.106	11.842	.006[b]
	Residual	20363.602	7	2909.086		
	Total	89263.813	9			

a. Dependent Variable: PDC

b. Predictors: (Constant), Hours, DAC

Table 4. 14 : Model summary of PDC

Model Summary[b]

Model	R	R Square	Adjusted R Square	Std. Error of the Estimate	Durbin-Watson
1	.879[a]	.772	.707	53.93594	1.970

a. Predictors: (Constant), Hours, DAC

b. Dependent Variable: PDC

ANOVA table and the model summary are also providing evidence regarding the accuracy of the PDC model, as descried in the WPLA and CR models.

4.4.2.4 Mathematical Model – Remaining Load Bearing Capacity

$$\text{Remaining Load-Bearing Capacity} = 17152e^{-9E-04(WLPA)} \quad (24)$$

4.5 Validation of models

To ensure the accuracy and the correctiveness of the developed models, two sets of random samples were tested. Then the experimental values and the values obtained from the models were compared.

Validation samples:

Chemical composition:

Carbon content: 0.26 C / Plain carbon steel

Table 4. 15 : Chemical composition of 0.26% C steel

C %	Si%	Mn%	Cu%	P%	S%	Cr%	Ni%	Al%	Fe%
0.26	0.21	0.72	0.142	0.071	0.041	0.115	0.076	0.0034	98.3

Exposure time:

1. 216 hours
2. 352 hours

Total Attenuation Coefficient (TAC) :

216 hours -248 dB/mm

352 hours – 271 dB/mm

Experimental results:

216 h

Table 4. 16 : Experimental results for 216 h exposure time

Parameter	Experimental Value
WLPA	6125.471 g/m^2
CR	1.517 mm/yr
PDC	111.80 μm

352 h

Table 4. 17 : Experimental results for 352 h exposure time

Parameter	Experimental Value
WLPA	10780.584 g/m^2
CR	1.633 mm/yr

Results obtained from mathematical model:

<u>216 h:</u>

MATLAB plane for 216 h exposure time:

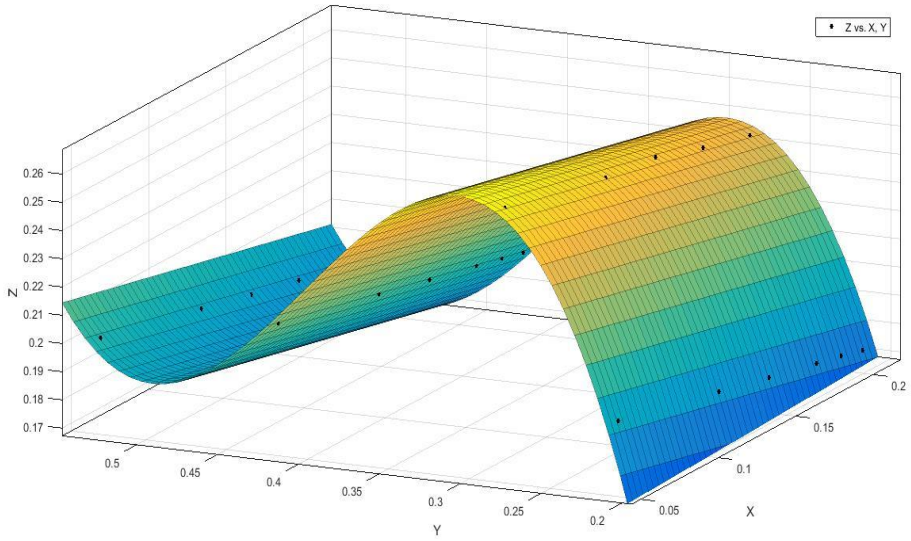

Figure 4. 33 : MATLAB plot -Validation of 0.26% C at 216 h grain size (x), carbon content (y), reference/base/initial attenuation coefficient [z – f(x,y)] plane

Linear model Poly13:

f(x,y) = p00 + p10*x + p01*y + p11*x*y + p02*y^2 + p12*x*y^2 + p03*y^3 (25)

Coefficients (with 95% confidence bounds):

p00 = -0.9848 (-0.9993, -0.9704)
p10 = -0.1349 (-0.1885, -0.08142)
p01 = 10.5 (10.39, 10.62)
p11 = 0.0002434 (-0.3171, 0.3176)
p02 = -28.11 (-28.42, -27.8)
p12 = -0.0003832 (-0.4265, 0.4257)
p03 = 23.66 (23.39, 23.92)

Goodness of fit:
SSE: 5.137e-06
R-square: 0.9997
Adjusted R-square: 0.9997
RMSE: 0.0005497

X, which denotes the relevant grain size of the specimen, could be found using following known parameters:

Y = C Content = 0.26

f(x,y) = Z = Total Attenuation Coefficient (dB/mm) = 0.248

Therefore,

X = Grain size (mm) = 0.095

This can be used to find the relevant Reference Attenuation Coefficient (RAC) for 0.26% C steel using the reference plane given in the Figure 4.28 in section 4.4.

X = Grain Size (mm) = 0.095

Y = Carbon Content = 0.26

Therefore,

f(x,y) = Z = Reference Attenuation Coefficient(dB/mm)= 0.154

Difference in Attenuation Coefficient (DAC) could be found.

DAC = TAC - RAC

DAC = 0.248 – 0.154 dB/mm = 0.094 dB/mm

<u>Using these values to SPSS Models:</u>

Carbon Content = 0.26 Hours = 216 DAC = 0.094

WLPA= -7719.656 + 8976.973(Carbon Content) +29.821(Hours) +58004.066(DAC)

WLPA= 6502.375 g/m^2

CR= 0.675 + 0.922(Carbon Content) +6.138(DAC)

CR = 1.517 mm/year

PDC= 1363.731(DAC)

PDC= 111.79 ɥm

352 h:

MATLAB plane for 352 h exposure time:

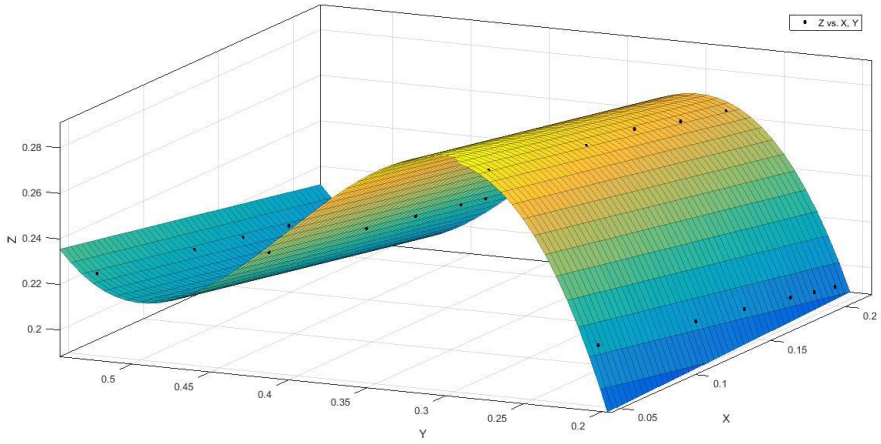

Figure 4. 34 : MATLAB plot -Validation of 0.26% C at 352 h

grain size (x), carbon content (y), reference/base/initial attenuation coefficient [z – f(x,y)] plane

Linear model Poly13:

f(x,y) = p00 + p10*x + p01*y + p11*x*y + p02*y^2 + p12*x*y^2 + p03*y^3 (26)

Coefficients (with 95% confidence bounds):

p00 = -0.9329 (-0.9474, -0.9185)
p10 = -0.1349 (-0.1885, -0.08142)
p01 = 10.16 (10.05, 10.28)
p11 = 0.0002434 (-0.3171, 0.3176)
p02 = -26.95 (-27.25, -26.64)
p12 = -0.0003832 (-0.4265, 0.4257)
p03 = 22.47 (22.2, 22.74)

Goodness of fit:

SSE: 5.137e-06
R-square: 0.9997
Adjusted R-square: 0.9997
RMSE: 0.0005497

X, which denotes the relevant grain size of the specimen, could be found using following known parameters:

Y = C Content = 0.26

f(x,y) = Z = Total Attenuation Coefficient (dB/mm) = 0.271

Therefore,

X = Grain size (mm) = 0.080

This can be used to find the relevant Reference Attenuation Coefficient (RAC) for 0.26% C steel using the reference plane given in the Figure 4.28 in section 4.4.

X = Grain Size (mm) = 0.080

Y = Carbon Content = 0.26

Therefore,

f(x,y) = Z = Reference Attenuation Coefficient(dB/mm) = 0.156

Difference in Attenuation Coefficient (DAC) could be found.

DAC = TAC - RAC

DAC = 0.271 – 0.156 dB/mm = 0.115 dB/mm

<u>Using these values to SPSS Models:</u>

Carbon Content = 0.26 Hours = 352 DAC = 0.115

WLPA= -7719.656 + 8976.973(Carbon Content) +29.821(Hours) +58004.066(DAC)

WLPA= 11774.799 g/m2

CR= 0.675 + 0.922(Carbon Content) +6.138(DAC)

CR = 1.620 mm/year

Validation - Summary:

Table 4. 18 : : Validation results - summary

216 h				
Parameter to express degree of corrosion	Value obtained from the mathematical model	Experimental Value	Difference	% Error
WLPA (g/mm^2)	6502.375	6125.471	-376.903	-6.153
CR (mm/yr)	1.491	1.517	0.0251	1.656
PDC (μm)	128.06	111.80	-16.258	14.541
352 h				
WLPA (g/mm^2)	11774.799	10780.584	-994.215	-9.222
CR (mm/yr)	1.620	1.633	0.013	0.798

The percentage errors of the results obtained from the model and the experiments are below 15 %. In most of the cases it is even below 10%. These provide the evidences that the developed model could be validated with an acceptable accuracy.

4.6 Analysis of the fatigue results

Table 4. 19: Experimental fatigue results

Set	Hours	Average Fatigue Cycles to failure (x100)	Minimum Fatigue Cycles to failure (x100)
1 (2 weeks)	336	2902	925
2 (4 weeks)	672	1900	1134
3 (6 weeks)	1008	1665	660
4 (8 weeks)	1344	1274	536
5 (10 weeks)	1680	738	330

The corroded samples (6 per each set) were tested by the fatigue machine. Average and the minimum fatigue lives are given in the Table 4.20.

Then the theoretical calculations based on the mass loss/weight loss analysis were done to see whether the theoretical (weight loss reduction based) calculations would be accurate enough to predict the fatigue live of corroded samples. The retained mass vs corrosion duration is given in the Figure 4.35 and using those values the remaining cross sectional area of corroded samples were calculated (Table 4.20).

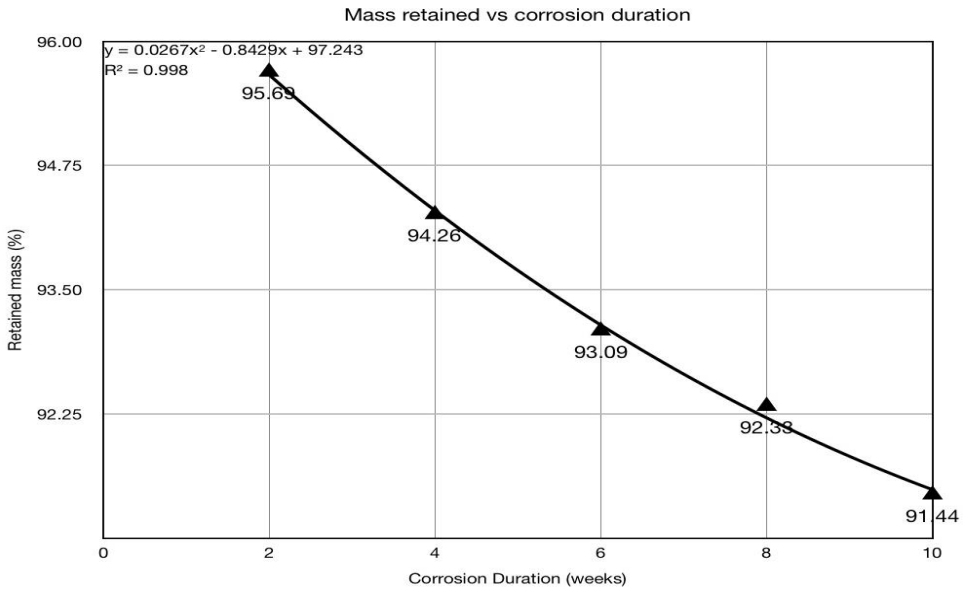

Figure 4. 35: Mass retained with the corrosion duration

Table 4. 20: Remaining thickness of the corroded samples

Calculated remaining thicknesses	
Set	**Calculated remaining thickness (mm)**
0 (Stock)	0.9 (stock)
1	0.860
2	0.848
3	0.838
4	0.831
5	0.823

Using these thickness values for each set, a fatigue sample was modeled in ABAQUS FEA software.

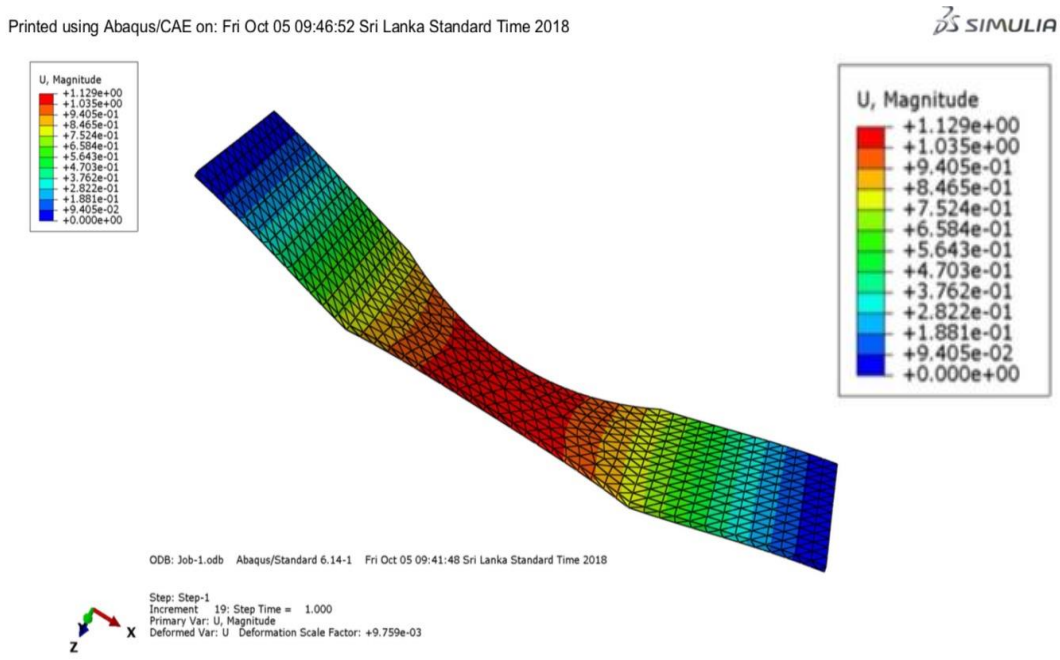

Figure 4. 36: Modeled fatigue sample for the stock

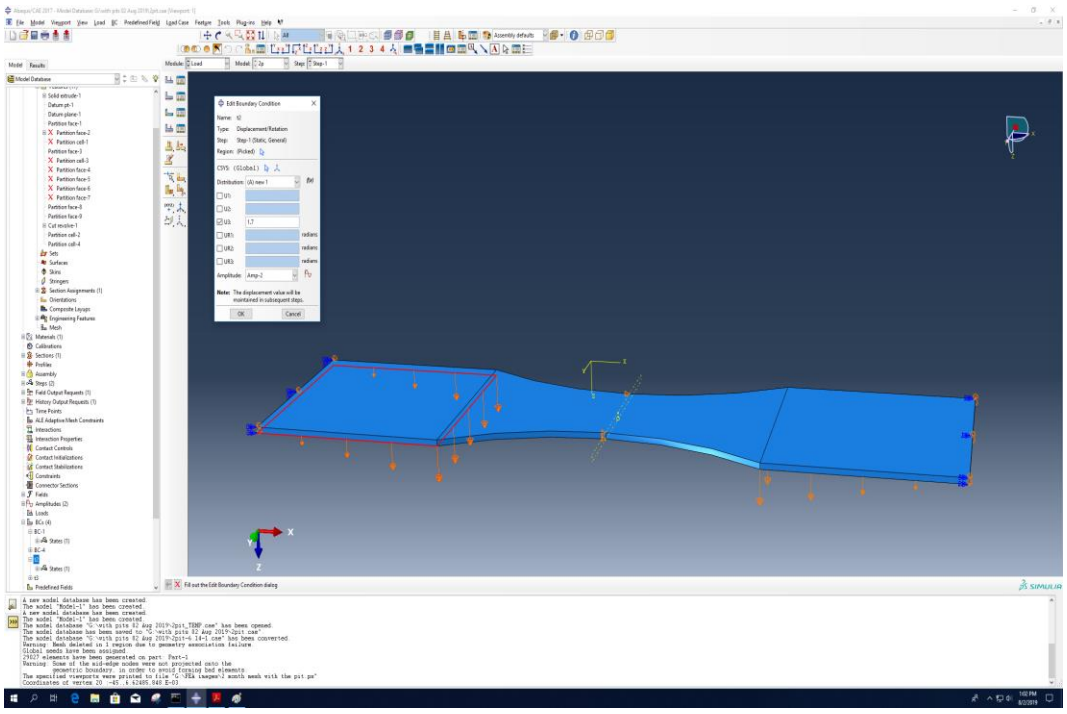

Figure 4. 37: Finite Element Methods – adding displacement equation and time function

FEA models were the run under fe-safe fatigue analysis software. This software provides fatigue lives once the FEA model files are feed. The above sample set which has thickness reductions with the time shows higher fatigue lives than the practical fatigue lives (Figure 4.38). Means there is a disparity. This result provides evidence that, there is some other factor which affects the fatigue life of corroded steels and the thickness reduction alone cannot be taken to predict the actual fatigue lives.

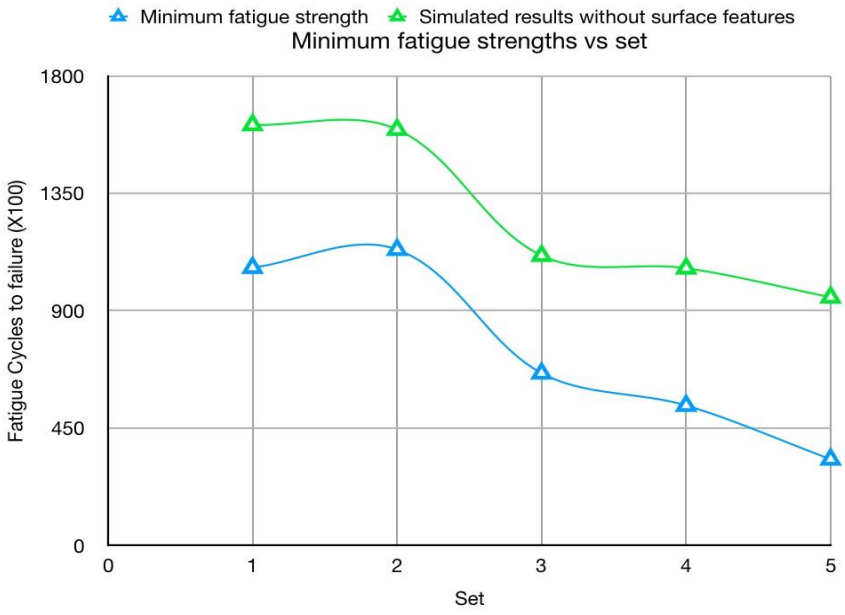

Figure 4. 38: Fatigue lives of corroded samples –Modeled and actual (Practical)

According to the literature [34][35][36] the fatigue life is also affected by the corrosion pits/penetrations and the roughened surface of the material. Therefore during this research work an attention was paid to incorporate the corrosion pits/penetrations in to the surface of the FEA model which already has the thickness reduction. MountainsMap®, surface developing software was utilized to construct the topology including the pits/penetrations occurred due to corrosion. First the corrosion

layers were removed from the sample. Then two SEM images were taken in two different tilt angles. These two images used as the input to the software and those could generate the 3D image with the roughened topology which happened due to corrosion damages.

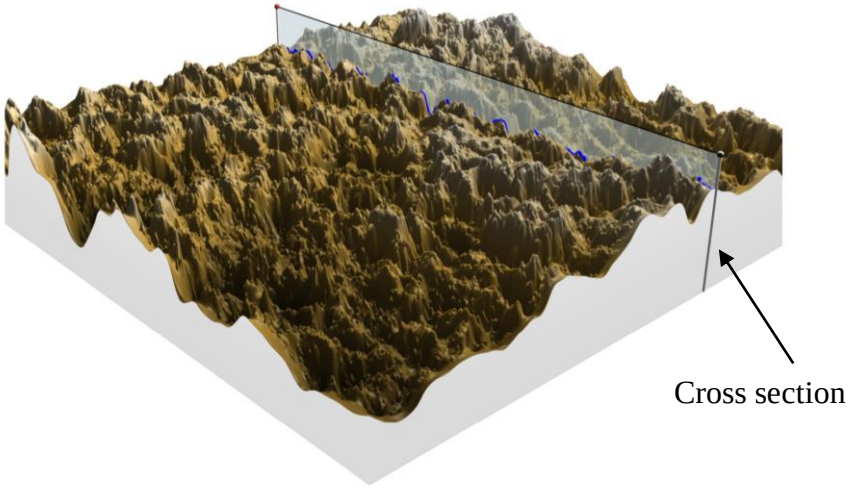

Figure 4. 39: 3D construction obtained from the SEM images

A cross section from the required place of the 3D image could be taken as shown in the Figure 4.39. The waviness depths (could be referred to as pits/penetrations) for the relevant cross section are also developed by the software (Figure 4.40). These profile curves provide the information for the evaluation of the pit geometry, the pit shape and the depth.

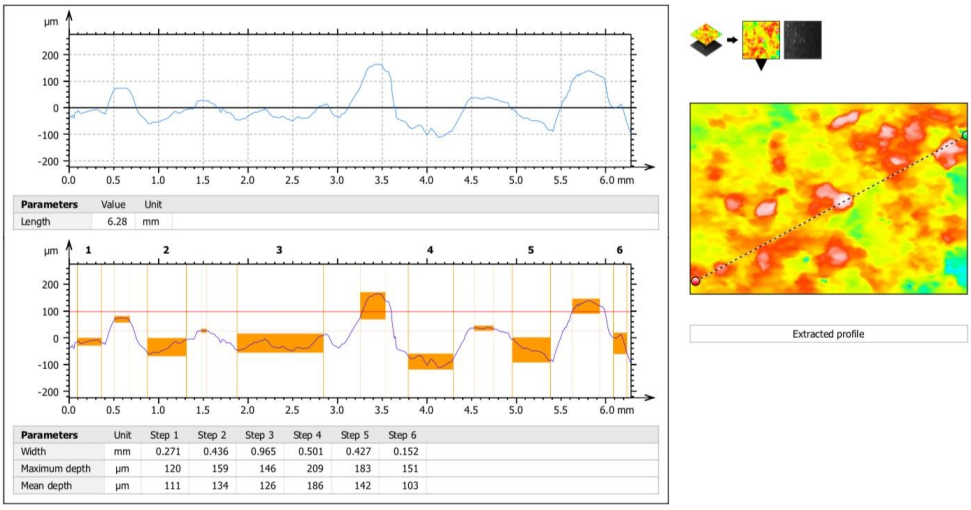

Figure 4. 40: Evaluation of pit geometries

Fatigue life strongly depends on the pit geometry. In this research, the particular critical geometry was found using the profile curves obtained from the 3D model (Figure 4.40 and 4.41).

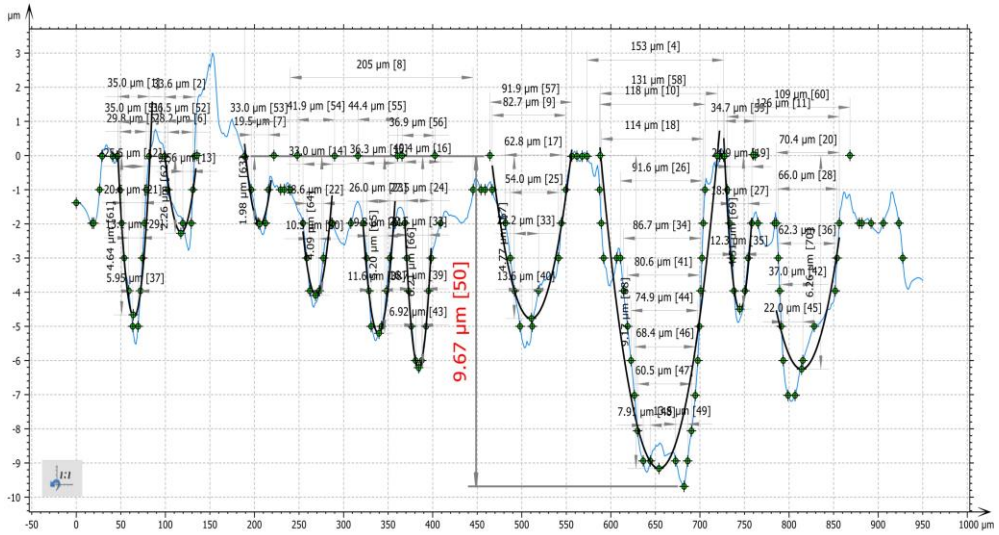

Figure 4. 41: Determination of the critical geometries

Table 4.22 shows the obtained depth/radius ratios of the pits in corroded sets.

Table 4. 21: Depth/Radius of the penetrations/pits in corroded samples

Set	Topographical depth/radius ratio
1	0.381465
2	0.403742
3	0.421633
4	0.114151
5	0.480714

Then the relevant critical pit geometries which were obtained as described above could be modeled in on surface of the FEA fatigue samples.

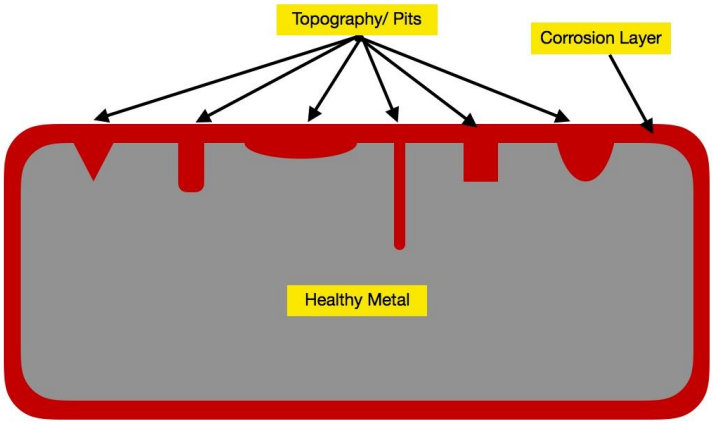

Figure 4. 42: Different pit geometries on a sample surface

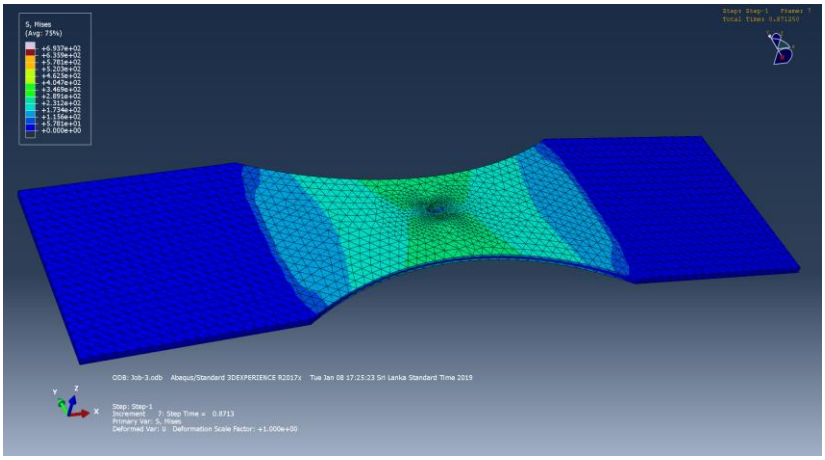

(a)

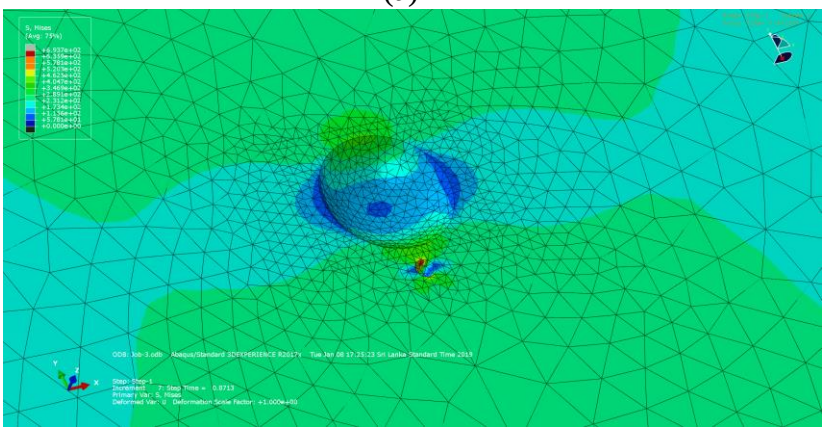

(b)

Figure 4. 43: (a) A modeled pit on a FEA fatigue model

(b) Magnified pit

Then the each model which represents the cumulative effect of the thickness reduction and the pit geometry/surface features were run under fe-safe software. Critical surface geometries were modeled in Abaqus FEA using 3D revolve cut followed by filleting of the edges. The cuts were placed in the middle of the specimen surface top in all models

as seen in Figure 4.43 (a). Fatigue life varies with the location of the surface feature. However as an initiative, the feature was placed in the middle of the surface.

Then the practical/experimental fatigue value, FEA fatigue value - without surface features, FEA fatigue value - with surface features were plotted against the sets (Figure 4.44) and against the relevant WLPA(Figure 4.45) of the samples.

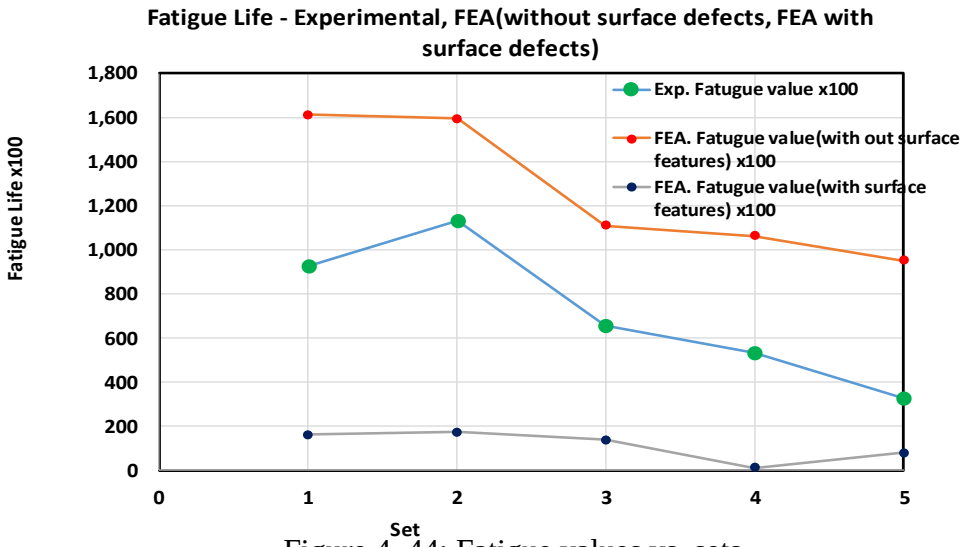

Figure 4. 44: Fatigue values vs. sets

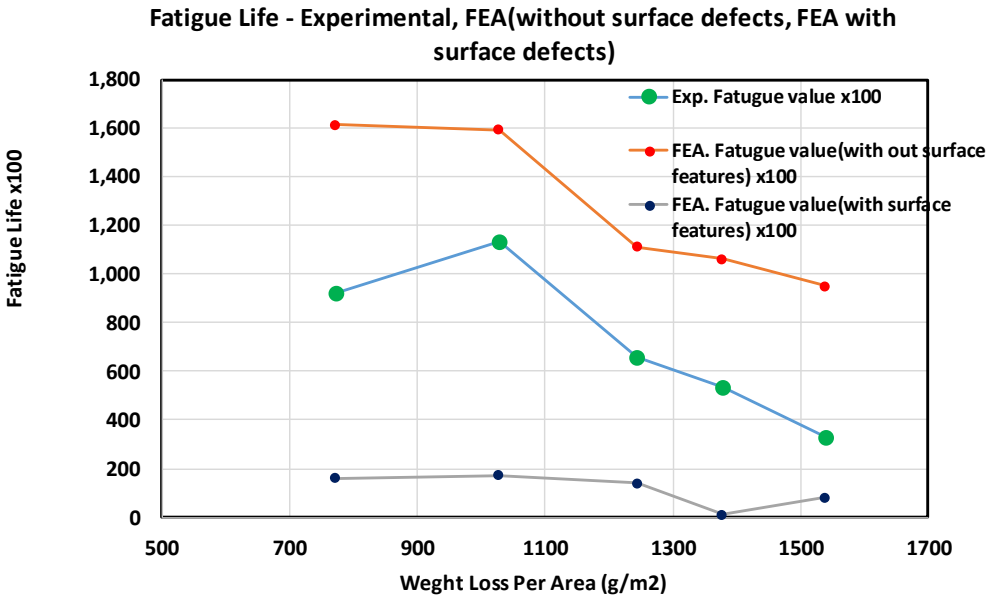

Figure 4. 45: Fatigue lives vs WLPA

Even though we expected to have similar values, the resulted fatigue lives for the models with surface features shows very low fatigue lives as seen in Figure 4.55 or Figure 4.56. These results are highly distant to experimental results. Few major reasons were accountable for this severe drop in fatigue strength. In finite element models with surface features, the stresses reached upper elastic region of the metal, making them prone to initiate the fatigue crack at pits (surface irregularities). However, the FEA models without surface features had no such high stressed regions. Therefore, a higher fatigue life prediction was made for all the regions in those models.

The metal stock used for the experimental fatigue testing had different properties compared to which was used in fe-safe. BS-1005 (the available material in the fe-safe library which is closer to the experimented steel) steel was used for the fatigue analysis in fe-safe, since its carbon content was similar to which in the experimental steel stock(0.05%.wt). BS-1005 has a young's modulus of 190MPa, however the experimental steel had only a Young's modulus of 3.1MPa, showing a great difference in ductility. This difference could be the reason for the drop-in fatigue strength of fe-safe model. FEA models were consisted with a single surface feature only. However, in reality there were hundred thousand of mild pits were present on the surface. As an initial step for an approach from Finite Element Modelling, this single feature model was developed. It is recommended that further improvements should be carried out considering the distribution and population of the surface features (pits) of the model.

Following conclusions could be obtained from the experiments and the study carried out.

- Finite Element Modelling in combination with fe-safe® and mountainsmap® is able to predict the effect of surface topography on fatigue life, more accurately compared to existing industrial practices. Utilization of both mass-loss analysis and topographical evaluation makes the result more accurate.

- Dimensions of topographical features were close ranged, throughout the surface of atmospherically corroded low carbon steel, due to the uniformity of the corrosion layer.
- Components with basic and complex surface topographical features can be evaluated for fatigue performance using FEA.

5 CONCLUSION

The outcome of this research revealed that the, conventional weight loss analysis cannot give a complete picture of the actual corrosion and also the loss of absolute load-bearing capacity due to corrosion cannot be predicted accurately using a conventional measurement of degree of corrosion (such as mass-loss analysis) alone. The ultrasound attenuation is an accurate, reliable and nondestructive method to determine the actual amount of the degree of corrosion and to predict regarding the remaining load bearing capacity and thereby the loss of performance under the load bearing ability. These finding can be summed up as,

WLPA= -7719.656 + 8976.973(Carbon Content)+29.821(Hours) +58004.066(DAC)

CR= 0.675 + 0.922(Carbon Content)+6.138(DAC)

PDC= 1363.731(DAC)

Remaining Load-Bearing Capacity = 17152e-9E-04(WLPA)

Where,

WLPA= Weight Loss Per unit Area

CR = Corrosion Rate

PDC = Penetration Depth of Corrosion

In the way of achieving these following are also concluded.

- A logarithmic relationship was found between attenuation coefficient and corrosion rate.
- Steel containing 0.28%C steel shows the highest rate of corrosion while 0.21%C steel shows the lowest rate; 0.42%C and 0.53%C steel show intermediate

corrosion rates. This implies that rate of corrosion does not linearly vary with the carbon content and it depends on the amount of ferrite and pearlite present.

- The penetration of corrosion beyond the general attack increases steadily with time in accordance with the power function proposed for the deterioration of properties of corroded members.

6 SUGGESIONS AND FURTHER DEVELOPMENTS

1. In the analysis of the effect of carbon content on corrosion, as a correction factor, more samples with different carbon contents should be get involved to finetune the results and also to find the exact carbon content which would have maximum corrosion.

2. The same recommendation given 2 should be carried our for more number of grain sizes which are related to more number of carbon contents.

3. Ferrite and pearlite percentages in corroded samples should be analyzed under scanning electron microscope to observe and quantify which would be more susceptible to corrosion attack. The differential corrosion of the ferrite and pearlite phases could be studied to determine whether the penetration of corrosion progresses along any one microstructure, since preliminary research has shown that pearlite is more susceptible to corrosion due to its forming a galvanic couple between the ferrite and cementite lamellae.

4. The measurement of penetration was done for a projected vertical depth. The use of an absolute fit and a higher number of readings may provide better results.

5. The entire methodology of the project ought to be re-simulated and carried out for an atmospheric corrosion/marine conditions scenario. This will be able to verify the applicability of the theories formulated herein, such as whether the penetration of corrosion progresses accordance with the derived correlations in such conditions or if it will be severely limited due to the absence of HCl as an accelerator.

6. Asymmetric double sigmoidal function or a similar function can be used to further analysis of the results related with C Content.

7. Develop the surface topology analysis model using roughness parameters for a better accuracy.
8. Further developments are recommended with appropriate material properties, preferably with a standard steel for the experimental fatigue testing. A result with a higher accuracy can be achieved with such apparatus. The research should be extended beyond 992 hours.

7 REFERENCES

[1] G. Koch, J. Varney, N. Thopson, O. Moghissi, M. Gould, and J. Payer, "International Measures of Prevention , Application , and Economics of Corrosion Technologies Study," *NACE International*, 2016. http://impact.nace.org (accessed May 29, 2017).

[2] V. S. Moura, L. D. Lima, J. M. Pardal, A. Y. Kina, R. R. A. Corte, and S. S. M. Tavares, "Influence of microstructure on the corrosion resistance of the duplex stainless steel UNS S31803," *Mater. Charact.*, vol. 59, no. 8, pp. 1127–1132, 2008, doi: 10.1016/j.matchar.2007.09.002.

[3] S. J. Oh, D. C. Cook, and H. E. Townsend, "Atmospheric corrosion of different steels in marine, rural and industrial environments," *Corros. Sci.*, vol. 41, no. 9, pp. 1687–1702, Aug. 1999, doi: 10.1016/S0010-938X(99)00005-0.

[4] J. F. Marco, M. Gracia, J. R. Gancedo, M. A. Martín-Luengo, and G. Joseph, "Characterization of the corrosion products formed on carbon steel after exposure to the open atmosphere in the Antarctic and Easter Island," *Corros. Sci.*, vol. 42, no. 4, pp. 753–771, Apr. 2000, doi: 10.1016/S0010-938X(99)00090-6.

[5] S. Feliu, M. Morcillo, and S. Feliu, "The prediction of atmospheric corrosion from meteorological and pollution parameters-II. Long-term forecasts," *Corros. Sci.*, vol. 34, no. 3, pp. 415–422, 1993, doi: 10.1016/0010-938X(93)90113-U.

[6] T. T. N. Lan *et al.*, "The effects of air pollution and climatic factors on atmospheric corrosion of marble under field exposure," *Corros. Sci.*, vol. 47, no. 4, pp. 1023–1038, 2005, doi: 10.1016/j.corsci.2004.06.013.

[7] A. R. Mendoza and F. Corvo, "Outdoor and indoor atmospheric corrosion of carbon steel," *Corros. Sci.*, vol. 41, no. 1, pp. 75–86, 1999, doi: 10.1016/S0010-938X(98)00081-X.

[8] S. Palraj, M. Selvaraj, K. Maruthan, and M. Natesan, “Kinetics of atmospheric corrosion of mild steel in marine and rural environments,” *J. Mar. Sci. Appl.*, vol. 14, no. 1, pp. 105–112, 2015, doi: 10.1007/s11804-015-1286-x.

[9] M. Morcillo, D. De La Fuente, I. Díaz, and H. Cano, “Atmospheric corrosion of mild steel,” *Rev. Metal.*, vol. 47, no. 5, pp. 426–444, 2011, doi: 10.3989/revmetalm.1125.

[10] D. de la Fuente, J. Alcántara, B. Chico, I. Díaz, J. A. Jiménez, and M. Morcillo, “Characterisation of rust surfaces formed on mild steel exposed to marine atmospheres using XRD and SEM/Micro-Raman techniques,” *Corros. Sci.*, vol. 110, pp. 253–264, 2016, doi: 10.1016/j.corsci.2016.04.034.

[11] P. Dillmann, F. Mazaudier, and S. Hœrlé, “Advances in understanding atmospheric corrosion of iron. I. Rust characterisation of ancient ferrous artefacts exposed to indoor atmospheric corrosion,” *Corros. Sci.*, vol. 46, no. 6, pp. 1401–1429, 2004, doi: 10.1016/j.corsci.2003.09.027.

[12] R. N. Parkins, “Pergamon THE INTERGRANULAR CORROSION AND STRESS CORROSION CRACKING OF MILD STEEL IN CLARKE ’ S SOLUTION removing corrosion products from steel samples , the exposure period to the stirred,” vol. 36, no. 12, pp. 2097–2110, 1994.

[13] K. K. and S. P. S. Lee, “Kinetics of intergranular corrosion and separation between initiation and propagation of stress corrosion crack in mild steel,” *Scr. Metall.*, vol. 22, no. 1, pp. 31–34, 1988, doi: 10.1016/B978-0-444-40976-8.50013-5.

[14] M. Morcillo, B. Chico, I. Díaz, H. Cano, and D. de la Fuente, “Atmospheric corrosion data of weathering steels. A review,” *Corros. Sci.*, vol. 77, pp. 6–24, 2013, doi: 10.1016/j.corsci.2013.08.021.

[15] Y. Ma, Y. Li, and F. Wang, “Corrosion of low carbon steel in atmospheric

environments of different chloride content," *Corros. Sci.*, vol. 51, no. 5, pp. 997–1006, 2009, doi: 10.1016/j.corsci.2009.02.009.

[16] Y. M. Panchenko and A. I. Marshakov, "Long-term prediction of metal corrosion losses in atmosphere using a power-linear function," *Corros. Sci.*, vol. 109, pp. 217–229, 2016, doi: 10.1016/j.corsci.2016.04.002.

[17] Y. M. Panchenko, A. I. Marshakov, T. N. Igonin, V. V. Kovtanyuk, and L. A. Nikolaeva, "Long-term forecast of corrosion mass losses of technically important metals in various world regions using a power function," *Corros. Sci.*, vol. 88, pp. 306–316, 2014, doi: 10.1016/j.corsci.2014.07.049.

[18] R. Landolfo, L. Cascini, and F. Portioli, "Modeling of metal structure corrosion damage: A state of the art report," *Sustainability*, vol. 2, no. 7, pp. 2163–2175, 2010, doi: 10.3390/su2072163.

[19] X. Zhong, X. Wu, and E. H. Han, "Characteristics of Oxidation and Oxygen Penetration of Alloy 690 in 600 °C Aerated Supercritical Water," *J. Mater. Sci. Technol.*, vol. 34, no. 3, pp. 561–569, 2018, doi: 10.1016/j.jmst.2016.11.001.

[20] R. Avci *et al.*, "A practical method for determining pit depths using X-ray attenuation in EDX spectra," *Corros. Sci.*, vol. 93, pp. 9–18, 2015, doi: 10.1016/j.corsci.2014.12.018.

[21] A. V. Girão, G. Caputo, and M. C. Ferro, "Application of Scanning Electron Microscopy–Energy Dispersive X-Ray Spectroscopy (SEM-EDS)," *Compr. Anal. Chem.*, vol. 75, pp. 153–168, 2017, doi: 10.1016/bs.coac.2016.10.002.

[22] Y. Zhou and Y. Zuo, "The Intergranular Corrosion of Mild Steel in CO2 + NaNO2 Solution," *Electrochim. Acta*, vol. 154, pp. 157–165, 2015, doi: 10.1016/j.electacta.2014.12.053.

[23] X. X. Ye *et al.*, "The high-temperature corrosion of Hastelloy N alloy (UNS

N10003) in molten fluoride salts analysed by STXM, XAS, XRD, SEM, EPMA, TEM/EDS," *Corros. Sci.*, vol. 106, pp. 249–259, 2016, doi: 10.1016/j.corsci.2016.02.010.

[24] T. C. and F.Lansing, "Corrosion Mechanism." .

[25] T. Bellezze, G. Giuliani, A. Viceré, and G. Roventi, "Study of stainless steels corrosion in a strong acid mixture. Part 2: anodic selective dissolution, weight loss and electrochemical impedance spectroscopy tests," *Corros. Sci.*, vol. 130, no. October, pp. 12–21, 2018, doi: 10.1016/j.corsci.2017.10.010.

[26] A. A. Almusallam, "Effect of degree of corrosion on the properties of reinforcing steel bars," *Constr. Build. Mater.*, vol. 15, no. 8, pp. 361–368, 2001, doi: 10.1016/S0950-0618(01)00009-5.

[27] H. S. Lee and Y. S. Cho, "Evaluation of the mechanical properties of steel reinforcement embedded in concrete specimen as a function of the degree of reinforcement corrosion," *Int. J. Fract.*, vol. 157, no. 1–2, pp. 81–88, 2009, doi: 10.1007/s10704-009-9334-7.

[28] C. A. Apostolopoulos and V. G. Papadakis, "Consequences of steel corrosion on the ductility properties of reinforcement bar," *Constr. Build. Mater.*, vol. 22, no. 12, pp. 2316–2324, 2008, doi: 10.1016/j.conbuildmat.2007.10.006.

[29] W. Zhang, X. Song, X. Gu, and S. Li, "Tensile and fatigue behavior of corroded rebars," *Constr. Build. Mater.*, vol. 34, pp. 409–417, 2012, doi: 10.1016/j.conbuildmat.2012.02.071.

[30] Ohga, M, Appuhamy, J.M.R.S, Kaita, T, Fujii, K, and Dissanayake, P.B.R, "Evaluation of Tensile Strength Deterioration of Bridge Plates Due To Corrosion," *Int. Conf. Sustain. Built Environ.*, no. December, pp. 521–528, 2010.

[31] T. Kaita, J. M. R. S. Appuhamy, K. Itogawa, M. Ohga, and K. Fujii,

"Experimental study on remaining strength estimation of corroded wide steel plates under tensile force," *Procedia Eng.*, vol. 14, pp. 2707–2713, 2011, doi: 10.1016/j.proeng.2011.07.340.

[32] Y. Wang, J. A. Wharton, and R. A. Shenoi, "Ultimate strength analysis of aged steel-plated structures exposed to marine corrosion damage: A review," *Corros. Sci.*, vol. 86, pp. 42–60, 2014, doi: 10.1016/j.corsci.2014.04.043.

[33] Y. Wang, S. Xu, H. Wang, and A. Li, "Predicting the residual strength and deformability of corroded steel plate based on the corrosion morphology," *Constr. Build. Mater.*, vol. 152, pp. 777–793, 2017, doi: 10.1016/j.conbuildmat.2017.07.035.

[34] M. Weber, P. D. Eason, H. Özdeş, and M. Tiryakioğlu, "The Effect of Surface Corrosion Damage on the Fatigue Life of Extruded Aluminum Alloy 6061-T6," University of North Florida, 2017.

[35] X. Y. Zhang, S. X. Li, R. Liang, and R. Akid, "Effect of corrosion pits on fatigue life and crack initiation," *13th Int. Conf. Fract. 2013, ICF 2013*, vol. 2, pp. 1667–1675, 2013.

[36] R. Rahgozar and Y. Sharifi, "Remaining fatigue life of corroded steel structural members," *Adv. Struct. Eng.*, vol. 14, no. 5, pp. 881–890, 2011, doi: 10.1260/1369-4332.14.5.881.

[37] S. Al-Shahrani and T. J. Marrow, "Effect of surface finish on fatigue of stainless steels," *12th Int. Conf. Fract. 2009, ICF-12*, vol. 2, no. 5, pp. 861–870, 2009.

[38] N. Jothilakshmi, P. P. Nanekar, and V. Kain, "Assessment of intergranular corrosion attack in austenitic stainless steel using ultrasonic measurements," *Corrosion*, 2013, doi: 10.5006/0714.

[39] J. Jiao, Z. Fan, F. Zhong, C. He, and B. Wu, "Application of Ultrasonic Methods

for Early Detection of Intergranular Corrosion in Austenitic Stainless Steel," *Res. Nondestruct. Eval.*, 2016, doi: 10.1080/09349847.2015.1103922.

[40] K. R. Olsen, "Ultrasonic Detection of Simulated Corrosion in 1 Inch Diameter Steel Tieback Rods," no. August 2009, 2009.

[41] K. K. Maddumahewa, N. P. A. Madusanka, S. A. K. V. M. Piyathilake, and V. Sivahar, "Ultrasonic Nondestructive Evaluation Of Corrosion Damage In Concrete Reinforcement Bars," pp. 79–82, 2017.

[42] X. Li, Y. Song, F. Liu, H. Hu, and P. Ni, "Evaluation of mean grain size using the multi-scale ultrasonic attenuation coefficient," *NDT E Int.*, vol. 72, pp. 25–32, 2015, doi: 10.1016/j.ndteint.2015.02.002.

[43] B. Peirson, "Comparison of the ASTM Comparative Chart Method and the Mean Line Intercept Method in Determining the Effect of Solidification Rate on the Yield Strength of AA5182," Grand Valley State University, 2005.

[44] H. Ogi, M. Hirao, and T. Honda, "Ultrasonic attenuation and grain-size electromagnetic acoustic resonance," *J. Acoust. Soc. Am.*, vol. 98, no. 1, pp. 458–464, 2014, [Online]. Available: https://doi.org/10.1121/1.413703.

[45] J. Schijve, "Fatigue as a Phenomenon in the Material," in *Fatigue of Structures and Materials*, SpringerLink, 2009.

[46] P. Behjati, H. Vahid Dastjerdi, R. Mahdavi, and D. Rasouli, "Effect of microstructure on attenuation mechanism of ultrasonic waves in carbon steels," *Mater. Sci. Technol.*, vol. 26, no. 4, pp. 482–486, 2010, doi: 10.1179/026708309X12495548508509.

8 RESULTS TABLES

8.1 Appendix I

(Following table includes of these are calculated values /experimental readings. Calculation procedures are discussed in the relevant sections in the thesis)

Carbon content	Time (h)	Weight Loss (Average)	Weight Loss STDV	WL per unit area (g/m^2)	Corrosion Rate (mm/yr)	Attenuation Coefficient (dB/mm) (Average)	Attenuation Coefficient (dB/mm) STDV
0.21	0	-	-	-	-	0.151	0.013
	192	1.59	0.16	990.68	0.984	0.187	0.054
	360	4.09	0.21	2557.34	1.372	0.22	0.05
	528	7.69	0.43	4808.05		0.233	0.028
	688	7.78	0.15	4859.75	1.35	0.238	0.03
	840	11.23	1.04	7020.09	1.598	0.239	0.013
	992	12.37	1.92	7731.43	1.491	0.272	0.029
0.28	0	-	-	-	-	0.163	0.037
	192	2.62	0.36	1636.3	1.63	0.258	0.017
	360	5.15	1.51	3217.47	1.712	0.292	0.059
	528	7.57	1.28	4733.78	1.716	0.3	0.046
	688	10.9	1.2	6814.57	1.893	0.317	0.058
	840	13.53	2.12	8453.64	1.926	0.329	0.042
	992	16.43	0.2	10269.25	1.979	0.332	0.092
0.42	0	-	-	-	-	0.173	0.043
	128	1.35	0.48	842.29	1.259	0.207	0.021
	280	3.75	0.02	2344.79	1.601	0.242	0.051
	368	4.76	0.25	2973.89	1.545	0.268	0.009
	528	7.62	0.09	4762.74	1.724	0.274	0.042
	640	9.26	1.63	5786.7	1.728	0.282	0.012

	-	-	-	-	-	0.306	0.021
0.53	0	-	-	-	-	0.184	0.039
	192	1.78	0.14	1114.17	1.103	0.198	0.047
	360	4.37	0.29	2730.29	1.447	0.224	0.043
	528	7.12	0.73	4449.39	1.611	0.236	0.037
	688	8.57	0.99	5354.88	1.487	0.249	0.041
	840	12.84	0.59	8025.74	1.826	0.268	0.036
	992	13.73	0.73	8580.35	1.654	0.276	0.014

8.2 Appendix II

Carbon content	Exposure time in the corrosive environment	Attenuation coefficient (dB/mm) in average grain diameters					
		0.052 mm	0.117 mm	0.150 mm	0.180 mm	0.196 mm	0.210 mm
0.21	0	0.151	0.142	0.137	0.133	0.131	0.129
0.28	0	0.162	0.153	0.151	0.146	0.142	0.141
0.42	0	0.173	0.164	0.160	0.156	0.154	0.152
0.53	0	0.184	0.175	0.171	0.166	0.164	0.162
0.21	192	0.187	0.178	0.174	0.169	0.167	0.165
0.28	192	0.258	0.249	0.247	0.241	0.237	0.236
0.42	192	0.207	0.198	0.194	0.190	0.187	0.186
0.53	192	0.198	0.189	0.185	0.181	0.179	0.177
0.21	360	0.220	0.212	0.207	0.203	0.201	0.199
0.28	360	0.292	0.283	0.281	0.275	0.272	0.271
0.42	360	0.242	0.234	0.229	0.225	0.223	0.221
0.53	360	0.224	0.216	0.211	0.207	0.205	0.203
0.21	528	0.233	0.224	0.220	0.216	0.213	0.211
0.28	528	0.300	0.291	0.289	0.284	0.280	0.279
0.42	528	0.268	0.259	0.254	0.250	0.248	0.246
0.53	528	0.236	0.228	0.223	0.219	0.217	0.215
0.21	688	0.238	0.229	0.225	0.221	0.218	0.216
0.28	688	0.317	0.308	0.306	0.300	0.297	0.296
0.42	688	0.274	0.265	0.261	0.257	0.255	0.253
0.53	688	0.249	0.240	0.236	0.232	0.230	0.228
0.21	840	0.239	0.230	0.226	0.222	0.220	0.218
0.28	840	0.329	0.320	0.318	0.313	0.309	0.308
0.42	840	0.282	0.273	0.268	0.264	0.262	0.260
0.53	840	0.268	0.260	0.255	0.251	0.249	0.247
0.21	992	0.272	0.263	0.258	0.254	0.252	0.250
0.28	992	0.332	0.324	0.321	0.316	0.312	0.311
0.42	992	0.305	0.297	0.292	0.288	0.286	0.284
0.53	992	0.276	0.268	0.263	0.259	0.257	0.255

8.3 Appendix III

SEM images of the 0.53 % C steel

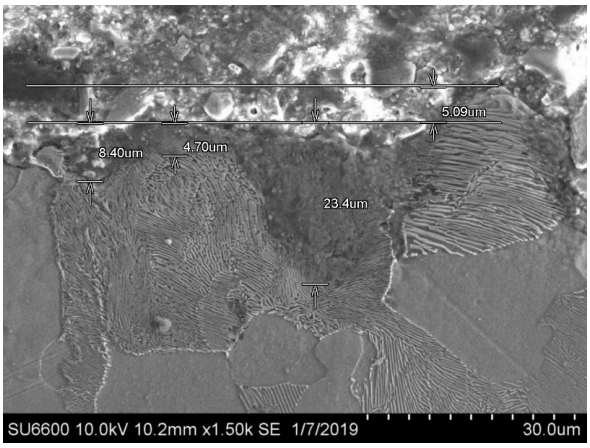

After 1 month in accelerated corrosion environment

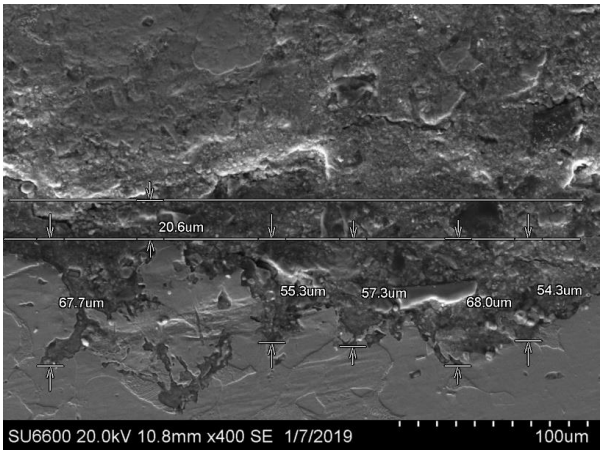

After 2 months in accelerated corrosion environment

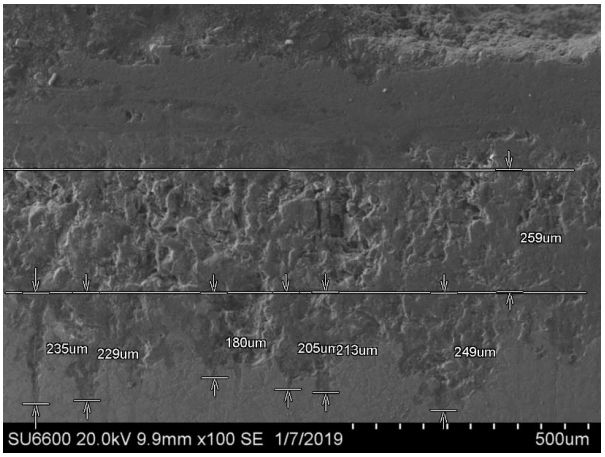

After 3 months in accelerated corrosion environment